PHASE STUDIES OF INORGANIC SULPHATES AT HIGH TEMPERATURES

David Alexander Campbell

A Thesis Submitted for the Degree of PhD
at the
University of St Andrews

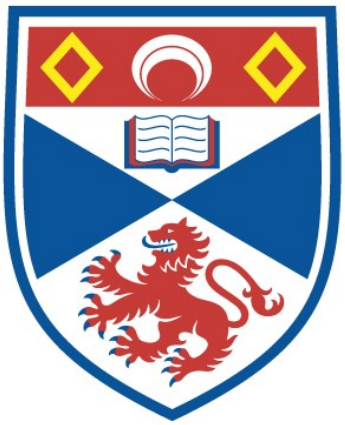

1985

PHASE STUDIES OF INORGANIC SULPHATES

AT HIGH TEMPERATURES

A Thesis

presented for the degree of

Doctor of Philosophy

in the Faculty of Science of the

University of St. Andrews

February 1985

DECLARATION

I declare that this thesis is my own composition, that the work of which it is a record has been carried out by me, and that it has not been submitted in any previous application for a Higher Degree.

This thesis describes results of the research carried out at the Department of Chemistry, United College of St. Salvator and St. Leonard, University of St. Andrews, under the supervision of Professor P.A.H. Wyatt since the 1st of October 1981.

David Alexander Campbell.

CERTIFICATE

I hereby certify that David Alexander Campbell B.Sc. has spent twelve terms of research work under my supervision, has fulfilled the conditions of Ordinance General no. 12 and resolution of the University Court, 1967, no. 1, and is qualified to submit the accompanying thesis in application for the degree of Doctor of Philosophy.

P.A.H. Wyatt

Professor

ACKNOWLEDGEMENTS

I wish to thank Professor P.A.H. Wyatt for his encouragement and support throughout this project.

I am indebted to the Science and Engineering Research Council of Great Britain for provision of the Research Studentship which financed this work.

I am especially grateful to members of the technical staff of the University of St. Andrews Chemistry Department without whose expertise this work would not have been possible: Mr. J. Rennie, Mr D.S. Clark and Mr. R.E. Cathcart of the engineering workshop, Mr. J.G. Ward and Mr. D. Wilkie of the electronics workshop, Mr. C.F.M. Smith for his glassblowing expertise and Mr.J.R. Bews of the microprocessor workshop.

I am grateful to Dr. G.S. Harris for his help and encouragement and also to Mr. G.K. Johnson of The Argonne National Laboratory, Chicago for useful discussions relating to the drop calorimeter.

I wish to acknowledge the computing laboratory of the University of St. Andrews for use of mainframe and microcomputer facilities.

Finally, I wish to express my sincere gratitude to my wife Isleen, who not only provided invaluable moral support but who also painstakingly checked and typed this thesis.

Summary

The theme of this thesis is the high-temperature phase studies of inorganic metal sulphates and the aspects specifically dealt with are phase diagrams and drop calorimetry.

Chapters 1,2, and 3 are concerned with the first of these. Chapter 1 briefly describes the features encountered in one and two-component systems and provides the thermodynamic background which allows such systems to be calculated.

Chapter 2 describes a selection of experimental techniques used to determine phase diagrams. Apparatus to perform Differential Thermal Analysis (DTA) was constructed as part of the work of this thesis and so this technique is fully described, including details of the apparatus, and a section on interpretation of DTA results relating to phase studies. Pointers are included as to further applications of this technique and improvements or modifications that might be made to the present apparatus.

Chapter 3 presents the phase diagram of the previously undetermined system Ag_2SO_4 - $La_2(SO_4)_3$ and also includes some observations on the kinetics of some phase changes and a description of the optical furnace which was built to study them. Also presented is a re-investigation of the system Ag_2SO_4 - $CdSO_4$, which contains many features not evident in an earlier study.

Chapter 4 is concerned with the thermodynamics of substances at high-temperatures and describes in detail the design, construction and experimental procedure for a drop calorimeter. This apparatus allows the equilibrium temperature of high-temperature polymorphic phase transitions and their enthalpies of transition to be determined.

A preliminary study on $CdSO_4$ was performed, which ties in with the study in Chapter 3, and an attempt was made to resolve the long standing controversy on the temperatures of the $CdSO_4$ phase transitions.

Drop Calorimetry can provide some of the data necessary for the calculation of phase diagrams as described in Chapter 1, and so a brief introduction to the thermodynamics of non-reacting systems and the treatment of results is presented.

To Isleen

CONTENTS

1 PHASE THEORY

1.1 Phase Diagrams and the Phase Rule

1.1.1 Introduction

This Section is intended as a brief introduction to the Gibbs Phase Rule and its application to the binary phase diagrams of condensed systems and their essential features where these are relevant to the experimentally determined diagrams featured in this thesis (Chapter 3).

1.1.2 The Phase Rule

The Gibbs Phase Rule is a statement of the relationships that exist between the variables temperature (T), pressure (p) and composition (x) in a system which may be composed of a number of phases and which is in a state of thermal and chemical equilibrium. A phase diagram is in essence a graphical representation of these relationships.

The phase rule is represented by the equation:

$$P + F = C + 2 \qquad (1.1.1)$$

(for the derivation of the phase rule see references 1 and 2).

P is the number of phases present at equilibrium; a phase being defined as any part of the system which is homogeneous within itself and bounded by a surface which allows it to be mechanically separated from any other parts. A phase need not be continuous.

C is the number of components. This term is defined as being the minimum number of independently variable chemical constituents which are necessary and sufficient to express the composition of each phase present at equilibrium, in the form of a chemical expression. In the case of systems in which the components do not chemically interact this is straightforward: water and ethanol is a two component example of such a system.

Consider the equilibrium equation:

$$CaCO_{3(s)} \rightleftharpoons CaO_{(s)} + CO_{2(g)} \qquad (1.1.2)$$

This system contains three phases (two solid and one gaseous). To determine the composition of any given phase it is necessary to specify only two of the constituents. Since each constituent is related by the equilibrium equation, none is independent of the

others; so the above is an example of a two component system.

F, the number of degrees of freedom (or variance) of the system, is defined as the number of intensive variables (composition, temperature and pressure) which may be changed without causing the appearance of a new phase or the disappearance of an old one.

However, the phase rule, though widely recognised as a most elegant and comprehensive generalisation of chemical thermodynamics, does have limitations: firstly, it is applicable only to systems in a state of equilibrium; secondly, it ignores the influence of gravitational and magnetic fields. Within these limitations, however, the rule provides certain criteria by which a system may be judged to be in equilibrium; a system which does not obey the phase rule is definitely not in equilibrium but a system may contain metastable phases and still obey the phase rule.

The following examples illustrate the application and validity of the phase rule. For a more exhaustive treatment see references 3-6.

1.1.3 Single Component Systems

In a single component system, the phase rule is:

$$F = 3 - P \qquad (1.1.3)$$

Figure 1.1 shows the p-T diagram for RbI.[7] If, to take an example, the system is maintained at 4 kbar and cooled along isobar abcd, then at point a, pure liquid is the only phase present, therefore F = 2. This is a bivariant region; both T and p can be continuously and independently varied without bringing about the appearance of a new phase. On cooling to 740 ^{o}C however, two phases are present and so RbI begins to crystallise with the NaCl structure. Here, F = 1 (ie this is an univariant point) and since the pressure is fixed there is no degree of freedom left. Therefore, at 4 kbar, liquid and solid will be in equilibrium at a unique temperature (740 ^{o}C). Before the system can undergo further cooling, crystallisation of RbI must be complete. Immediately below 740 ^{o}C only one phase is present. At 400 ^{o}C, RbI transforms into the CsCl structure and again this represents a univariant transition.

The point, e on the diagram represents the equilibrium between three phases: RbI-(I), RbI-(II), and RbI (l); it occurs at a unique temperature and pressure (5.0 kbar, 760 ^{o}C), is invariant (F = 0) and is termed the Triple Point.

The line ef represents the equilibrium:

$$RbI(II) \rightleftharpoons RbI(l) \qquad (1.1.4)$$

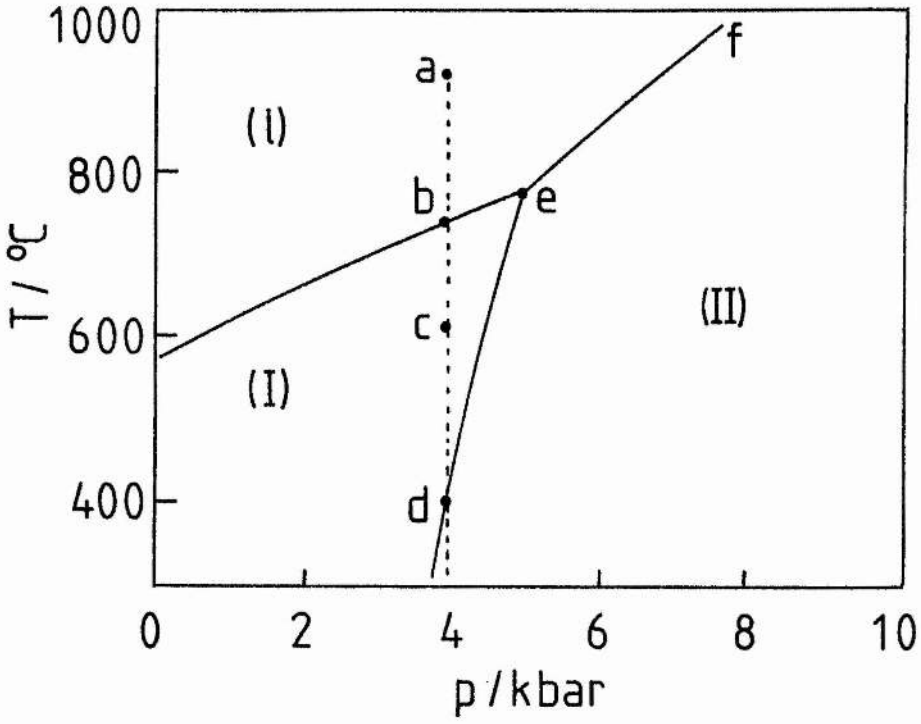

Figure 1.1 p-T diagram for RbI. (I) = NaCl structure (II) = CsCl structure.

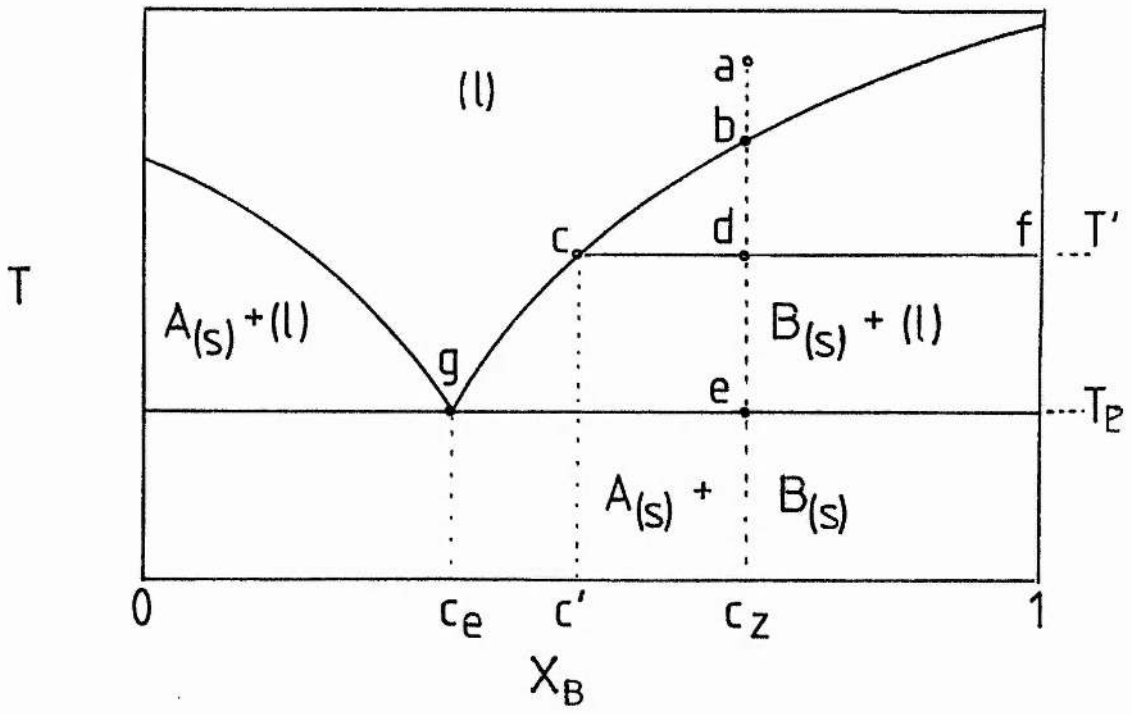

Figure 1.2 Phase diagram of the Binary system A-B; X_B is the composition of the system expressed as mole fraction of component B.

1.1.4 Binary Diagrams

The original studies contained in this thesis are concerned with diagrams for two component (or binary) systems in which the pressure is assumed to be constant or to have negligible effect upon the phase equilibria, and so in such systems one degree of freedom is removed. The system is condensed because the vapour phase is ignored and for the sake of convenience the phase rule again reduces to $F = 3 - P$.

Binary diagrams can be placed in one of three classes depending on whether the two solid components are:

(1) Completely immiscible.

(2) Completely miscible.

(3) Partially miscible.

1.1.4.1 Systems With Completely Immiscible Components.

The simplest of the class (1) diagrams is the so-called eutectic diagram (figure 1.2). The eutectic occurs at the intersection of the liquidus curves, g. If liquid of this composition is cooled to T_e, the eutectic temperature, then the phase reaction

$$l \rightarrow A(s) + B(s) \qquad (1.1.5)$$

occurs. At this point $F = 0$ and so the eutectic is invariant, and

appears as a horizontal line, which is a characteristic of all invariant phase reactions. The structure of the solidified eutectic is an intimate mixture of solids A and B. If the system is cooled along isopleth c_z, then at point a only pure liquid is present; at b, the liquidus curve, crystallisation of pure solid B commences at a temperature unique to the overall composition (since F = 1). Cooling along bd two conjugate phases are present and the composition of the liquid varies along the liquidus curve bc. The composition along any given isotherm in this region is fixed (eg df). If for example, the overall composition of the system is c_z, then the composition of the liquid is c', while that of the solid is pure B. The relative amounts of the two phases vary in accordance with the so-called Lever rule which, for overall composition c_z (lying on the tie-line cdf) is given as:

$$\frac{\text{amount liquid phase}}{\text{amount solid phase}} = \frac{df}{dc} \qquad (1.1.6)$$

Decreasing the temperature causes further crystallisation of B, while the composition of the liquid becomes richer in component A and traverses the liquidus curve cg until the temperature of the system reaches that of the eutectic where it remains until all the liquid has solidified.

1.1.4.2 Compound Formation

Figure 1.3 illustrates the occurrence of an intermediate compound of stoichiometry AB_2, which is stable until the melting point T_m is reached. On melting the phase reaction is:

$$AB_2(s) \longrightarrow AB_2(l) \qquad (1.1.7)$$

ie solid becomes liquid of the same composition. The stability of a compound is indicated by the sharpness of the curve.

An unstable compound exhibits a submerged maximum (shown by dotted lines in figure 1.4). If a mixture of stoichiometry AB_2 is heated, then a meritectic reaction will occur at T_i (known as the incongruent melting point):

$$AB_2(s) \rightleftharpoons B(s) + l \qquad (1.1.8)$$

(ie solid decomposes to a liquid of a different composition depositing a pure solid component). The liquid phase has composition c_m.

All mixtures in the composition range c_m to $x_A = 0$ will undergo this invariant transition.

Figure 1.5 illustrates another possible fate of the compound; that of solid-state decomposition which in this example occurs at T_s and is represented by equation (1.1.9):

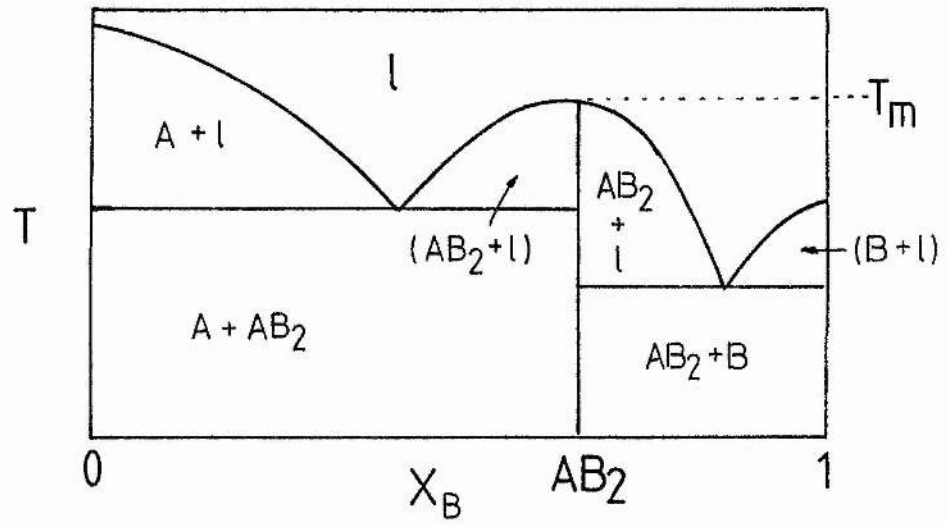

Figure 1.3 Binary system A-B with congruently melting compound, AB_2
$A = A_{(s)}$; $B = B_{(s)}$

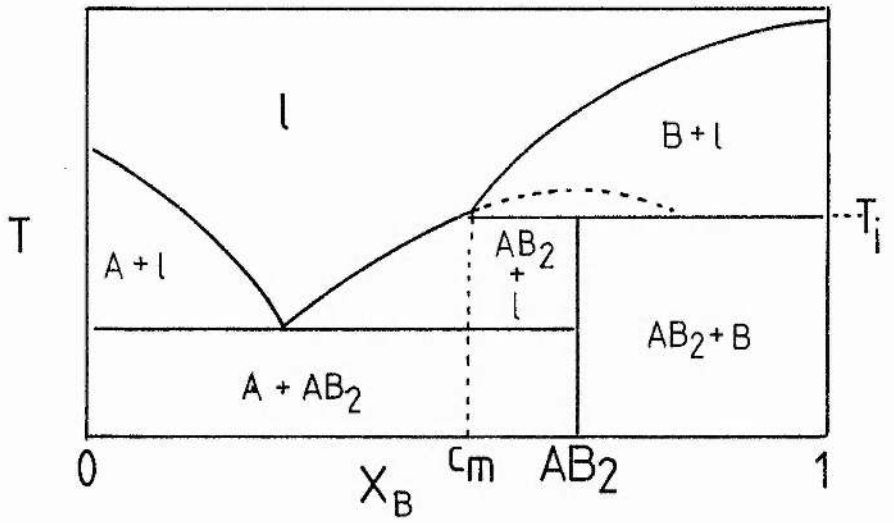

Figure 1.4 System A-B with incongruently melting compound, AB_2

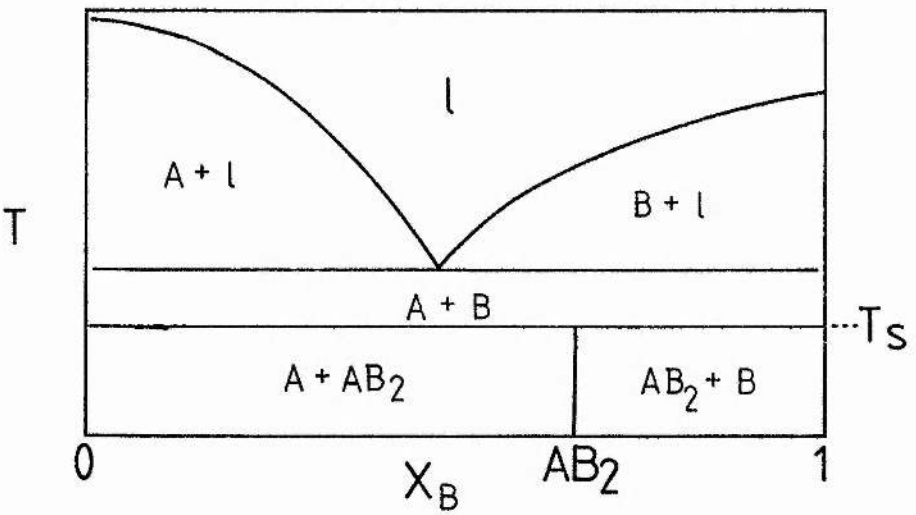

Figure 1.5 System A-B with intermediate compound, AB_2 undergoing solid state decomposition.

$$AB_2(s) \rightleftharpoons A(s) + 2B(s) \qquad (1.1.9)$$

Compound formation may be observed in all classes of binary system.

1.1.4.3 Systems With Completely Miscible Components

A solid solution is a single homogeneous crystalline phase, the composition of which may be varied within finite limits without causing the appearance of another phase. The components must be mutually soluble in much the same way as in liquid or gaseous phases.

There are two general categories into which solid solutions may fall. Cu and Ni form a series of continuous solid solutions in which Cu atoms are substituted for those of Ni atoms which adopt an fcc lattice (figure 1.6). This type of solid solution is termed substitutional and may occur when metal atoms are of a comparable size.

Alternatively, solute atoms may occupy interstitial sites in the parent crystal structure and this may occur when solute atoms are small in comparison to those of the solvent. C dissolved in Ni is an example of an interstitial solid solution.

In the case of figure 1.6 the solutions formed do not exhibit a minimum or a maximum in either the freezing point (liquidus) curve or the melting curve (solidus). The conjugate phases at any given temperature (eg T`) are joined by tie lines.

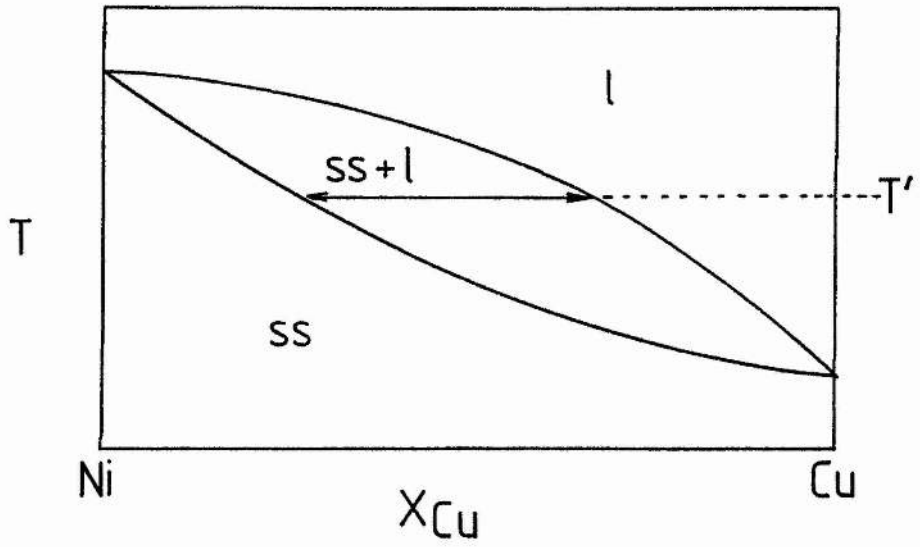

Figure 1.6 The system Ni-Cu. ss = solid solution phase.

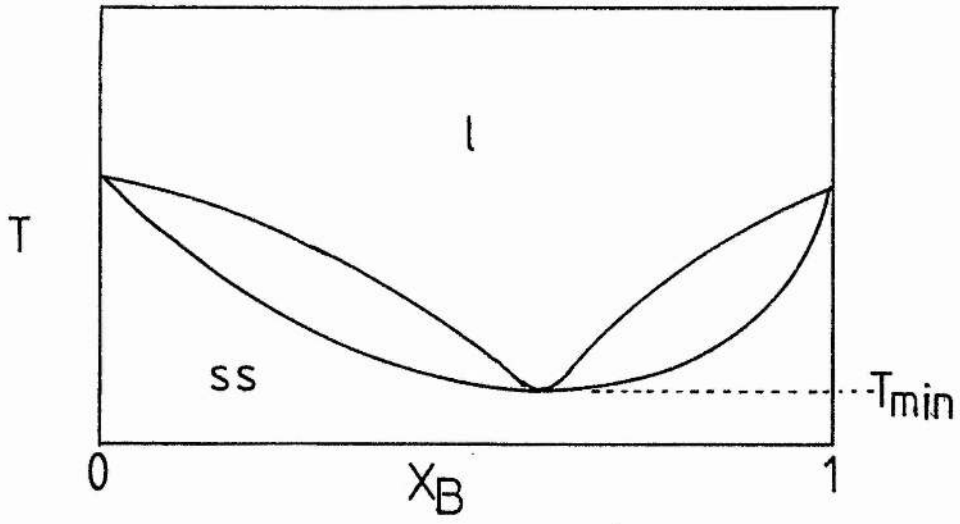

Figure 1.7 The system A-B. Minimum-melting solid solution (T_{min}).

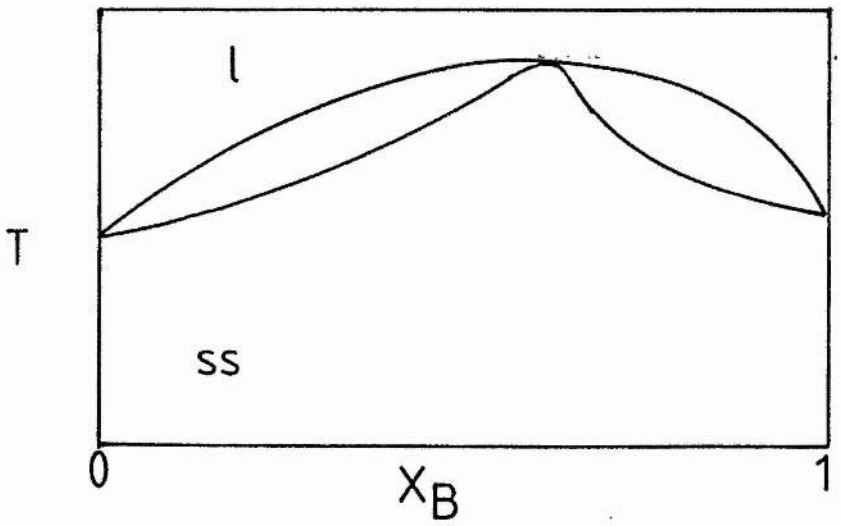

Figure 1.8 The system A-B, displaying a maximum-melting solid solution.

Figure 1.7 shows a system which exhibits a minimum in the melting point, T_{min}, and which differs from that in figure 1.6 in that this minimum occurs at only one temperature and one composition. These curves have counterparts in vapour-liquid equilibria. Figure 1.8 shows a maximum-melting solid solution.

1.1.4.4 Systems With Partially Miscible Components.

Although solid-solubility is expected in most solid-state diagrams, in many cases the composition range over which solid solutions are formed may be so small that they may not be detected when using conventional methods of analysis; a fact evidenced by many published diagrams.[8]

An example of a phase diagram peculiar to systems with limited solid solubility is that involving the peritectic reaction which on heating occurs at T_p and is represented by the equation:

$$\alpha \rightleftharpoons \beta + l \qquad (1.1.10)$$

(where α and β are solid solution phases). Since the equilibrium involves three phases, then F = 0, ie it is invariant. A hypothetical peritectic phase diagram is shown in figure 1.9.

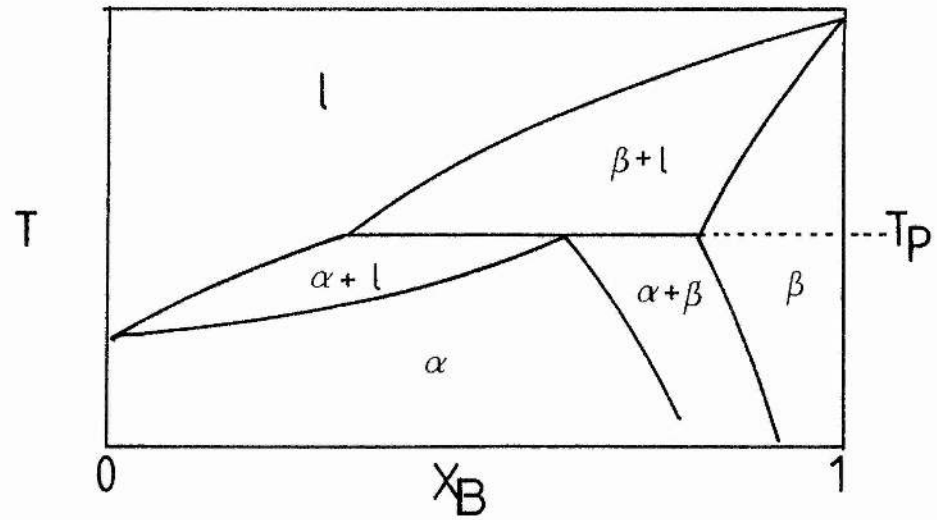

Figure 1.9 A peritectic system. The peritectic transition occurs at T_p.

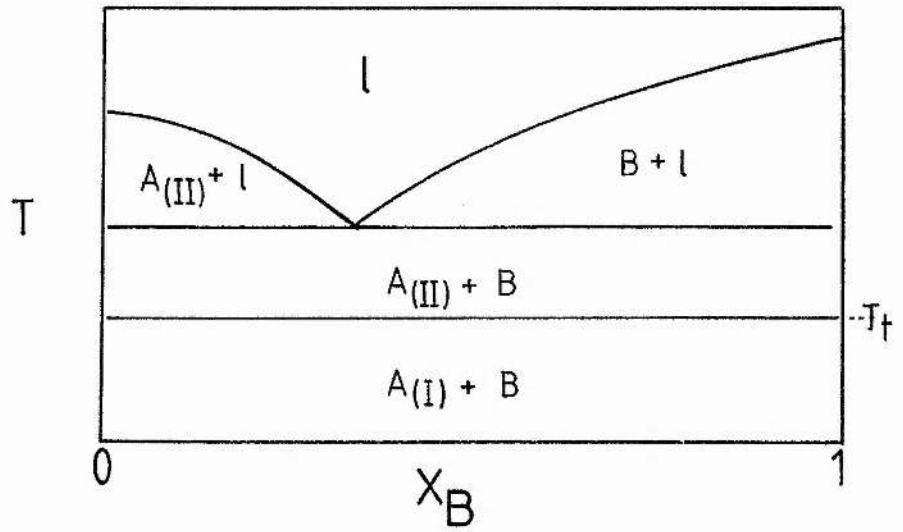

Figure 1.10 Component A exists in two modifications (I) and (II) for which the transition temperature is T_t.

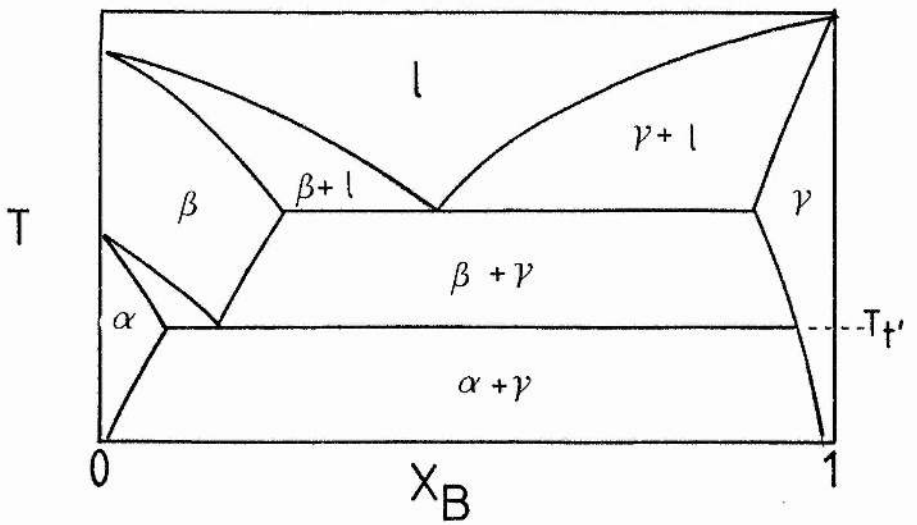

Figure 1.11 Two solid solutions related to A(I) and A(II); α and β respectively, form a eutectoid at $T_{t'}$ with γ.

Other features to be found in binary diagrams include polymorphic transitions. Figure 1.10 illustrates the case in which only component A exists in a high-temperature form, A(II). At constant atmospheric pressure, the transition

$$A(I) \rightleftharpoons A(II) \qquad (1.1.11)$$

occurs at constant temperature and is unaffected by composition unless the compound is soluble in the other component in which case a eutectoid is observed (see figure 1.11), which is analogous to the eutectic, in as much as it is the lowest temperature T' at which the two solid solution phases α and β may co-exist. The reaction is:

$$\alpha \rightleftharpoons \beta + \gamma \qquad (1.1.12)$$

and takes place solely within the solid state.

The system shown in figure 1.12 has a region containing two liquid phases and exhibits an upper critical point, c. T_m, the monotectic temperature, represents an invariant point for which the phase reaction is:

$$A(s) + l_2 \rightleftharpoons l_1 \qquad (1.1.13)$$

This is a monotectic reaction. Such regions are commonly found in the SiO_2-rich regions of silicate systems.

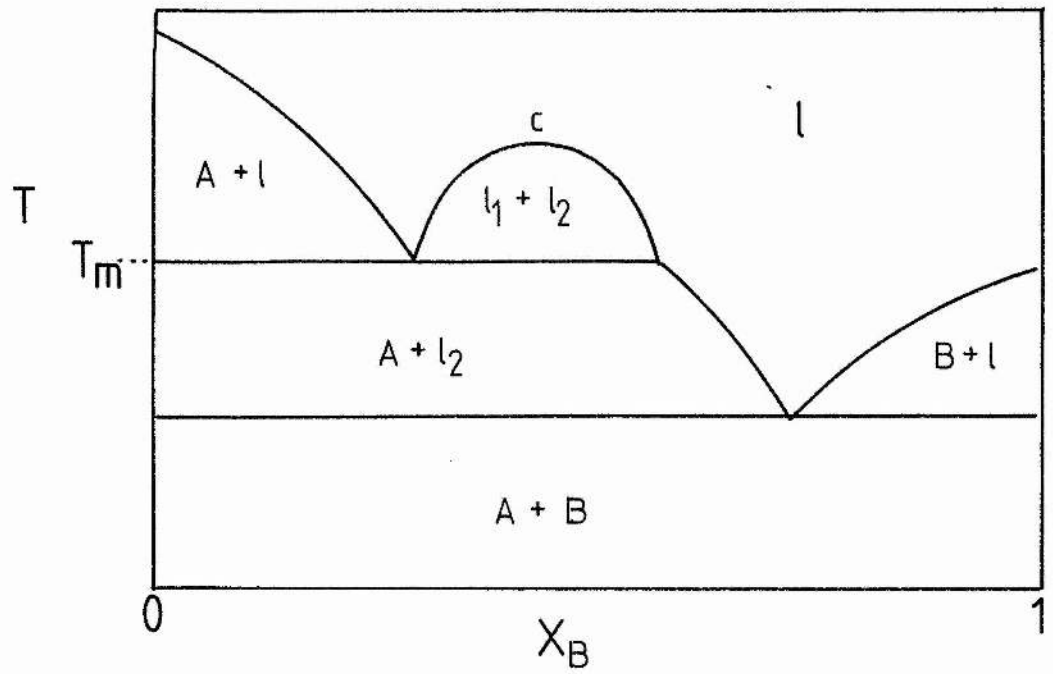

Figure 1.12 System A-B for which a two liquid region $l_1 + l_2$ is observed.

As discussed in a later Section, obtaining equilibrium diagrams is no easy task since persistent metastable phases may not always be screened out by applying the phase rule. (The existence of a metastable phase does not affect the usefulness of a diagram if that phase is of technological importance.) The phase rule does help test the validity of a diagram and it may also be used in conjunction with some additional rules,[9] which are as follows:

(1) The Boundary Rule: any P phase region may be bounded only by regions containing $P \pm 1$ phases.

(2) Curvature Boundaries: curvature boundaries of one phase region must meet with curvature and extrapolate into adjacent two phase regions.

(3) Solubility Rule: all components are mutually soluble to a greater or lesser degree.

Phase diagrams are usually a combination of several of the basic features illustrated in this Section, but they may be of far greater complexity than those shown.

1.1.5 Literature on Phase Diagrams

The three available volumes of Levin et al [8] illustrate five thousand phase diagrams of inorganic systems having up to four components, giving sources (these are diagrams published up to 1973). A recent book by Wisniak[10] gives the literature sources of all phase diagrams published up until 1980.

1.2 The Thermodynamic Basis of Phase Diagrams

1.2.1 Introduction

In this Section some basic thermodynamic equations applicable to one and two component systems are derived to show how the isobaric two component (or binary) phase diagrams of condensed systems may be constructed from thermochemical data available for the pure components, if simple models are assumed. Mention is also made of computer methods and their use in the calculation of ternary diagrams by critical analysis of the binary systems from which they are constructed.

1.2.2 Thermodynamics of Single Component Systems

At any given temperature T, a pure component A, which is present in its most thermodynamically stable condition, will lie at its minimum chemical potential (hereafter referred to as Gibbs function, G), which will decrease with increasing T (figure 1.13(a)).

If A can exist in two crystalline modifications A(I) and A(II), the low and high-temperature forms respectively, when these satisfy the equilibrium (1.2.1) at T_t:

$$A(I) \rightleftharpoons A(II) \qquad (1.2.1)$$

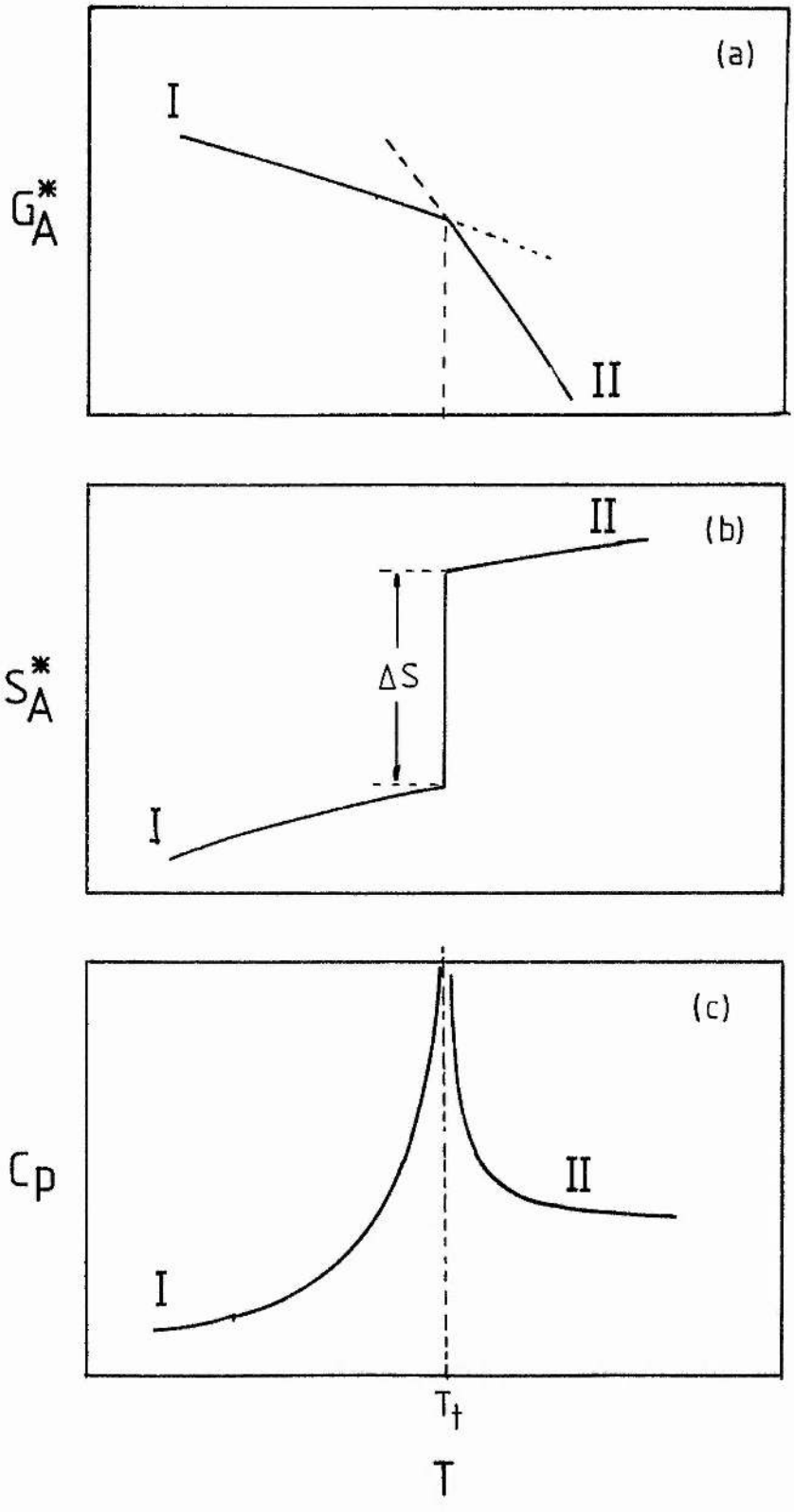

Figure 1.13 The variation of (a) Gibbs function, G_A^*, (b) Entropy, S_A^*, and (c) Heat capacity, C_p , as a function of temperature, T, around the transition, A(I) $\rightleftharpoons$ A(II).

then

$$G^{*}_{A(I)} = G^{*}_{A(II)} \qquad (1.2.2)$$

The entropy (S) of A (figure 1.13(b)) will exhibit a discontinuity at T_t due to the difference in slopes between the Gibbs function curves, ie:

$$(\delta G / \delta T)p = -S \qquad (1.2.3)$$

Discontinuities would also be apparent in the enthalpy (H) and volume (V). Since these discontinuities are observed for first order derivatives of G, this transition is termed First Order. Heat capacity (Cp) will tend towards infinity as this transition is approached (figure 1.13(c)).

Although not observed in the course of the work presented in this thesis, the phenomenon of the second order transition exists. On passing through such a transition H, S and V change continuously with temperature while Cp exhibits a discontinuity. The order-disorder transition is an example.

Gibbs function curves analogous to those in figure 1.13(a) may be constructed from data contained in thermochemical tables.[11] For the sake of convenience, the Gibbs function of the low-temperature modification is arbitrarily assigned a value of zero at 298.15 K and the Gibbs function of the high-temperature crystalline or liquid states are calculated relative to that standard state.

1.2.3 Thermodynamics of Simple Binary Systems

When two components, A and B, mix to form a solid or liquid solution, the change in the molar Gibbs function is:

$$\Delta_{mix}G_m = \Delta_{mix}H_m - T\Delta_{mix}S_m \qquad (1.2.4)$$

Where an ideal solution is formed, the average intermolecular interactions in the solution are the same as those in each pure component. Thus:

$$\Delta_{mix}H_m = 0 \qquad (1.2.5)$$

and the solution obeys Raoult's Law over the entire composition range; thus the mixing process must be driven purely by entropy. On the assumption that species A and B are placed in solution entirely at random, statistical thermodynamics shows that:

$$\Delta_{mix}S_m = -R\,(x \ln x + (1-x) \ln (1-x)) \qquad (1.2.6)$$

where x is the mole fraction of component A.

On the assumption of equation (1.2.5), then substitution of (1.2.6) into (1.2.4) will give:

$$\Delta_{mix}G = RT(x \ln x + (1 - x) \ln (1 - x)) \qquad (1.2.7)$$

$\Delta_{mix}G / RT$ as a function of x, for an ideal solution, is shown in figure 1.14.

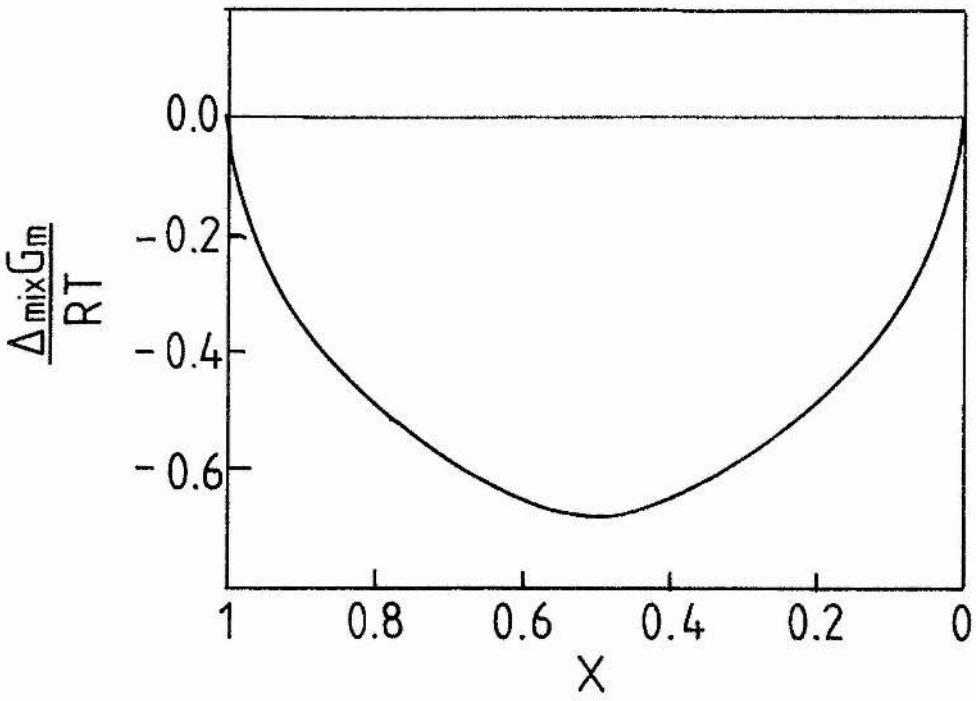

Figure 1.14 The variation of $\Delta_{mix}G$ / RT for an ideal solution, A-B, as a function of the mole fraction of component A, x.

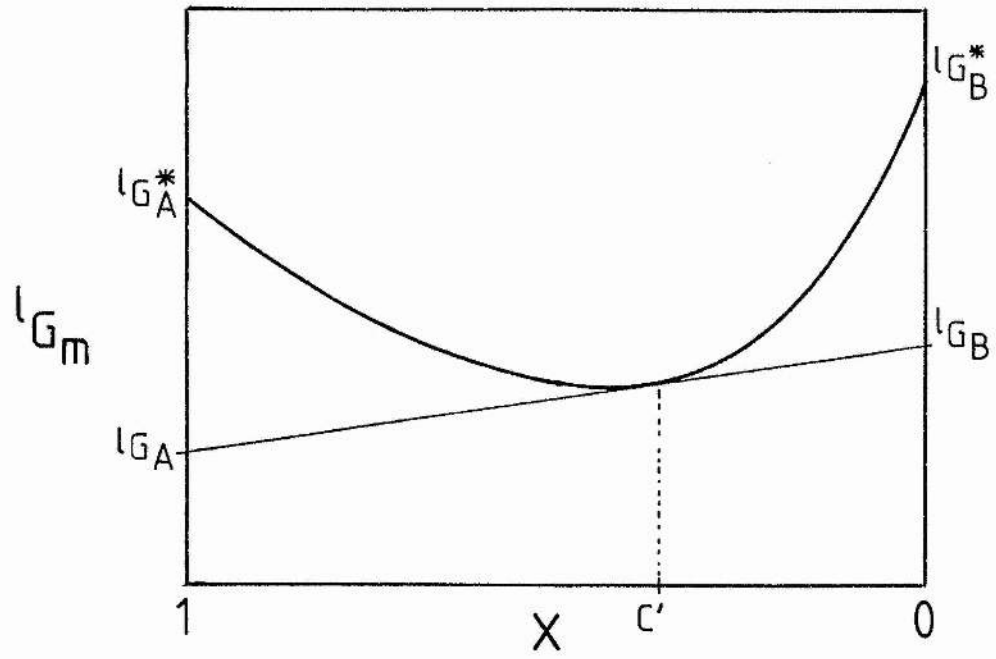

Figure 1.15 Gibbs function for the ideal solution A-B at constant temperature, as a function of x.

The partial molar Gibbs function of A in solution, ${}^{l}G_{A}$ is expressed as:

$$ {}^{l}G_{A} = {}^{l}G_{A}^{*} + RT \ln {}^{l}a_{A} \qquad (1.2.8) $$

where the superscript l denotes liquid and ${}^{l}G_{A}^{*}$ is the molar Gibbs function of pure liquid A.

The relative partial molar Gibbs function of A, ${}^{l}G_{A}^{M}$ is

$$ {}^{l}G_{A}^{M} = {}^{l}G_{A} - {}^{l}G_{A}^{*} = RT \ln {}^{l}a_{A} \qquad (1.2.9) $$

where superscript M denotes a relative partial molar quantity.

The activity of A in solution, ${}^{l}a_{A}$, is expressed in terms of x as:

$$ {}^{l}a_{A} = f_{A}\,{}^{l}x \qquad (1.2.10) $$

where f_{A} is the activity coefficient. In an ideal solution $f_{A} = 1$ and so ${}^{l}a_{A} = {}^{l}x$. The integral molar Gibbs function of an ideal liquid solution ${}^{l}G_{m}$, is:

$$ {}^{l}G_{m} = x\,{}^{l}G_{A}^{*} + (1 - x)G_{B}^{*} + RT\,(x \ln x + (1 - x) \ln (1 - x)) \qquad (1.2.11) $$

Comparing equations (1.2.11) and (1.2.7) shows that the right hand term in equation (1.2.11) equates to $\Delta_{mix}G$ for an ideal solution.

The Gibbs function curves for an ideal solution at temperature T, are shown as a function of x in figure 1.15. ${}^{l}G_{A}$ and ${}^{l}G_{B}$, the partial molar Gibbs functions at c', are the intercepts of the tangent drawn to the curve at c', at x = 1 and x = 0 respectively.

If in addition a continuous solid solution is formed, the relationship between the Gibbs function curves and the phase diagram at T' is shown in figure 1.16. Although the curves intersect at point e, the minimum Gibbs function for the system at that composition (c_e) will lie on the common tangent. The composition of liquid and solid solution will be c_l and c_s respectively; the relative amounts of the two phases are given by the Lever Rule.

Figure 1.17 shows Gibbs function curves at four isothermal sections T_1, T_2, T_3, T_4, for a simple class 1 eutectic system (figure 1.17(a)).

There are three possible phases, solid A, solid B, and liquid. Only for the last of these will the Gibbs function vary with composition at a fixed temperature. At temperature T_1, liquid has the lowest Gibbs function at all compositions (figure 1.17(b)). Along isotherm T_2, A is in equilibrium with liquid of composition c_1. The tangent (figure 1.17(c)) sets the composition limits over which A and l co-exist. At temperature T_3, all three phases are in equilibrium and so lie on a common tangent (figure 1.17(d)). Below T_3 no liquid is present (figure 1.17(e)).

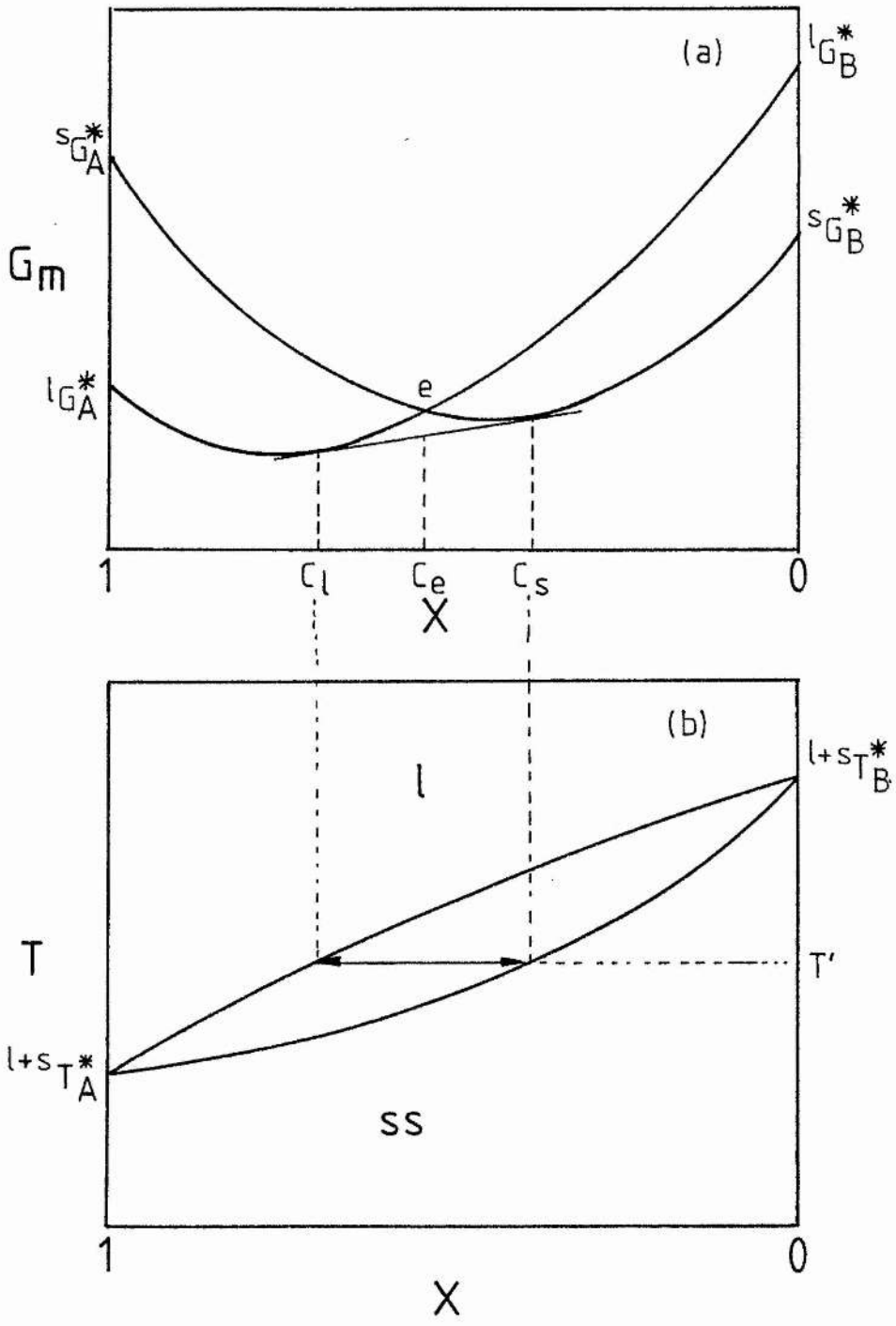

Figure 1.16 (a) Gibbs function curves as a function of x at temperature T', for the system A-B (b), which forms a continuous solid solution (ss = solid solution, l = liquid).

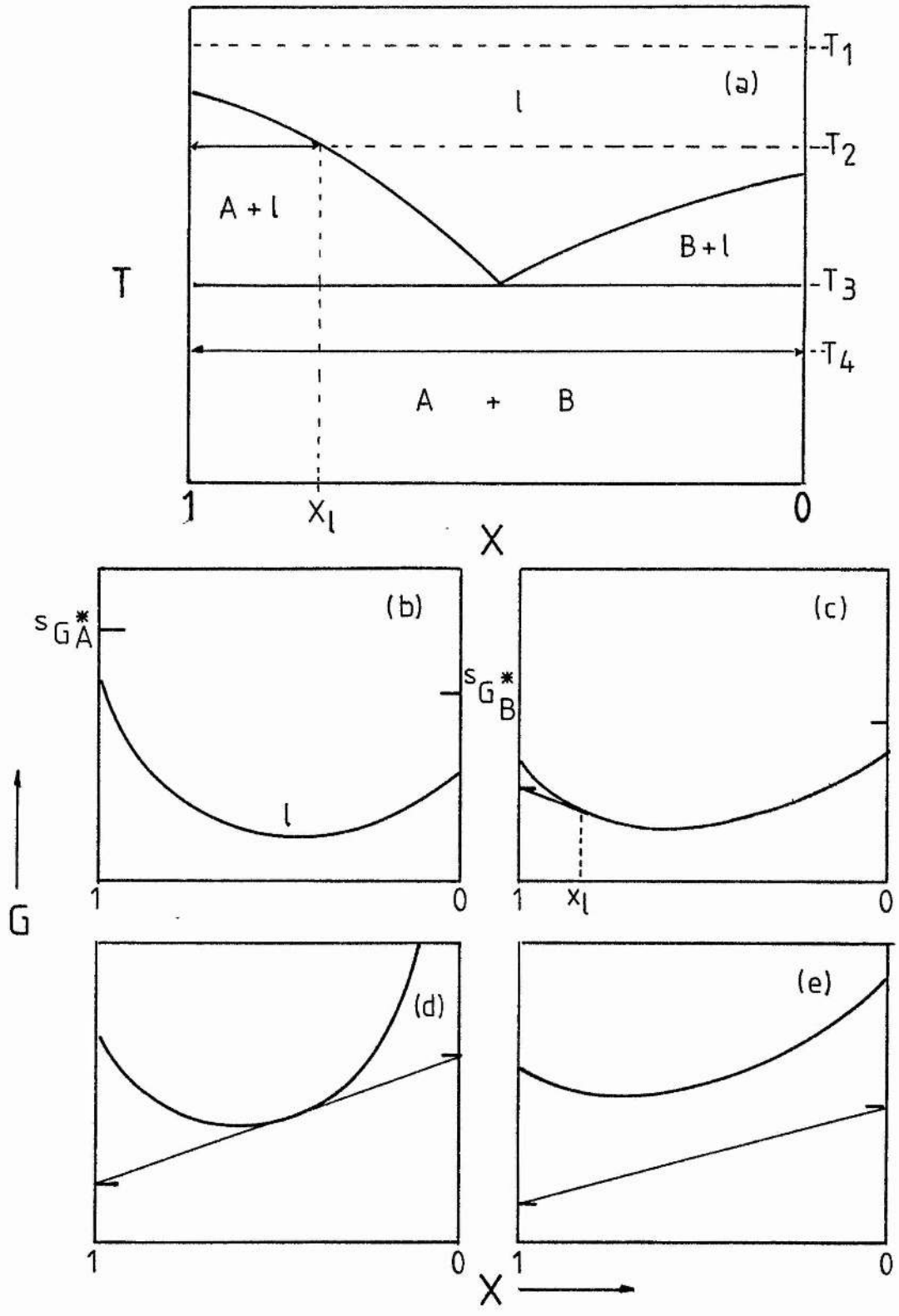

Figure 1.17 (a) The phase diagram of a simple binary system, A-B, and (b-e) the complementary Gibbs function curves along the isothermal sections T_1, T_2, T_3 and T_4 respectively.

Figure 1.18(a) shows a system featuring a stable compound, AB, and regions of solid solution, α and β; G^{*}_{AB} is represented on the G-X diagrams as a point.

Along isotherm T_1, the liquid phase possesses the lowest Gibbs function (figure 1.18(b)). Figure 1.18(c) illustrates the melting of AB at T_2, represented by the equilibrium:

$$AB(s) \rightleftharpoons AB(l) \qquad (1.2.12)$$

On isotherm T_3 there are a number of co-existing phases (figure 1.18(d)), while along T_4 AB is in equilibrium with both solid solution phases.

1.2.4 Excess Functions

Ideal solutions are rarely met in practice (although some examples are given later) and so there is generally some deviation from Raoult's Law except in very dilute solutions. This deviation may be expressed in terms of excess functions, Z^E ie:

$$Z^E_{mix} = Z^{obs}_{mix} - Z^{ideal}_{mix} \qquad (1.2.13)$$

where Z is any molar quantity, such as G,H,S or V.

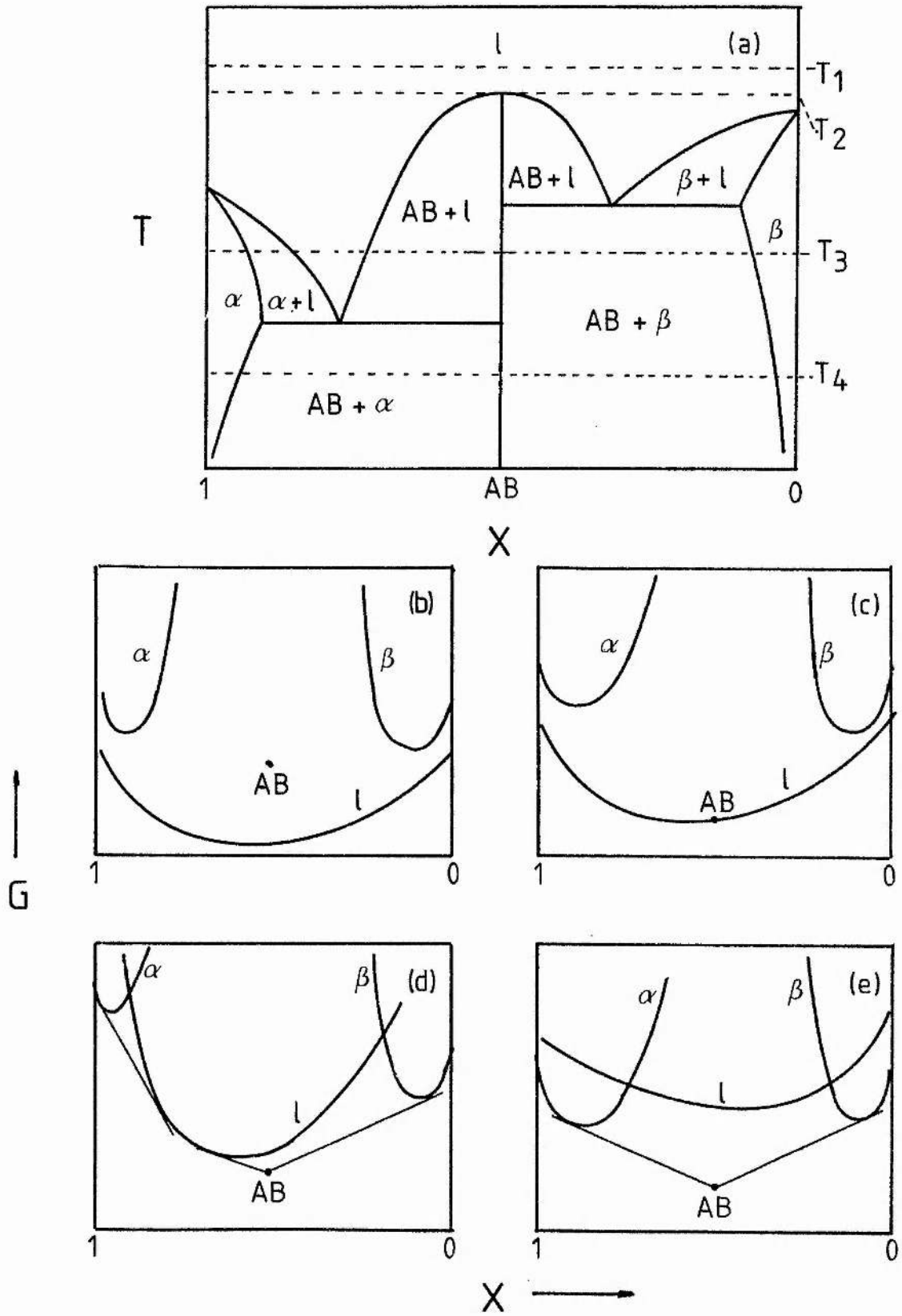

Figure 1.18 (a) The binary system A-B, which features regions of solid solution α and β, and a stable double salt, AB. (b-e) The Gibbs function curves along the isothermal sections T_1, T_2, T_3 and T_4 respectively.

In the case of a binary solution, the molar excess Gibbs function on mixing, G^E is expressed as:

$$G^E = RT\ (x \ln f_A + (1 - x) \ln f_B) \qquad (1.2.14)$$

By definition a regular solution has $S^E = 0$ and:

$$H^E = k_o(1 - x)(x) \qquad (1.2.15)$$

where k_o is a temperature-independent constant which takes into account interaction energies and co-ordination number. In the sub-regular approximation, $S^E = 0$ and

$$H^E = x\ (1 - x)(k_o + k_1 x) \qquad (1.2.16)$$

1.2.5 Calculation of Phase Diagrams

Consider the system shown in figure 1.16(b). On isotherm T' the compositions of the co-existing solid solution and liquid phases are c_s and c_l respectively. At equilibrium the Gibbs function of each component in both phases is equal, ie: ${}^sG_A = {}^lG_A$ and ${}^sG_B = {}^lG_B$.

For component A:

$$\Delta_{fus}G_A^* + RT \ln ({}^la_A / {}^sa_A) = 0 \qquad (1.2.17)$$

where $\Delta_{fus}G_A^* = {}^lG_A^* - {}^sG_A^*$; $\Delta_{fus}G_A^*$ is the change in Gibbs function on fusion at any temperature T.

Also:

$$\Delta_{fus}G_A^* = \Delta_{fus}H_A^* - T\Delta_{fus}S_A^* \qquad (1.2.18)$$

and

$$\Delta_{fus}G_A^* = \Delta_{fus}H_A^*(1 - T / T_{fus,A}) \qquad (1.2.19)$$

Substitution of (1.2.18) into (1.2.19) gives:

$$\ln({}^sa_A / {}^la_A) = \Delta_{fus}H_A^* / R(1 / T - 1 / T_{fus,A}) \qquad (1.2.20)$$

which for an ideal solution is expressed as:

$$\ln({}^sx / {}^lx) = \Delta_{fus}H_A^* / R(1 / T - 1 / T_{fus,A}) \qquad (1.2.21)$$

similarly for component B:

$$\ln({}^s(1 - x) / {}^l(1 - x)) = \Delta_{fus}H_B^* / R(1 / T - 1 / T_{fus,B}) \qquad (1.2.22)$$

By solving equations (1.2.21) and (1.2.22) as a function of T, the phase diagram, figure 1.16(b), may be calculated assuming that heat capacities are constant over the temperature range of interest. $\Delta_{fus}H$ may be obtained from thermochemical tables.

An example of a similar Class 2 system, is that of Si-Ge.[12] Ideal liquid solutions are formed amongst binary systems of the molten salts, Na_2SO_4, Na_2CrO_4 and Na_2MoO_4.[13]

If the eutectic system AB (figure 1.17(a)) is held at T_2 at composition c_1 on the liquidus curve then pure solid A and liquid of composition c_1 are in equilibrium; therefore:

$$ {}^{s}G_A^* = {}^{l}G_A \qquad (1.2.23) $$

and

$$ \Delta_{fus}G_A^* + RT \ln {}^{l}a = 0 \qquad (1.2.24) $$

$\Delta_{fus}G_A^*$ may be obtained from thermochemical tables and is expressed as a function of T over the temperature range of interest. The quantity ${}^{l}a_A$ may be measured using electrochemical or vapour pressure techniques over a range of temperatures at each of a number of compositions, $x = 0 < x < x = 1$. Plotting $-R \ln {}^{l}a_A$ against $1 / T$ gives a straight line and the temperature at which this intersects the plot of $\Delta_{fus}G_A^* / T$ versus $1 / T$, is the liquidus temperature for the composition in question. By repeating this procedure for a number of compositions on the A-rich side of the diagram, that liquidus curve may be determined. The liquidus curve for the B-rich side is determined by performing a similar analysis on $\Delta_{fus}G_B^*$ and ${}^{l}a_B$, the latter being obtained by applying the integrated form of the Gibbs-Duhem equation to the activity data for component A.

An example of such a calculation is that performed on the system Zn-Sn by Dunkerly and Mills[14] using existing thermodynamic data which had been obtained by Taylor,[15] who used electrochemical techniques to determine the activity of Zn in Zn-Sn mixtures at several temperatures and a number of compositions. The calculated diagram was virtually identical to that obtained experimentally.

A variation of the above method was used by Belton and Rao to obtain diagrams for the system Mg-Ge.[16]

1.2.6 Computer Methods

The importance of modern computer methods was illustrated by Kaufmann[17,18] who calculated the binary phase diagrams of seventy- two refractory metal systems (eg Mo, Ir, Ta, W). The method used required the Gibbs functions of all possible phases and because no thermodynamic data were available for these systems, semi-empirical methods were employed to calculate the interaction parameters, based on regular solution models. The calculated diagrams duplicated the essential features of existing experimental diagrams although serious temperature discrepancies were apparent.

It is possible to generate ternary phase diagrams by analysis of existing binary diagrams as demonstrated by Bale et al[19,20] who examined the experimentally obtained diagrams of fifteen binary metal chloride systems (Li, Na, Ca, and Sr). By critical analysis of the

diagrams and through use of equations similar to (1.2.11) and (1.2.14), component activities in the various solutions were obtained. This allowed analytical expressions for all the excess thermodynamic mixing properties of the binary systems to be determined. On the assumption that all ternary solutions formed were regular in nature, interpolation procedures were applied to equate the partial Gibbs functions of all three components in all phases.

The results achieved with this method were seen to be very favourable when the calculated diagrams were compared to their experimental counterparts: important features such as eutectics, peritectic valleys and liquidus temperatures being accurately reproduced.

The importance of this type of calculation lies in the fact that critical analysis of only a few experimental binary diagrams allows a far greater number of ternary systems to be calculated.

2 EXPERIMENTAL METHODS IN HIGH-TEMPERATURE PHASE STUDIES

2.1 Introduction

This Chapter surveys experimental techniques currently used to determine phase diagrams at temperatures in the range 100 - 2000 ^{o}C.* These techniques may be divided into two categories: Static and Dynamic.

In the former, the material to be studied is allowed to attain thermal equilibrium at the temperature of interest and a measurement is taken which is a function of the true equilibrium state of the system; eg, an X-ray diffraction spectrum.

A dynamic technique, on the other hand, measures the variation of some quantity (usually temperature) with time.

Some techniques, such as electrical conductivity, may be used both dynamically and statically.

* NB : The use of the degree Celsius (^{o}C) as the unit of temperature is recommended by the International Confederation for Thermal Analysis (ICTA)[21,22] when presenting thermal analysis results in the chemical literature, and, since the bulk of the material in this Chapter is concerned with thermal analysis, that convention will be followed by the author.

The two major dynamic techniques in current use are Differential Thermal Analysis (DTA) and its more modern counterpart, Differential Scanning Calorimetry (DSC). The former is the principal experimental technique used in this work and so will be discussed in considerable detail in Section 2.3.

2.2 Static Techniques

2.2.1 High-Temperature X-ray Diffraction

This technique is most often used to obtain information on the crystal structures and the transition temperatures of high-temperature polymorphs. Studies at temperatures greater than 1500 ^{o}C have been reported.[23] The onset of chemical decomposition may give rise to spurious lines however, and this may limit the use of this technique.

2.2.2 Quenching

If high-temperature X-ray diffraction cannot be used it may be possible to quench any high-temperature modification of the specimen to ambient temperature by rapid cooling, and assuming that the sample has not reverted to its most thermodynamically stable state, examine it by conventional X-ray diffraction or by optical microscopy.

In practice, quenching may be achieved by suspending the sample, which is enclosed within a thin-walled container (preferably made of Pt), in the hot-zone of a vertical furnace. When the sample has reached thermal equilibrium it is dropped into liquid coolant (eg Hg) which is below ambient temperature. Some of the liquid may vaporise as the sample enters the liquid and this reduces the efficiency of the process.

High-temperature polymorphs are not generally amenable to quenching but the technique is of assistance in determining liquidus curves which cannot be detected by thermal analysis. If a liquid is quenched complete vitrification may occur, especially with molten sulphates.[24] If a specimen is held at a temperature slightly below the liquidus curve some solid will be present. After quenching, the specimen is examined under plane-polarized light and the solid appears as crystals embedded within a glass matrix.[25-27]

Owing to heat transfer problems, the degree of quenching may not be uniform throughout the specimen and this will limit both the accuracy and the precision of the results.

2.2.3 Hot-Stage Microscopy

Phase reactions such as crystallisation, melting and polymorphic transitions may be directly observed using this technique.[28]

In the apparatus described by Shepherd[29] the sample rests on a window which allows the passage of plane-polarized light. The window is set in a small block which is heated by an internal coil. The block may be flushed with liquid nitrogen, thus quenching the sample, if further examination by X-ray diffraction is required. The block is contained within a water-cooled assembly which prevents heat conduction to the objective lens.

Instruments of this type can be used at temperatures greater than 1000 ^{o}C and tend to be expensive.

A simpler and less expensive device is described by Schultze.[30] It requires only a small amount of sample (1 mg) and this is supported on the junction of a thermocouple, which itself acts as a heater. One half-cycle of ac current is applied to the thermocouple and a measuring circuit is automatically switched in and out during alternating half-cycles. An ordinary microscope is used to examine the sample whilst provision of a second thermocouple allows simultaneous DTA.

The present author has adapted a furnace and microscope to provide low—resolution in situ observations at high temperatures and this apparatus is described in Chapter 3.

2.2.4 Electrical Conductivity

Phase boundaries, such as liquidus and solidus curves and polymorphic transitions, may be detected using this technique.[23] A conductivity cell is constructed by embedding two noble metal wires in the sample. The conductivity is obtained by measuring a voltage drop across a standard resistor placed in series with the cell. The conductivity is determined at several temperatures and at a number of compositions and the phase boundary is indicated by a discontinuity or change in slope of conductivity with temperature.

The phase diagram of the binary system Ag_2SO_4 - Li_2SO_4 was determined by setting the system up as a concentration cell[31]:

$$Ag(s) \mid Li_2SO_4, Ag_2SO_4 \mid Ag_2SO_4 \mid Ag(s)$$
$$S_1 \mid \text{mixture}_2 (T)$$

The cell was placed in a furnace and the emf measured. The diagram obtained displayed features which were not evident on an earlier study made using thermal analysis.

2.2.5 Calorimetric Techniques

The discontinuity in enthalpy on crossing a phase boundary (see Section 1.1) may be directly measured using a calorimeter. The liquidus curves for the systems NaBr - $NaNO_3$ and KBr - KNO_3[32] were determined by measuring the variation of enthalpy of mixing of the molten salts, with temperature and composition. The departure of the mixing function from the quasi-parabolic shape indicates the occurrence of a solid-liquid boundary. Calorimeters are discussed in greater detail in Chapter 4.

2.3 Dynamic Techniques: Differential Thermal Analysis

2.3.1 Historical Development of DTA

Modern DTA evolved from the method of cooling-curves developed by Rudberg (1829) in which a large sample (150 g) is raised to above its melting point and allowed to cool naturally, the temperature being read from a thermometer embedded in the sample. Transitions, such as freezing-points, show up as plateaux or inflexions in the cooling curves (figure 2.1).

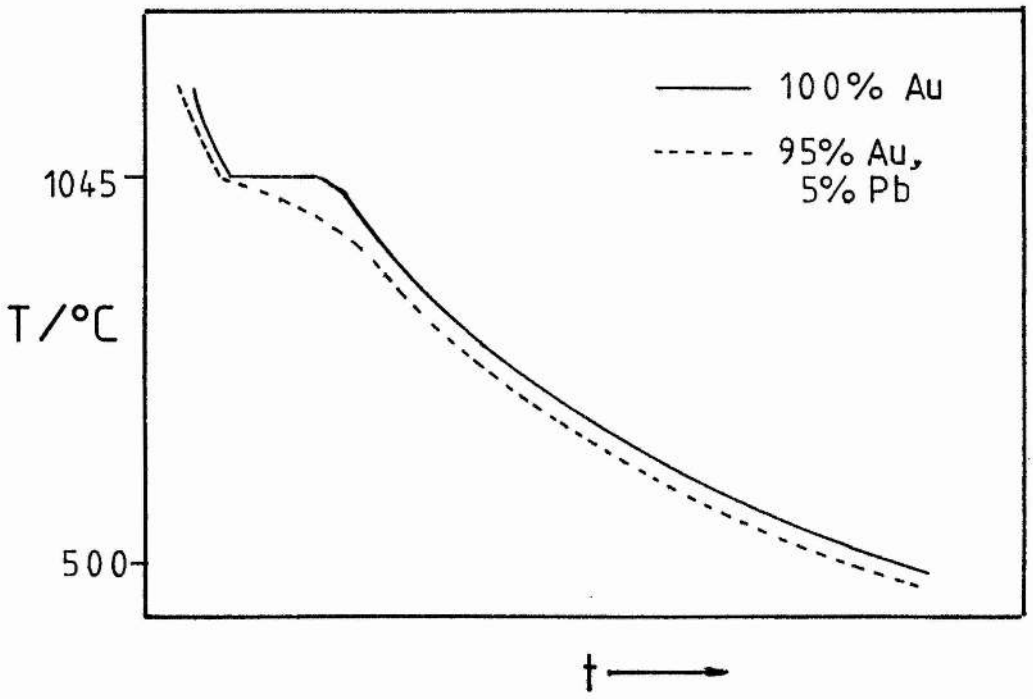

Figure 2.1 Cooling curves for pure Au (———) and Au/Pb alloy (- - - - -).

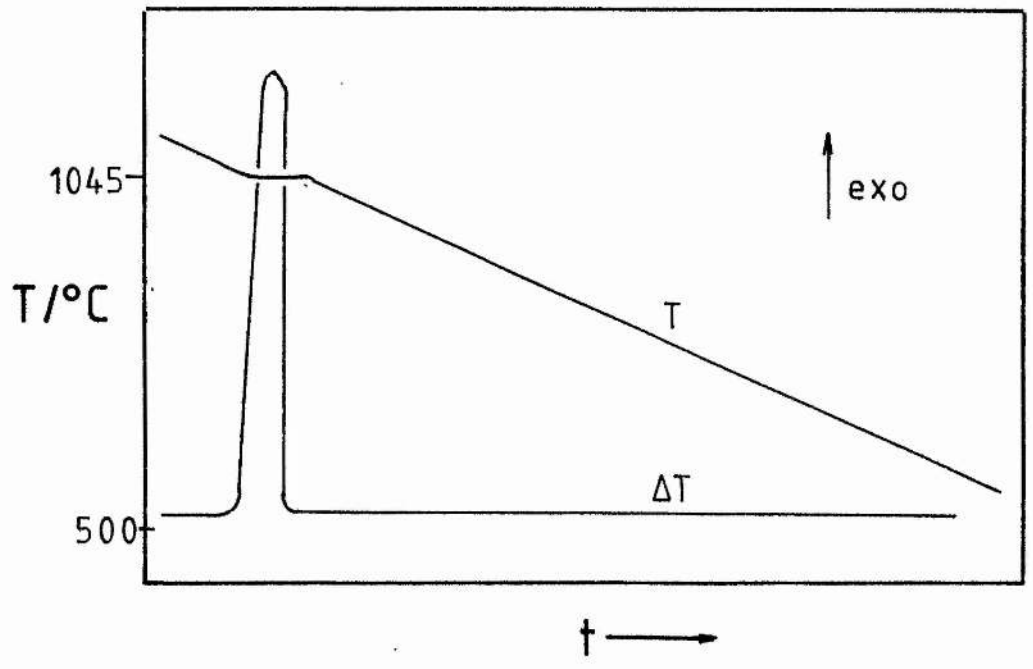

Figure 2.2 DTA curve obtained on cooling pure Gold.

The use of differential thermocouples was first demonstrated at the end of the last century by Roberts-Austen, who used twin Pt/Pt-10%Rh thermocouples, the signals from these being fed into twin galvanometers, so allowing the temperature T, and differential temperature ΔT, to be measured. The principle of the technique is as follows: the sample and an inert reference material are subjected to cooling at the same rate; they are both at the same temperature initially and the thermocouples' emfs are balanced. When the sample undergoes a transition its cooling rate is retarded while that of the reference material remains steady. The thermocouples' emfs are unbalanced and a signal is obtained which is proportional to the difference in temperature and this difference in signal persists until the temperatures of sample and reference are once again equal. The results of a typical DTA experiment are shown in figure 2.2.

The technique has not changed in concept in recent times, but modern instruments are easier to use and allow more accurate and precise results.

The evolution of DTA instrumentation is described by Mackenzie.[33]

2.3.2 DTA Apparatus

Figure 2.3 shows a modern DTA apparatus in schematic form. The sample and reference materials are contained within glass or metal cups which rest in a metal or ceramic holder, this assembly being situated in the hot zone of the furnace. The furnace is controlled by a temperature programmer which heats or cools it at a constant rate. Thermocouples are placed in contact with the cups or the sample itself and their emfs are measured by a device such as a twin-pen chart recorder or a microcomputer.

The apparatus can be considered in terms of five main components and each will be discussed in more detail below.

2.3.2.1 Furnaces

The furnace should provide a region of constant temperature (known as the hot zone) which will accommodate the sample block, reach the desired maximum temperature, and be suitably designed to allow for the desired heating and cooling rates. A resistance furnace, based around a tube of refractory material (silica or alumina), with uniformly spaced wire windings along its length and placed within a thermally and electrically insulated container, is generally the most satisfactory design. The choice of winding will depend on the intended maximum working temperature. For applications below 1100 ^{o}C, Nichrome is most suitable, while to achieve temperatures in the range 1200 - 1400 ^{o}C, Kanthal A may be used. To reach temperatures above

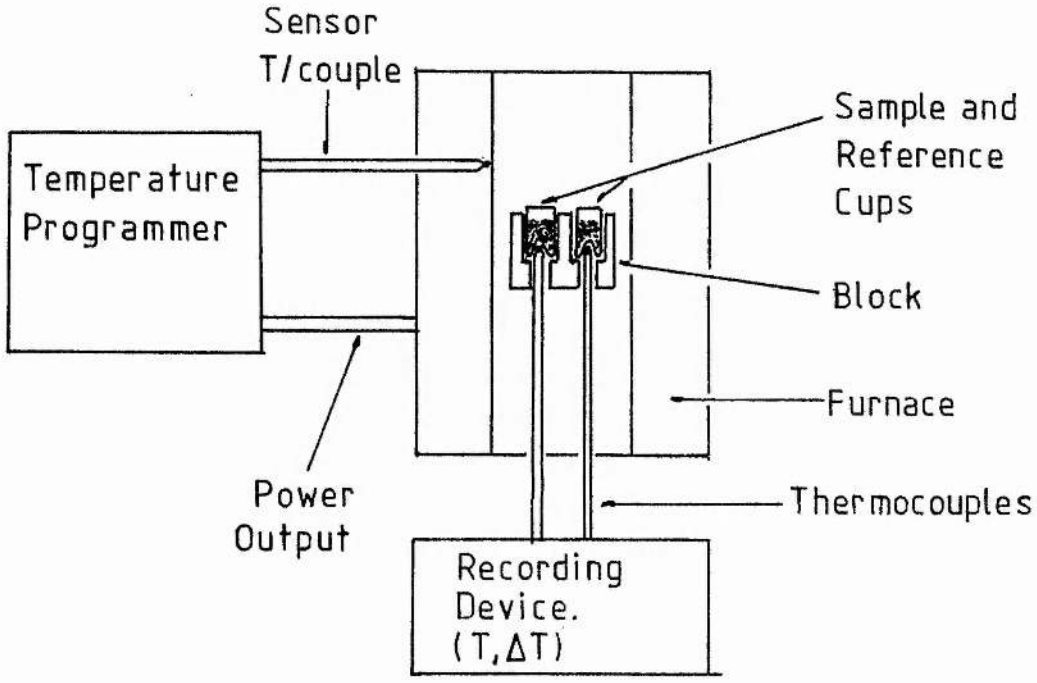

Figure 2.3 Schematic diagram of DTA apparatus.

1500 ^{o}C Pt or Pt-13%Rh windings, although extremely expensive, provide very good reliability and do not necessitate the use of a vacuum or reducing atmosphere. Mo has been claimed to work but this certainly requires a reducing atmosphere.[34]

If a high working temperature is the major consideration then heavy lagging of the furnace will help. Figure 2.4(b) shows the temperature profile of a lagged furnace. An unlagged (or low mass) furnace (figure 2.4(a)) will not reach such a high working temperature but the hot zone is more extensive and the furnace will heat and cool at far greater rates (a lagged furnace may however be force-cooled if faster cooling rates are desired). The unlagged furnace requires a larger amount of current to drive it to high temperatures and this must be borne in mind. The use of radiation shields (figure 2.5) will greatly reduce end-losses and the need for lagging.

An alternative method of achieving both a uniform temperature zone and a high working temperature is to have three separate sets of windings along the furnace tube, each with its own controlled power supply (figure 2.4(c)).

Resistance furnaces in which current is passed through the refractory furnace core itself may also be used to reach higher temperatures, although inert or reducing atmospheres are required. SiC can be operated up to 1600 ^{o}C, while graphite may be used at temperatures in excess of 2500 ^{o}C and is particularly useful in view of its high mechanical strength and low coefficient of resistance.

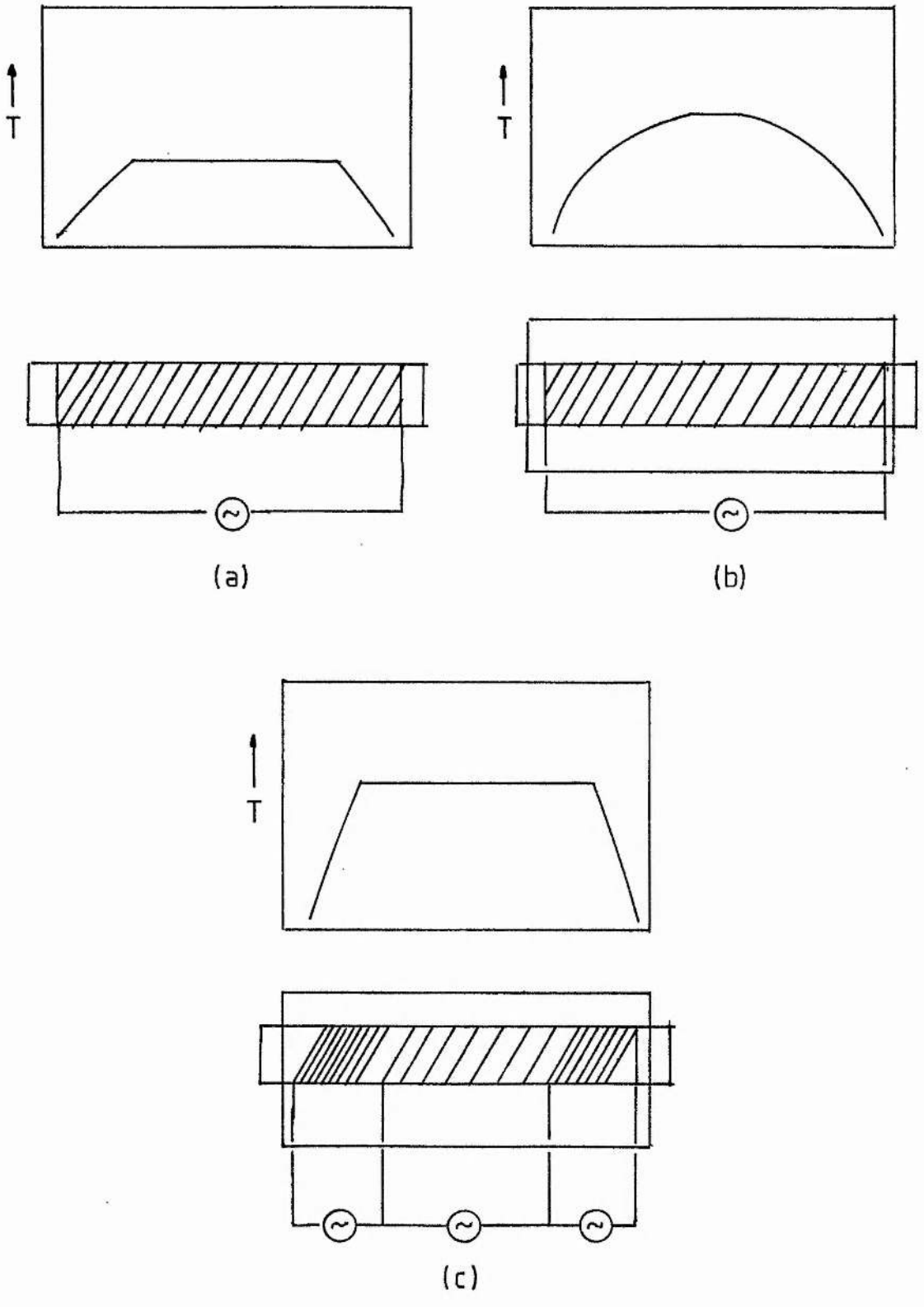

Figure 2.4 Temperature profiles for (a) unlagged furnace (b) lagged furnace (c) 3-phase lagged furnace.

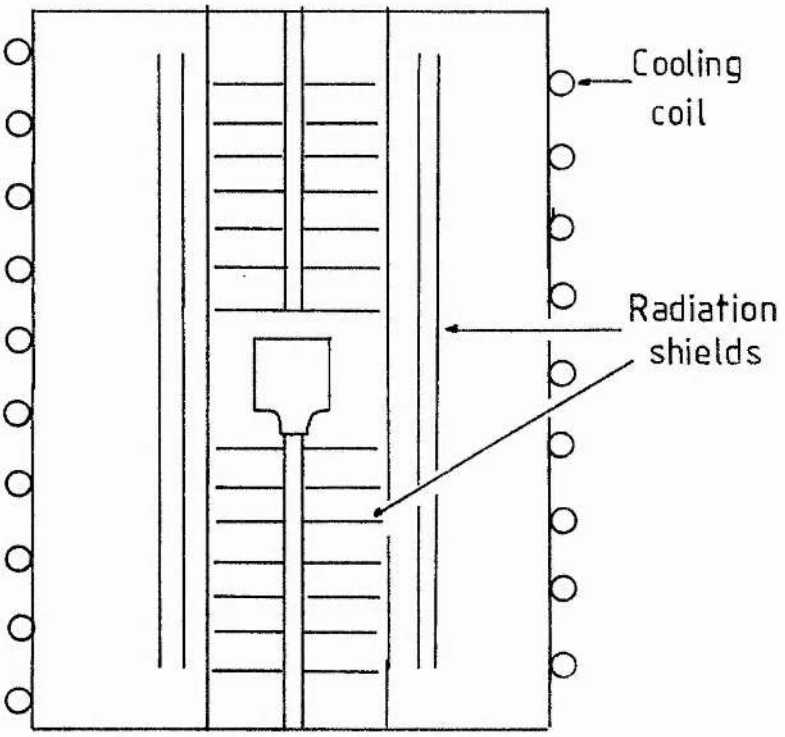

Figure 2.5 DTA furnace with radiation shields and water cooling for advanced performance.

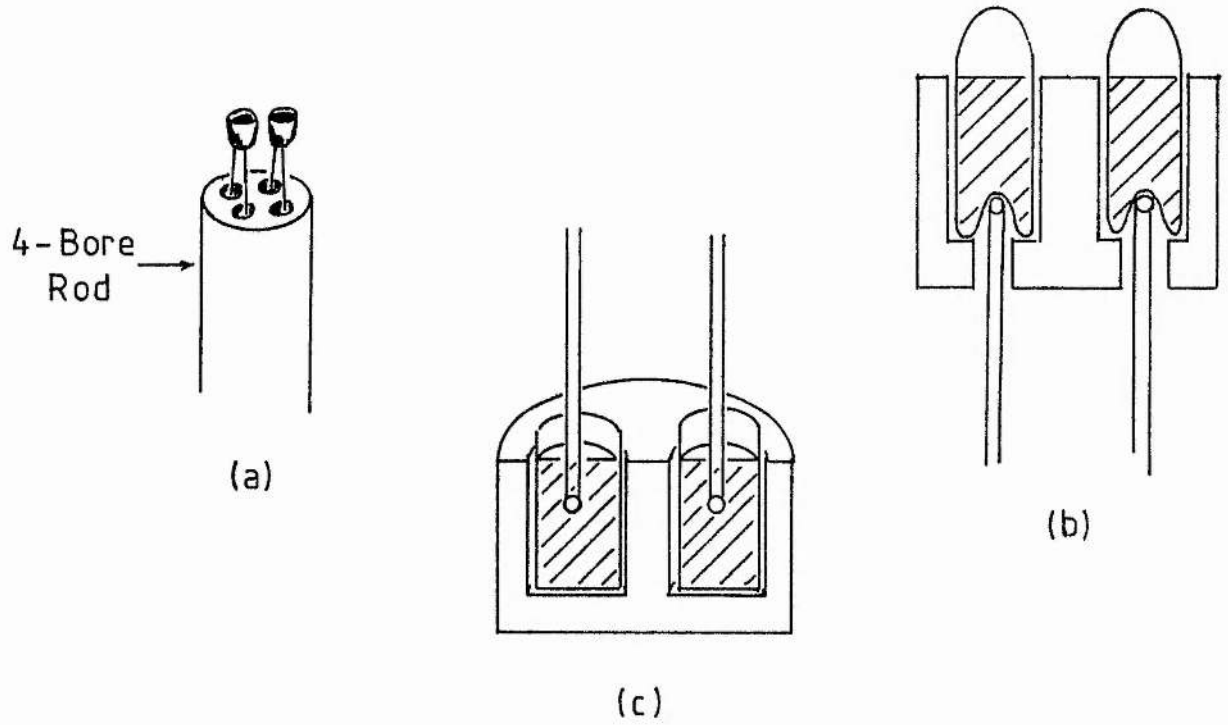

Figure 2.6 Thermocouple/block/sample arrangements.

Resistance furnaces are most conveniently used vertically, since then they provide better temperature homogeneity than horizontal furnaces, although the latter will be less susceptible to convection currents.

In pursuit of convenience and compactness, it has become more common for manufacturers of complete DTA apparatus to provide internally heated sample blocks within an insulated environment. It has been argued however, that these suffer from temperature inhomogeneity.[35]

The body of available literature on all aspects of furnace design is large. There are a number of discussions particularly relevant to DTA apparatus.[34-39]

2.3.2.2 Temperature Programmer/Controller

This unit should fulfil two basic requirements:

1) To provide a good range of linear ramp rates (heating and cooling rates) typically in the range 1 - 20 $K\ min^{-1}$.

2) To provide accurate temperature control (better than $\pm$ 1 K) on both ramps and isothermal control.

The methods of achieving these objectives are described in Chapter 3.

All modern programmers rely on a sensor thermocouple positioned as close as possible to the furnace windings at the hot zone.[35] The programmer compares the output of the sensor thermocouple with an electronically generated voltage, corresponding to the thermocouple emf at the set temperature. The programmer increases or diminishes the power output to the furnace depending upon the magnitude and sign of the difference between the two signals.

NB: The performance of the system is not affected by the ageing of the furnace windings.

2.3.2.3 Sample Block

The mass of sample used in DTA experiments varies from several hundred milligrams to a few micrograms and so the size and shape of the sample block must be chosen accordingly. There are some general factors to be considered however and it is helpful if these are considered with regard to the one-dimensional heat flow equation, which for a homogeneous system is :

$$(d^2T / dx^2) = pc / k(dT / dt) \qquad (2.3.1)$$

where:

x = distance from reference point

p = density of block

c = heat capacity of block

k = thermal conductivity of block

dT / dt = heating rate

The inverse of the proportionality constant, viz k / pc, is given the symbol a and is called the thermal diffusivity of the block. Since equation (2.3.1) applies only to homogeneous systems, then if there are any boundaries in the system, for example between sample and sample cup, there will be a discontinuity and new values of p, c, and k will apply beyond this boundary. Even within a pure substance which undergoes a phase transition, the appearance of new phases generates new boundaries.

In ideal circumstances both the sample and reference materials will be in the same thermal environment and will possess identical thermal properties. The sample and reference materials are contained in cylindrical cups or ampoules which are placed in symmetrically spaced wells within a cylindrical sample block, which is usually no larger than 2 cm in diameter and 2 cm high. The block will have to withstand high temperatures and possibly corrosive or oxidising atmospheres.

Metals such as nickel and stainless steel are commonly used at temperatures of up to 1000 ^{o}C (although an inert atmosphere must also be used) and aluminium is used up to 600 ^{o}C.

The advantages of a metal holder are that it has a high heat capacity with respect to that of the sample and reference materials and heat conductivity is extremely high, consequently heat is rapidly conducted from the surface of the block and this results in good temperature homogeneity and minimal baseline drift. Peaks will be sharp because of the fast rate at which the sample equilibrates after

it has undergone a transition. This does however tend to result in a loss of sensitivity.

Metal blocks are easily machined and can be fabricated rapidly and cheaply to adapt to changing requirements.

Ceramic materials such as sintered alumina, boron nitride and silica may be successfully used at temperatures above 1000 ^{o}C where the use of noble metals is prohibitively expensive. These materials have lower thermal conductivity than metals and give larger, broader peaks with greater baseline drift. They possess a greater emissivity than metals and so heat transfer to the ceramic block is more efficient at moderate to high temperatures (> 500 ^{o}C) where heat transfer occurs by radiation.

Ceramic or glass blocks can be used in corrosive atmospheres such as SO_3 and Cl_2[40] but are difficult to machine, although pyrophyllite (which has been available for some time) and the newer glass ceramics such as "Macor" (manufactured by Corning) may be used.

The sample is usually held in cups that fit snugly into the block cavities. Pt-Rh is particularly suitable for use at high temperatures as it can be made with a thin wall and is resistant to a wide range of melts and corrosive atmospheres. In cases where chemical decomposition or convection currents are a problem then lids should be fitted; alternatively quartz containers could be used. These are readily sealed, have good resistance to corrosive melts and atmospheres and are disposable.

Where sensitivity (peak size) is of prime importance then the sample block may be discarded and the sample and reference materials supported on the thermocouples themselves.[41]

2.3.2.4 Thermocouples

Chromel-Alumel thermocouples are the most widely used base-metal system in DTA. Their main attributes are a high sensitivity (4.0×10^{-2} mV K^{-1}, 20 - 1000 ^{o}C) which is linear with temperature, and they are inexpensive. However, they become unstable if used at high temperatures over long periods of time and they require periodic recalibration; they are also susceptible to oxidation.

At temperatures in the range 1000 - 1600 ^{o}C, Pt Ptx%Rh thermocouples are almost always used, where x is in the range 10 to 15. They are stable over long periods of time and are resistant to oxidising atmospheres. They are less sensitive than base-metal thermocouples (5.6×10^{-3}mV K^{-1} at 20 ^{o}C, 1.2×10^{-2}mV K^{-1},500 - 1000 ^{o}C), are non-linear at temperatures between ambient and 500 ^{o}C but are very expensive.

The thickness of the thermocouple wire is critical, particularly if the wires are immersed in the sample, as this constitutes a heat leak and may reduce peak size. If the wire is too thin, the strain induced in the junction through constant use will affect both the emf and the working life of the thermocouple. Wire of diameter 0.25 mm is

a suitable compromise.

The practice of using the thermocouples themselves to hold microgram quantities of the sample (see figure 2.6(a)) can be self - defeating. The gain in sensitivity obtained by discarding the sample block may be nullified by the large heat leak of the thermocouple itself, this quite apart from the fact that such a small sample may not be representative of the parent material. This arrangement is therefore not recommended except in cases where only small quantities of material are available for analysis.[42]

The placement of the thermocouples with respect to both the sample or reference and to each other is critical. Both thermocouple junctions should be located on the central axis of the sample/reference and preferably at the centre of the specimen itself. This will minimise baseline drift and peak asymmetry. It is important that the location of the thermocouples is reproducible from experiment to experiment and it is the present author's opinion that the arrangement shown in figure 2.6(b) is preferable in this respect to that shown in figure 2.6(c), where the flexible nature of the thermocouples makes it more difficult to reproduce the centring accurately.

2.3.2.5 Temperature Measurement

The device used for this purpose is a twin-pen strip chart recorder, allowing both the T and ΔT signals to be displayed in convenient form. The sensitivity of modern chart recorders is generally greater than 10 mV fsd (full scale deflection), so that base-metal thermocouples can be directly connected to such devices. The use of noble-metal thermocouples requires a resolution of a few microvolts in order to detect small transitions, and so additional dc amplification is needed.

With the recent developments in semi-conductor technology and the consequent availability of powerful micro-processors and low cost semi-conductor memory, the trend for manufacturers of complete DTA systems (such as Stanton Redcroft Ltd and the Du Pont Corporation) is to provide digital processing of signals. There are numerous advantages in this: computation of peak areas, deconvolution of complex peak envelopes, storage of data on floppy disks which allows the creation of a data base to provide classification and identification of materials. These are all functions which may be performed by the system itself or by existing mini or mainframe computing facilities interfaced to it.[48]

2.3.3 Scope of DTA

The use of DTA in the present thesis has been limited to phase diagram studies, as described in the next Chapter. However, this technique finds applications in a number of fields including studies on cements, ceramics, glasses, soils, explosives, catalysts, textiles, lipids, and increasingly, polymers. A more exhaustive discussion of these topics may be found in Mackenzie.[43]

In complex materials the phase transitions are used to identify individual components and to categorise the chemical reactions which occur in the course of decomposition. Quantitative DTA techniques have been developed to obtain kinetic data on chemical reactions[44-46] and to obtain calorimetric data.[47] These applications require careful calibration of the apparatus and even then the accuracy obtained may be less than that from a more specialised technique.

DTA may therefore be considered as a good general purpose technique for the investigation of thermal phenomena. It is particularly suited to work of an exploratory nature where accuracy and precision are not of prime importance. The use of DTA is enhanced if performed simultaneously with other thermoanalytical techniques such as Thermogravimetric Analysis (TGA) (which is particularly useful in obtaining kinetic data[49]), Evolved Gas Analysis (EGA),[50] and Thermal Conductivity.[51]

It is important to remember when comparing several sets of DTA results drawn from different laboratories, that there will be differences in experimental parameters, both in apparatus design and sample. ICTA recommend that these parameters be reported so that discrepancies between results may be accounted for.[52]

2.3.4 DTA and Phase Diagrams

2.3.4.1 Introduction

On crossing a phase boundary the heat evolved or absorbed can generally be detected by DTA and the use of this technique in phase studies is described by Gutt and Majumdar.[53] The following discussion on DTA and phase studies is limited to binary systems at constant pressure, but it should be said that DTA is perhaps the most widely used technique in high pressure - high temperature phase studies.[54,55]

In practice, a phase diagram is determined by making mixtures of the two components A and B at some twenty to thirty compositions and performing DTA on each mixture. The transition temperatures from each analysis are plotted against composition and so a T-x diagram is created. A pattern of curves and horizontal lines should be obvious, but usually other details arising from the analysis, such as peak heights and shape, have to be considered and auxiliary techniques such

as X-ray diffraction may also be required.

The relationship between DTA results and the features found in the phase diagrams, when ideal conditions apply, is explained below for the hypothetical phase diagram shown in figure 2.7(a). The system A-B features a congruent melting compound AB, which has limited solubility in A but is completely insoluble in B. Component B has a high—temperature polymorph, B(II). Figure 2.7(b) shows the peak transitions obtained on heating the system at six compositions or isopleths.

The correct method of determining the transition temperature from a DTA curve is a matter of some debate.[53] The onset of a phase change may not be easily pinpointed and so the sample temperature at the maximum of the ΔT signal is generally selected. The occurrence of a reversible transition should ideally be indicated by a plateau in the sample temperature. The present author has observed that the peak of the ΔT signal occurs after the plateau has been passed. Thus, the peak temperature does not correspond to any particular event during the transition but it is recognised as providing greater reproducibility than the onset.

On heating along isopleth 1 (figure 2.7(b)) the first transition encountered, 1(a), is that due to crossing from a two-phase region, α + AB(s), into a homogeneous solid solution, α. The peak is broad and of low intensity. Transition (b) is broad because the phase reaction, $\alpha \rightarrow$ l, involves the absorption of heat as melting takes place, this being gradual initially but increasing at higher

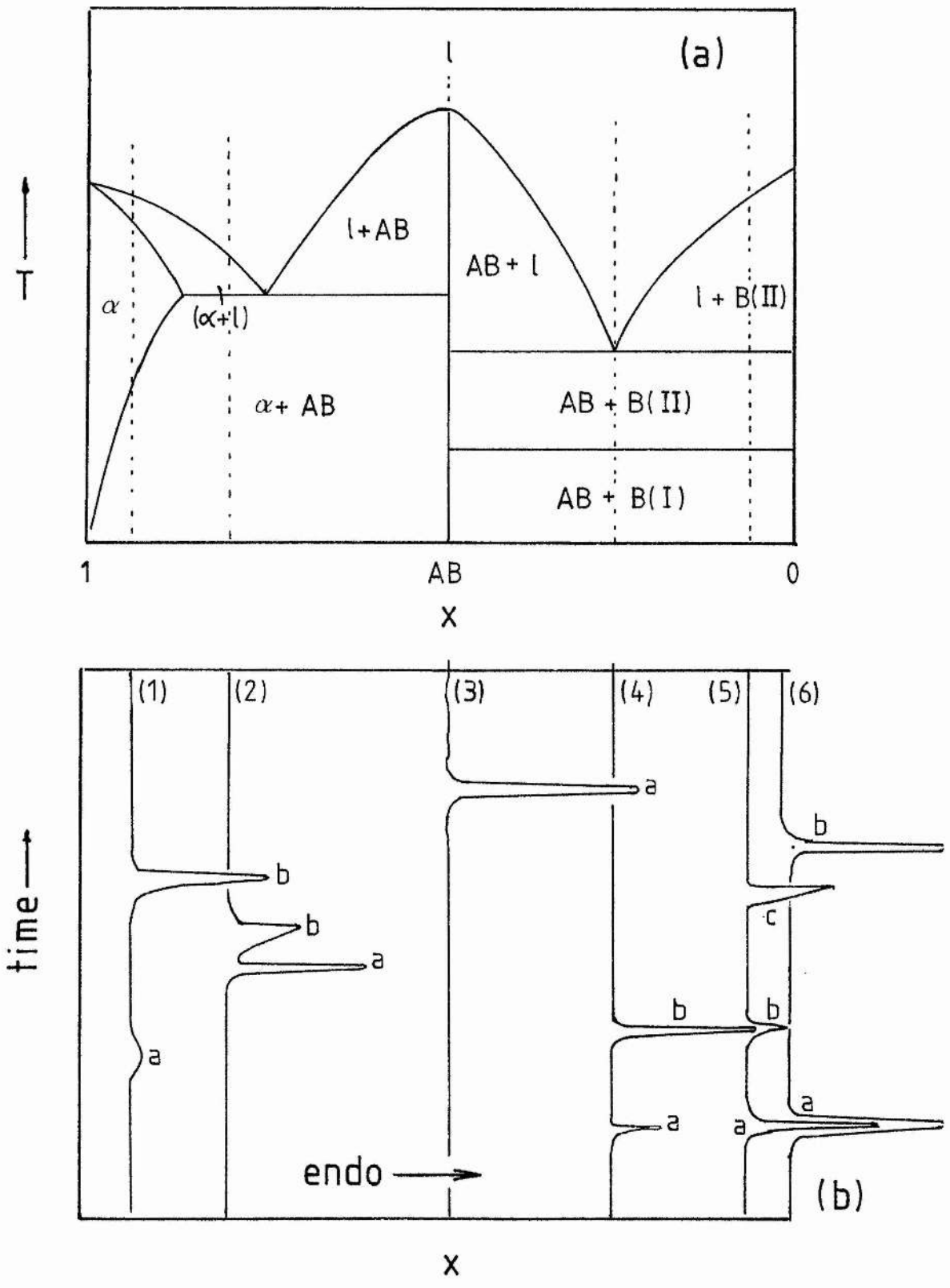

Figure 2.7 The relationship between binary phase diagram (a) and DTA heating curves obtained for 6 compositions (b).

temperatures as more liquid is formed. The size of the peak is dependent on the magnitude of $\Delta_{fus}H_A^*$. The asymmetry of the peak is due to a rapid return to baseline after the last trace of α has melted and this occurs at a rate limited by the thermal diffusivity of the liquid phase; this is also the case for transitions 2(b) and 5(c). The eutectic transitions 2(a), 4(b) and 5(b) are sharp because complete melting takes place within a very narrow temperature range, and the peak size will increase in magnitude as the eutectic composition is approached. The congruent melting of AB occurs at a temperature greater than that of other compositions in the vicinity. The ΔT peak is sharp, as would be expected for a pure compound. The polymorphic transition B(I)$\longrightarrow$ B(II) is represented by peaks 4(a), 5(a) and 6(a), which increase in magnitude as component B becomes more concentrated. Isopleth 6 portrays the DTA curve for pure component B.

The situation described above is idealised and many factors combine to cause deviation from the ideal. The fact that conditions, such as thermal diffusivities, are different after a transition from those immediately preceding it means that the ΔT peak is unlikely to be symmetrical.

Kinetics of phase transitions have a marked effect on the shape and position of ΔT peaks. Thermal hysteresis is the term used to describe the deviation of the observed transition temperature from the true equilibrium value, which takes place on both heating and cooling, due to heating or supercooling respectively. Hysteresis arises from the need to drive the process at a measurable rate.[56] The present

author has noted that superheating occurs to a lesser degree than supercooling, the former being a few K, the latter sometimes exceeding 50 K. Decreasing ramp rates will reduce the degree of hysteresis but in many cases these would have to be less than 1 K min^{-1} to have any effect and this would result in very low peak intensity.

2.3.4.2 Ramp Rates

As already indicated, ramp rates have a considerable effect on the appearance of DTA peaks and this phenomenon will now be described using the one-dimensional heat flow equation (2.3.1) to illustrate the effect on heating.

A temperature gradient will be present in a specimen which is being heated; the centre of the sample, where the thermocouple junction is located, will be at a lower temperature than any other part of the sample. A phase boundary at transition temperature T_t will travel through the sample as it undergoes a phase change and will be retarded due to absorption of heat as it does so. The reference material will not offer such resistance to heat flow.

In the case of a low heating rate the time delay in the transition front reaching the sample thermocouple will be small, relative to the rate of diffusion of heat. Consequently, the differential temperature will also be small, but because the heating rate is low the peak is broad relative to its height. With a fast heating rate, a large temperature differential will rapidly build up

and dissipate as the reaction front reaches the sample thermocouple. A low heating rate (< 1 K min^{-1}) will be used if equilibrium temperature values are desired, but only where the peak is of sufficiently high magnitude. Fast heating rates (> 10 K min^{-1}) are used to gain sensitivity but superheating may occur, baseline drift will be exaggerated and there will be poor resolution of adjacent transitions.

The above comments apply equally to cooling rates but it should be noted that supercooling will be exacerbated by faster cooling rates. Ramp rates of 4 - 6 K min^{-1} are generally of most use in practice.

2.3.4.3 Sample parameters

The size, shape, packing, and previous history of the sample will affect the shape of the DTA peak in many ways.[57] In a tightly packed sample there is increased contact area between the particles and gas voids are eliminated, thus increasing effective thermal diffusivity. This has the effect of sharpening the peaks during transitions (although there is some loss of sensitivity) but decomposition reactions may be hindered if gaseous products are unable to diffuse rapidly away from the reaction interface, thus broadening peaks.

Particle size is a difficult parameter to generalise upon, since several effects may be superimposed, so complicating the picture. Reducing the particle size results in tighter packing with the consequences listed above. The larger effective surface area will speed up certain types of decomposition reaction, though phase transitions are not generally affected.

The physical size of the sample will also affect the shape of the DTA peak. A large sample will increase sensitivity but will also broaden the peak considerably, while a sample of low mass (< 200 mg) in a thin container will give sharper peaks and more accurate transition temperatures.

The previous history of the sample is an important factor to be considered when analysing DTA results. Peaks may sharpen up and change position after several heating/cooling cycles due to homogenisation, crystallisation (or devitrification) and sintering effects.

It is common practice when performing quantitative DTA to dilute the sample with an inert material of similar thermal diffusivity. An unknown enthalpy of transition for a sample may be determined by comparison to a standard material with a transition of precisely known ΔH and which occurs at a similar temperature. The sample is diluted until the two peaks have similar shapes and areas and this will allow a better comparison to be made.

2.3.4.4 Other Factors

If a reference material is used it should have a thermal diffusivity similar to that of the sample, be chemically inert and undergo no phase transitions in the temperature range of interest. Metal oxides are commonly used for this purpose, eg alumina, which may be used up to temperatures of 1200 ^{o}C. In certain cases it may be convenient to dispense with reference materials and this will be discussed in Chapter 3.

The nature of the atmosphere in contact with the sample may be an important consideration if chemical decomposition occurs and this is discussed further in Chapter 3. Otherwise it is customary to have a stationary atmosphere of air, or a flow of some inert gas such as nitrogen or helium if there is a possibility of oxidation of the sample, holder or thermocouples.

By adopting standard procedures the reproducibility between experiments done on one particular instrument should be excellent: peak temperatures should be precise to within 2 K for transitions and for certain types of work it is possible, with careful calibration of the thermocouples, to achieve an accuracy of 0.1 - 0.5 K. This may however be negated by the interference of kinetic effects.

2.3.5 DTA Literature

Details on many aspects of DTA are to be found in the books by Garn[35], Mackenzie[58] and others.[59,60] There are concise reviews by Pistorius,[61] Wunderlich,[62] and Wendlandt[63,64] (which is published bi-annually). Additionally there are two journals devoted to all aspects of thermal analysis: The Journal of Thermal Analysis and Thermochimica Acta.

2.3.6 Differential Scanning Calorimetry (DSC)

This technique evolved from DTA and made its first appearance as a commercial instrument (manufactured by the Perkin-Elmer corporation) in 1964.

Disposable aluminium containers holding up to 100 mg of the sample and reference materials are placed in steel cups, each equipped with a small heater and temperature sensor. A signal proportional to the desired temperature is sent by a temperature programmer to the average temperature amplifier which in turn provides power to the sample and reference cups, thus heating or cooling them at a constant rate. When a phase transition occurs the differential temperature amplifier senses the temperature imbalance between the two holders and transfers energy to the cooler of the two and so minimises the temperature difference. The differential temperature amplifier also feeds the difference signal to a chart recorder; this signal is recorded as function of time and hence of temperature. The transition

is recorded as a peak whose area is directly proportional to the enthalpy of transition and may be measured using a planimeter or electronic integrator. The instrument is calibrated using standard compounds whose enthalpies of fusion are accurately known, eg indium, lead, or benzoic acid.

The technique is capable of obtaining accurate transition enthalpies at temperatures up to 600 ^{o}C, using small amounts of sample[65,66] and may be used to generate thermodynamic data from heat capacity measurements,[67] but the accuracy must be considered inferior to that which can be achieved by so-called classical calorimetric techniques.

3 ORIGINAL INVESTIGATIONS - PHASE DIAGRAMS OF BINARY METAL SULPHATE SYSTEMS

3.1 Experimental

This section describes and contrasts two techniques used for suppressing the decomposition of metal sulphate salts. The apparatus used in the high-temperature phase studies presented in Sections 3.2 and 3.3 is also described in detail.

3.1.1 Suppression of Decomposition

In the investigation of the phase diagram of any system it is essential that the number of components remains constant. If,for example, the number of components were to be increased by chemical decomposition then the results would not be valid. Since most metal sulphates decompose at temperatures above 600 ^{o}C, the phase diagrams of many systems involving sulphates are incomplete at higher temperatures[68,69] and because of decomposition important features such as high-temperature polymorphic transitions may be masked. To avoid this problem, conventional DTA methods, which employ open sample cups in an inert atmosphere, require modification and this may be done in two ways as follows.

3.1.1.1 The Method of Dewing and Richardson[70]

Assume that decomposition of a metal sulphate, MSO_4, proceeds as follows:

$$MSO_4(s) \rightleftharpoons MO(s) + SO_3(g) \qquad (3.1.1)$$

Therefore applying an atmosphere of $SO_3(g)$ around the sample will cause decomposition to be suppressed. In practice this is achieved by passing mixtures of SO_2 and O_2 gases through a ceramic tube in the centre of which is placed a spiral of Pt foil which catalyses the rate of attainment of equilibrium:

$$SO_2(g) + 1/2\ O_2(g) \rightleftharpoons SO_3(g) \qquad (3.1.2)$$

The sample is contained in an open cup using a differential thermocouple arrangement similar to that shown in figure 3.1 which was used by the present author in a previous investigation.[26] The sample is then heated at a constant rate and decomposition will be suppressed until the equilibrium decomposition pressure of the substance exceeds the pressure of the applied atmosphere.

This technique suffers from the disadvantage of requiring much of the apparatus to be constructed from materials which are resistant to constant exposure to highly corrosive gases. This difficulty is increased if a pressure greater than atmospheric pressure is required.

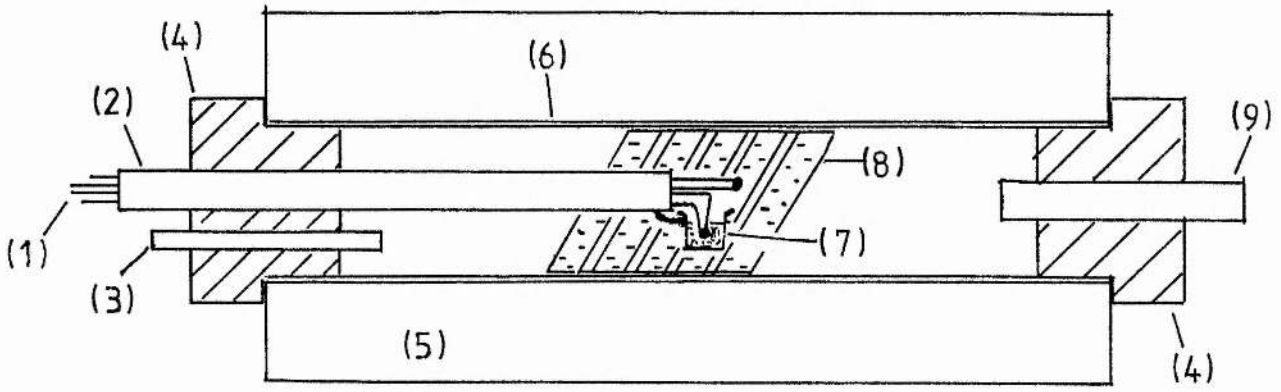

Figure 3.1 DTA apparatus with provision for flowing gas. (1) differential thermocouple, (2) 4-bore silica rod, (3) gas outlet, (4) PTFE inserts, (5) furnace insulation, (6) furnace windings, (7) Pt cup and sample, (8) Pt foil spiral, (9) gas inlet.

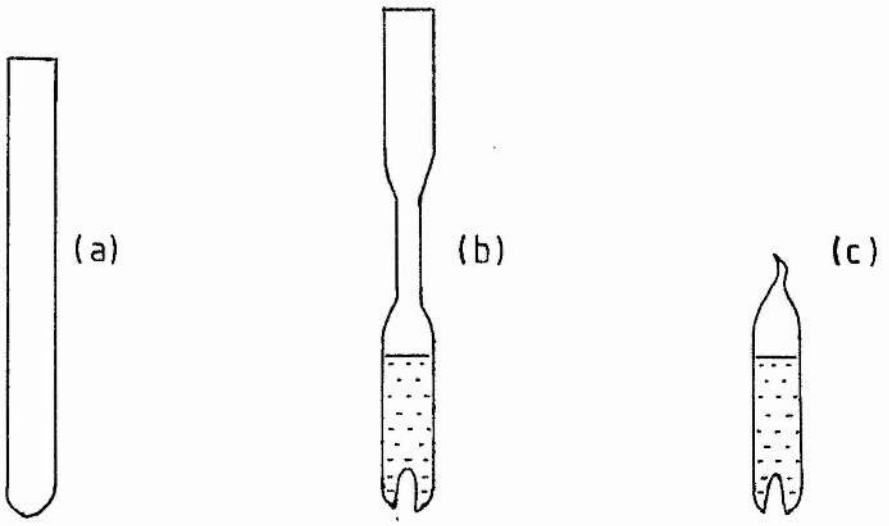

Figure 3.2 Stages in preparing a sealed ampoule. (a) basic tube after cutting to length and sealing, (b) tube packed with sample prior to mounting on vacuum line and (c) the finished sealed ampoule.

3.1.1.2 Sealed Ampoule Technique[71,72]

This method of suppressing decomposition was first employed in 1935[73] and consists of sealing the sample in a container made of quartz, stainless steel, gold, or platinum.[53] If the capsule is of small volume (< 0.1 cm^3) then decomposition of only a negligible amount of sample (< 1 mole %) will be required to set up the equilibrium decomposition pressure; this will be particularly true in the case of compounds such as Ag_2SO_4, $La_2(SO_4)_3$ and $CdSO_4$ (the components of the phase diagrams described in this Chapter) where the decomposition pressures are less than 0.1 atm at 950 °C.[74]

The fact that pressure is not constant throughout the course of the sealed ampoule DTA may seem to invalidate the application of the phase rule. However, the effect of pressure upon the temperature at which a phase change takes place, dp / dT, is given by the Clapeyron equation:

$$dp / dT = \Delta H_t / T_t \Delta V_t \qquad (3.1.3)$$

where ΔH_t and ΔV_t are the changes of enthalpy and volume respectively, on undergoing a transition at temperature T_t. It may be seen that dT / dp will be of low magnitude due to ΔH_t being very large in comparison to ΔV_t which will be small for solid-solid and solid-liquid phase reactions. In the case of K_2SO_4 for example, the variation of transition temperature (between hexagonal and orthorhombic forms) with pressure is 0.0184 K bar^{-1}, which in DTA terms is negligible.[75]

Other applications of this technique as applied to metal sulphates are in the decomposition of hydrates[76,77] and in high-temperature phase studies of $CaSO_4$.[78]

The advantages of this method are that it can be conveniently used with a standard DTA apparatus and that pressures > 1 atm of gas can be generated within the ampoule. Having the thermocouples in contact with the ampoule wall, rather than in direct contact with the sample itself, reduces sensitivity however.

A comparison between the two suppression techniques was made on pure compounds obtained from identical sources ($BeSO_4$ and $ZnSO_4$). Both compounds undergo polymorphic transitions at temperatures where decomposition is already noticeable.

Table 3.1 gives both sets of results. Those for the flowing gas method are taken from previous work by Gimzewski et al.[26,79] In each case the powders were given similar treatment before investigation; the thermocouples were calibrated using the same compounds and ramp rates of 5 - 6 K min^{-1} were used in both instances.

The results in table 3.1 show that in nearly all cases the transition temperatures differ by less than 4 K. When the various factors involved in performing DTA on two different sets of apparatus are taken into account, this indicates very good agreement between the two methods.

Table 3.1

Comparison of Suppression Techniques

Transition	Transition Temperature/°C	
	Sealed Ampoule Technique	Dewing and Richardson Technique
$ZnSO_4$ (h)	749 ± 3	751 ± 1
($\alpha \rightarrow \beta$) (c)	727 ± 2*	730.5 ± 1*
$BeSO_4$ (h)	606 ± 2.5	609 ± 2
($\alpha \rightarrow \beta$) (c)	586 ± 4	587 ± 2
$BeSO_4$ (h)	644 ± 1.2	646 ± 1
($\beta \rightarrow \gamma$) (c)	640 ± 1,632 ± 2	640 ± 2,636 ± 2

(h) refers to heating cycles and (c) refers to cooling cycles.

All temperatures recorded are peak temperatures (ΔT signal), except those marked *, which are the plateaux in the T signal.

NOTE: The $BeSO_4$ $\beta \rightarrow \gamma$ transition splits into two peaks, on cooling at 6 K min^{-1}.

3.1.1.3 Preparation of Sealed Ampoules

Ampoules are made as shown in figure 3.2. Quartz tubing 6.5 mm od and wall thickness 1 mm, is the starting material. This is cleaned by immersion in chromic acid followed by rinsing with copious amounts of distilled water. The tubing is dried in an oven at 120 ^{o}C before glassblowing. The tube is sealed at one end and the thermocouple recess (3-4 mm deep) is made by poking with a cold tungsten rod. A neck is made by heating, and pulling the tube gives the container shown in figure 3.2(b).

A sleeve of aluminium foil is inserted into the container and the sample is introduced through a funnel. The container is tapped to dislodge any sample trapped in the neck of the tube.

The quartz container may now be mounted on the vacuum line using a Quickfit ST52 screw-thread adaptor which uses a silicone ring and PTFE washer to give a vacuum-tight seal. The vacuum line is then pumped down, by oil pump, to a pressure of 0.01 torr. Any pre-treatment which the sample requires is carried out at this stage.

The quartz ampoule is sealed by applying a gas-oxygen flame to the narrow neck and pulling off. During this last operation, which takes approximately 3-4 s, a large pair of pliers is held round the sample and these act as a heat-sink and so the sample never gets hot.

3.1.2 DTA Apparatus

The DTA apparatus used to determine the phase diagrams presented in this Chapter is shown in schematic form in figure 3.3, and this will again be discussed in terms of five components, as in Chapter 2.

3.1.2.1 Furnace

The vertical furnace used is of commercial design (Stanton-Redcroft), and is of the straight-wound tubular resistance type, having a ceramic core wound with nichrome wire. The sensor thermocouple (Pt/Pt-13%Rh) is sited in the gap between the inner furnace wall and a mullite work tube which is in contact with the thermocouple hot junction. The wires of the sensor thermocouple are connected to a terminal block which serves as an ambient junction and this is held away from the furnace body by an extension piece thus maintaining the junction at ambient temperature.

To facilitate changing of the sample the furnace (held on a frame) is raised and lowered relative to the sample holder which is attached to the base plate of the furnace frame. The bottom of the furnace is plugged with a split sindanio insert, while a hollow ceramic plug filled with alumina powder is inserted in the top of the furnace to cut down on heat loss. An aluminium shield on the bottom of the furnace prevents radiation from reaching the cold junction of the differential thermocouple.

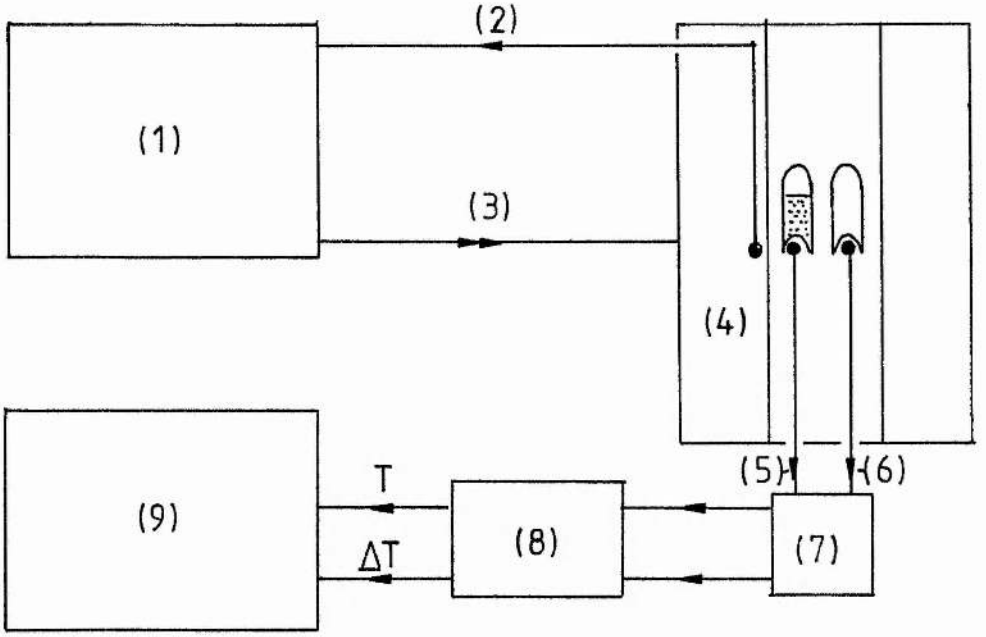

Figure 3.3 Sealed ampoule DTA apparatus (schematic).

(1) temperature programmer, (2) sensor thermocouple ,(3) regulated power to furnace, (4) furnace, (5) sample thermocouple, (6) reference thermocouple, (7) ice-bath cold junction, (8) dc amplifier, (9) twin-pen chart recorder.

—→ represents flow of data, ⇒ represents flow of power.

(1) 802KB temperature programmer.
(2) 802KB keyboard input unit.
(3) 407 three-term temp. controller.
(4) 505 thyristor power switch.
(5) furnace.

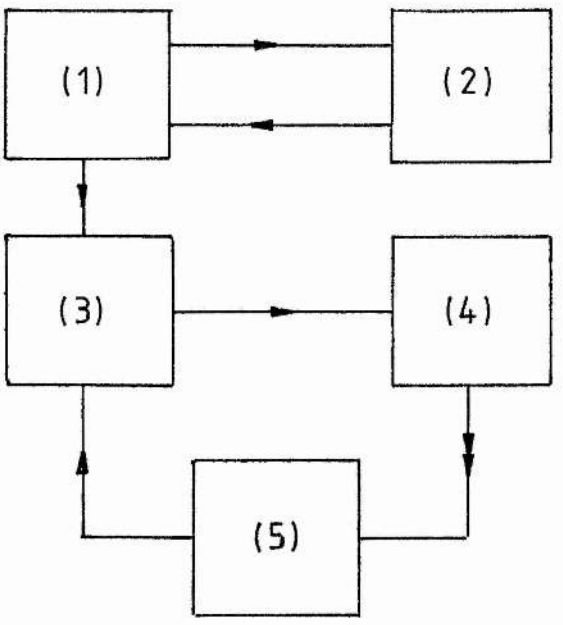

Figure 3.4 CRL temperature programming/controller system (schematic).

The hot zone of this furnace was located by moving a thermocouple along the axis and was found to be 2 cm long with a temperature uniformity of $\pm$ 1.5 K at temperatures between 710 ^{o}C and 910 ^{o}C. The maximum operating temperature of the furnace is 1100 ^{o}C.

3.1.2.2 Temperature Programmers

Two commercial temperature programmers were used in the course of this work: a Stanton-Redcroft LVP/cc20/R/250 Mark 3 variable rate linear temperature programmer and a Control and Readout LTD (CRL) 802KB/407/505 temperature programming system. Although the latter is a sophisticated and versatile unit, the basic means of achieving temperature control are the same for both programmers.

To obtain isothermal temperature control from the furnace, the signal from the sensor thermocouple is compared to a signal synthesised by the programmer; eg, if the furnace temperature setting is 548 ^{o}C then, for a programmer using a Pt/Pt-13%Rh sensor thermocouple, a signal of 5.00 mV is electronically generated by the controller. The difference between this value and the signal from the sensor thermocouple provides a so-called error signal or offset, and the power output to the furnace is increased or diminished in order to minimise the error signal. This form of control is known as Proportional control and the temperature range about the set point in which this operates is called the Proportional Band. Furnace characteristics vary with temperature and so to obtain optimum results

at any given temperature will require a particular setting of the proportional band otherwise the temperature will cycle about the set point. Temperature control is further increased by introducing additional control terms. Short term oscillation is detected by taking the derivative of the error signal, while longer term cycling is taken into account by examining the integral of the error signal.

Temperature controllers which operate by optimising on these three parameters are known as three-term or PID (Proportional-Integral-Derivative) controllers. These terms must be adjusted to provide good temperature control at all temperatures over which the furnace is to be used and they must be readjusted when a different furnace is used.

In both programmers, power output is by phase-angle firing where portions of the ac voltage are fed to the furnace windings and this is achieved by use of a thyristor with a fast response. Both units may deliver up to 25 A at 220 V when connected to a high current mains supply (output currents of up to 10 A may be obtained from the normal 13 A supply) and will do so even with difficult furnace windings such as Kanthal or platinum, whose resistance varies markedly with temperature. They will also provide isothermal control to within better than $\pm$ 0.5 K of the set point.

The means by which temperature programming (or ramping) are achieved are quite different for both programmers, as are the facilities offered.

The Stanton-Redcroft programmer is an integral unit which provides continuously variable ramp rates in the range 1 - 20 K min^{-1}. Programming is achieved by use of a motorised linearised potentiometer to provide the synthetic thermocouple emf. On heating ramps, programming will continue until a pre-set temperature is reached, at which point the furnace is held indefinitely (switching to the cooling programme has to be done manually). The temperature of the furnace is read from a dial on the front of the unit.

This programmer, while providing good isothermal control and linear ramp rates, cannot easily be adapted to provide multiple-cycle temperature programmes and the PID terms are not easily adjusted.

The CRL system is split into three components and was chosen to provide convenience and versatility which would allow for easy adaptation to future applications. The system is depicted in figure 3.4.

The 802 KB digital electronic keyboard programmer is itself split into two units. The temperature programmer consists of fifteen segments and each segment has a ramp and an isotherm or "hold" level. Ramp rates between 1 K h^{-1} and 999 K min^{-1} are theoretically possible in virtually continuously variable fashion. Hold levels can be set in increments of 1 K with dwell lines between 1 s and 999 h. The facility to activate up to 4 relays at the end of any given ramp or isotherm is available, although it is not present on the unit used in this work.

Programmes are entered segment-by-segment using a membrane-type keyboard. An LED display gives the current segment status and the user is prompted to enter the appropriate data, stepping through the sequence of ramp, hold level and dwell time. The user may use as many segments as necessary and programmes of up to 150 segments are possible by chaining together smaller programmes. A typical programme is shown in figure 3.5.

The keyboard unit can store 10 programmes indefinitely in its alterable memory while power is applied, and for up to 6 months while power is down. Up to 10 programmes may also be stored on permanent memory modules using a standard EPROM, the entire contents of which can be completely erased using UV light, for further use.

The second part of the 802 KB is the programming unit to which the keyboard unit passes all information regarding ramp rate, hold level etc. The programming unit selects the desired programme and the user is then able to review the selected programme by using the ADVANCE control which also permits temperature programming to commence at any point in the programme. During programme execution a display of set point, segment, ramp rate and dwell time is provided. The programme may be interrupted at any stage using the PAUSE facility and this allows the programme to be altered, using the keyboard unit, during execution.

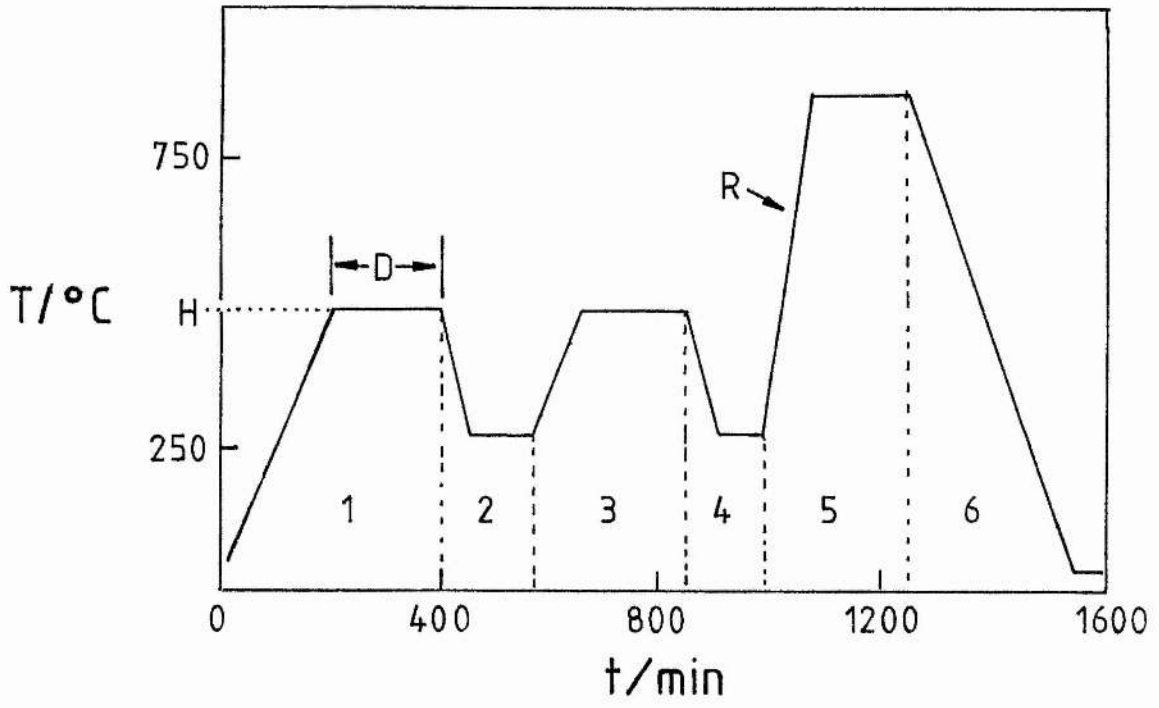

Figure 3.5 A typical furnace temperature-time profile set using the CRL system. H = hold level (°C), D = dwell time (min) and R = ramp rate (K min^{-1}).

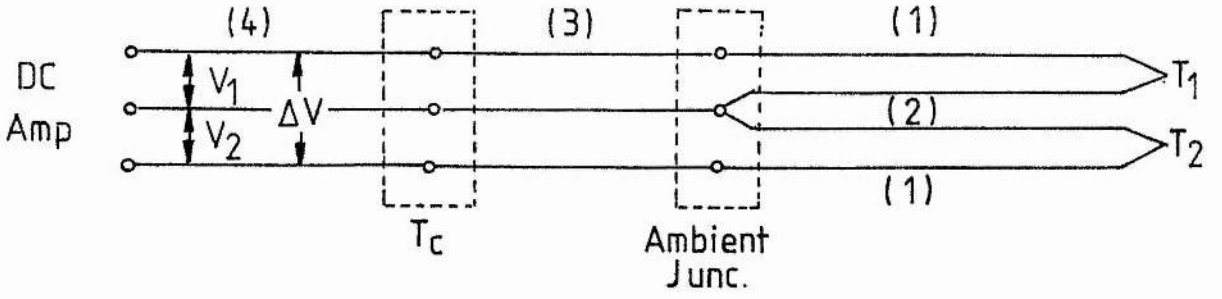

Figure 3.7 Differential thermocouple circuit. (1) Pt wires (+ve), (2) Pt/13%Rh wires (-ve), (3) compensating cable, (4) copper wires. T_c is maintained at 0 °C.

The 407 temperature controller receives information on the set point from the programming unit and compares this information to the emf of the sensor thermocouple, to which it is connected, and on the basis of the error voltage sends appropriate trigger pulses to the 505 thyristor power switch; this in turn feeds power to the furnace. The 407 and 505 can be used separately from the 802 KB to provide isothermal control. The set point is adjusted using thumbwheels on the 407 and the temperature at the sensor thermocouple is given on the LED display of the 407. The 407 can also be interfaced to a microcomputer for process control. Although fitted with a card for a Pt/Pt-13%Rh sensor thermocouple, other thermocouples may be used (eg chromel-alumel) with the appropriate card.

Adjustment of the PID terms on the 407 have been made to ensure good response from the Stanton-Redcroft vertical furnace over the temperature range 100 - 1000 ^{o}C. The use of other furnaces would require readjustment of these terms.

3.1.2.3 Sample Block

Two arrangements were used in this work. Figure 3.6(a) shows the arrangement used for sealed ampoules and this was manufactured by Stanton - Redcroft. The block is made of high-purity alumina and has two wells each of 6.7 mm diameter and 10 mm depth. The block is supported by a four-bore alumina rise-rod through which the thermocouples run and this rod is joined by means of an aluminium

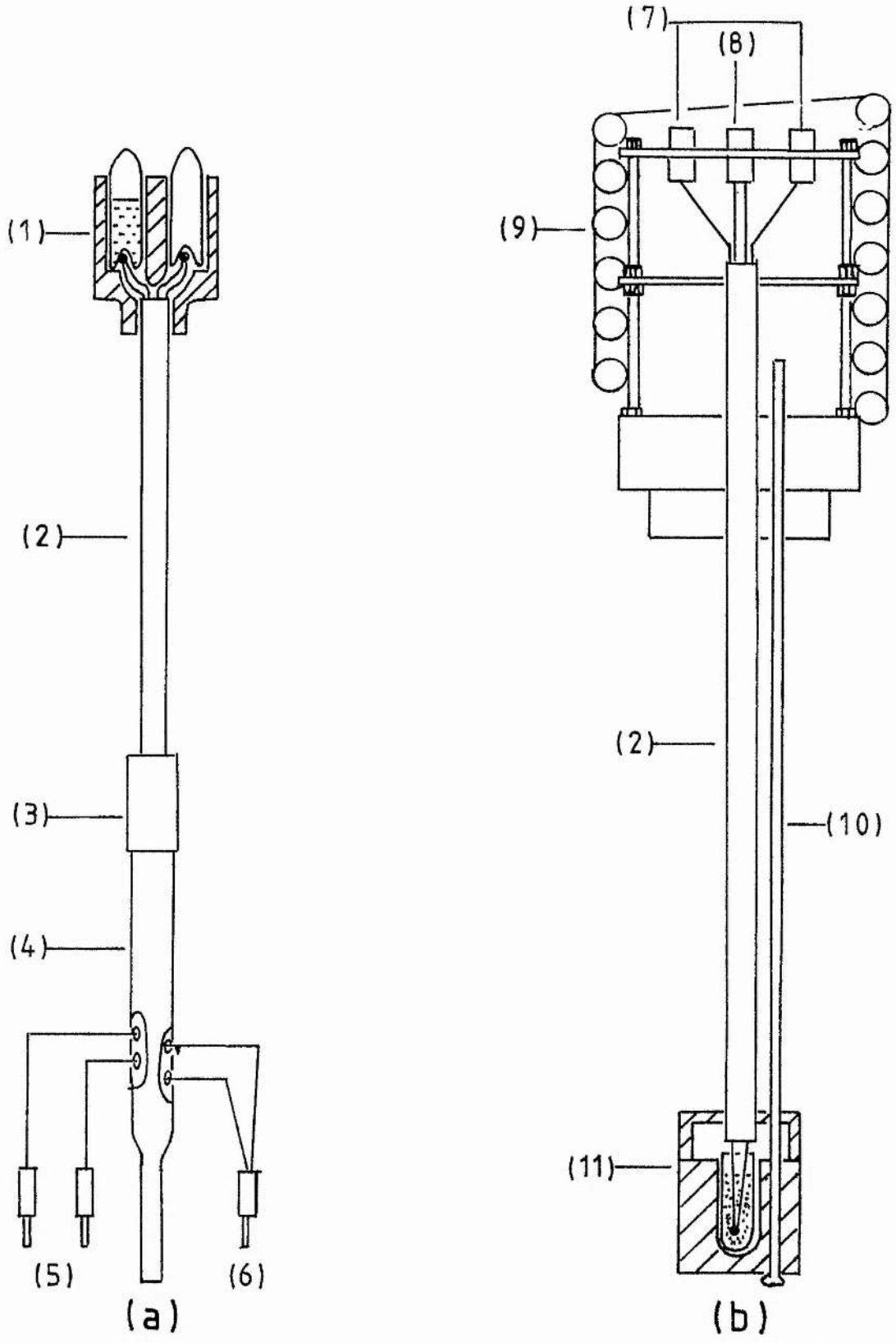

Figure 3.6 DTA sample holder/thermocouple arrangements for (a) sealed tube and (b) open-cup immersed-thermocouple situations. (1) high-purity alumina, sample and reference holder, (2) 4-bore alumina rod, (3) Al collar, (4) 4-bore silica rod, (5) sample and reference +ve thermocouple leads, (6) common -ve leads, (7) sample and reference +ve thermocouple sockets, (8) common -ve socket, (9) copper cooling-pipes, (10) silica rod, (11) pyrophyllite sample and reference holder and cap.

collar to a four-bore silica rod which slots into a brass holder fixed to the base plate of the furnace frame.

Figure 3.6(b) shows a custom-built arrangement designed to facilitate direct contact between thermocouple and sample and was used in the study of the system Ag_2SO_4 - $CdSO_4$. The sample block and lid were machined from pyrophyllite which was then cured at 1200 ^{o}C for 2 h. The block has a diameter of 20 mm and a height of 20 mm. The sample wells are 6.5 mm in diameter with a depth of 15 mm.

This arrangement is positioned on top of the furnace and due to this the ambient junction is affected by convection currents and this causes severe deterioration of the baseline. Placing a water-cooled jacket around the ambient junction obviates this problem.

While the above arrangement offered a higher sensitivity, peak temperatures obtained for transitions were identical to those obtained using the arrangement in figure 3.6(a), thereby justifying confidence in the overall accuracy of the system. However with the arrangement in figure 3.6(b), the thermocouples must be thoroughly cleaned after each run. This was accomplished by heating the thermocouple junctions to red heat in a gas-oxygen flame and plunging them into cold nitric acid. Repeated handling and cleaning operations will reduce the working life of the thermocouple.

3.1.2.4 Thermocouples

In both arrangements, Pt/Pt-13%Rh thermocouples were used. The wire, supplied by Goodfellows, had purities of > 99.9% for both Pt and Pt-13%Rh wires.

The thermocouples were calibrated using the melting points of Analar NaCl and Na_2SO_4 and BDH Aristar KNO_3 at heating rates of 6 K min^{-1}. The temperatures of fusion were taken from plateaux in the sample temperatures which were apparent during melting. The thermocouple emfs were interpreted using the IPTS (1968) tables[80] and the melting points were taken from the JANAF tables.[11]

In both arrangements the Pt/Pt-13%Rh wires are connected to a three-core compensating cable which in turn is joined to ordinary copper wire (figure 3.7). The compensating cable simulates the electrical characteristics of Pt and Pt-13%Rh wire at approximately ambient temperatures, so providing an "invisible junction". The junction between compensating cable and platinum wires (the ambient junction) must be kept in an environment which is free from temperature fluctuations.

The junction between the copper wire and the compensating cable (the cold junction) is sealed in resin and placed inside a tight-fitting glass tube with some liquid paraffin to increase thermal conductivity. The tube is inserted in a narrow-necked dewar flask containing a crushed ice/ water slurry. Temperature measurements made on this bath showed that the temperature variation was less than 0.1

^{o}C over 12 h. This 0 ^{o}C cold junction allows emfs to be directly read from the IPTS tables.

The voltages between the copper wires are:

$$V_1 = V_{T_1} - V_{T_c}$$
$$V_2 = V_{T_2} - V_{T_c}$$
$$\Delta V = V_1 - V_2 \cong \Delta T$$

Where T_1 and T_2 are the sample and reference temperatures respectively and T_c is the cold junction temperature. For convenience, voltage readings will be referred to below as the temperature or temperature differences to which they are proportional.

Since the emfs V_1 and V_2 are relatively large, between 0.1 and 11.0 mV in the temperature range 20-1000 ^{o}C, they can be accurately displayed on a chart recorder with that sensitivity. The ΔT signal however is of low magnitude and requires amplification before it can be fed to a chart recorder.

The amplifier used was a custom-built, low-noise, dc type amplifier, having two switchable gain settings, x 10 and x 100; the latter setting being used in the present work. Although both T and ΔT signals are connected to the amplifier's input, the T signal emerges on the amplifier's output sockets unaffected.

3.1.2.5 Temperature Measurement

A Linseis Series LS4 twin-pen flat-bed chart recorder was used to record the T and ΔT signals. Both input channels have identical specifications. The sensitivity setting used throughout this work was 10 mV fsd on both channels (calibrated). In situations where the T signal exceeded 10 mV, the variable sensitivity setting was used and this was calibrated using a DVM connected in parallel to the input signal.

The chart width is 250 mm which at 10 mV fsd allows a maximum resolution of 0.015 mV and this is equivalent to 2 K at 20 ^{o}C, 1.3 K at 500s ^{o}C and 1.1 K at 1000 ^{o}C. These errors are deemed to be small (< 0.3 %) in the temperature range of interest (400 - 1000 ^{o}C).

In situations where greater precision was required, eg during calibration, a Solartron 7045 digital voltmeter having a voltage resolution equivalent to 0.08 K was connected in parallel with the input signal. The chart recorder was modified to provide automatic zeroing of the pen displaying the T signal at regular intervals, continuously variable between 5 and 60 min. The chart drive was normally set at a rate of 100 mm h^{-1} when using ramp rates of 6 K min^{-1}. When taking readings from traces it must be borne in mind that the pens are offset by approximately 2.25 mm, the exact value being determined at the end of each run.

3.1.2.6 Optical Furnace

A furnace allowing "in situ" observations of phase reactions at high temperatures was built (see figure 3.8). The core consisted of a length of quartz tube (30 mm od x 200 mm) wound with nichrome ribbon and having a Pt/Pt-13%Rh thermocouple embedded in the wall. The tube had two quartz side-arms at its centre (14mm od x 75 mm) set at an angle of 180^{o} to each other. Microscope slides glued to brass washers were mounted on the ends of the arms to serve as windows. The sample holder was adjustable to provide suitable alignment of the sample in the field of view, and the the junction of a Pt/Pt-13%Rh thermocouple was held in close contact with the sample tube. The objective lens of a travelling microscope (magnification x 10) was sited 450 mm from the sample which was illuminated from front and rear by spotlights. The furnace temperature was programmed using the Stanton-Redcroft temperature programmer.

Although of relatively crude design (for example, heat loss through the windows was a major problem) the results obtained from this design in the study of the system Ag_2SO_4 - $La_2(SO_4)_3$ were very useful.

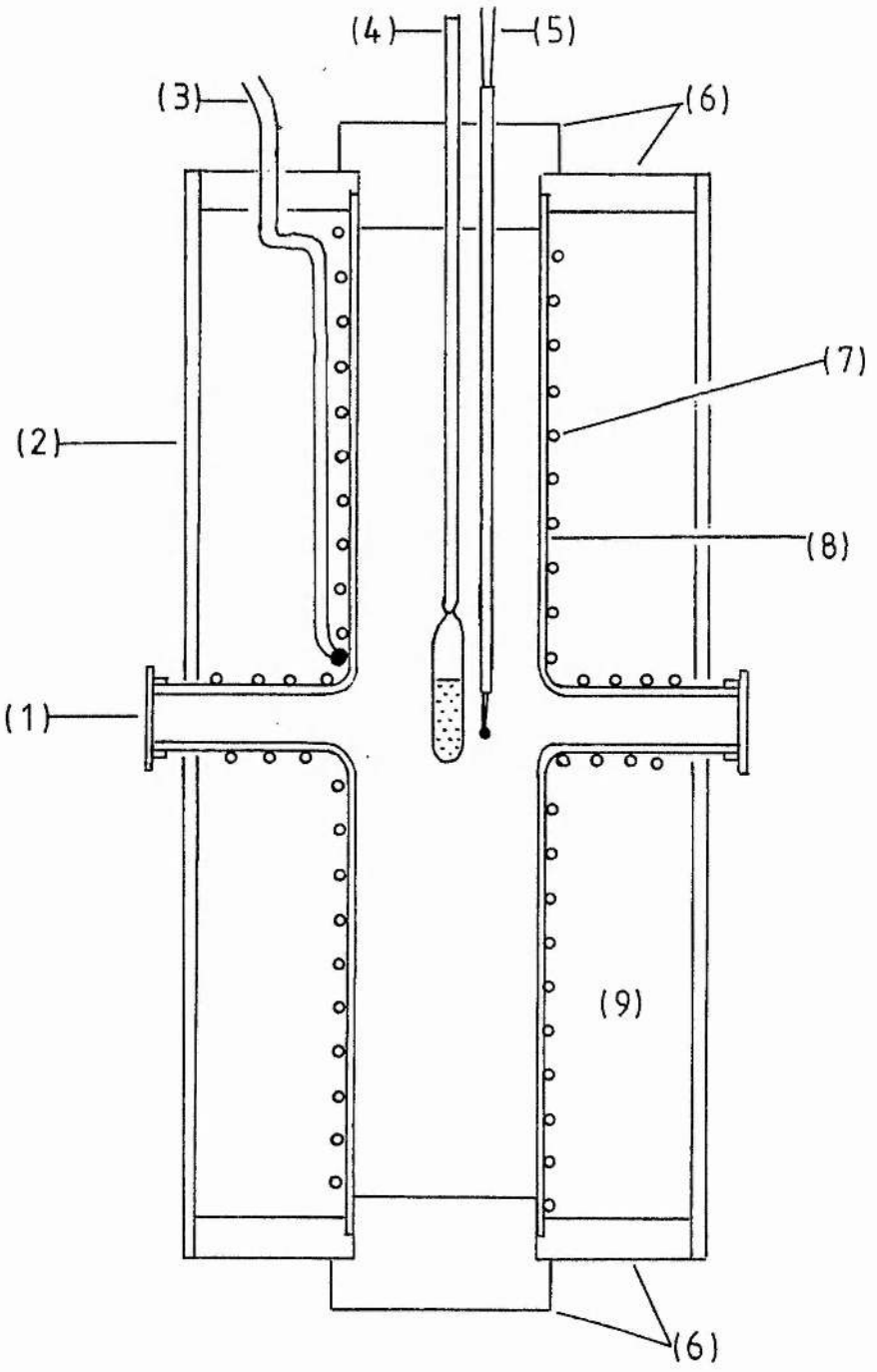

Figure 3.8 Custom-built optical furnace. (1) glass window, (2) aluminium body, (3) Pt/Pt-13%Rh sensor thermocouple, (4) silica rod, (5) Pt/Pt-13%Rh sample thermocouple, (6) sindanio inserts, (7) furnace windings, (8) quartz furnace core, (9) insulation.

3.1.3 Conclusions

Optimum DTA results are obtained by cycling a sample several times over the temperature range of interest. The DTA system described above, using the CRL programmer, provides a flexible system for acquisition of DTA results which may be run 24 hours a day. The accuracy and precision can be considered adequate for most applications although increased precision of the T signal and more convenient data handling could be achieved by computerised acquisition of thermocouple emfs.

3.2 The System Silver Sulphate - Lanthanum Sulphate

3.2.1 Introduction

The phase diagram of the previously undetermined system $La_2(SO_4)_3$ Ag_2SO_4 presented below, was studied using DTA, X-ray diffraction and optical techniques.

While there have been a number of high-temperature phase studies on Ag_2SO_4 both in single and multi-component systems,[8] investigations on $La_2(SO_4)_3$ are limited.

$La_2(SO_4)_3$ does not exhibit any high-temperature phase transitions and decomposes without melting, as shown by previous DTA and TGA studies.[81,82] Decomposition is a two-stage process the first stage being:

$$La_2(SO_4)_3(s) \rightleftharpoons La_2O_2(SO_4)(s) + 2SO_2(g) + O_2(g) \qquad (3.2.1)$$

The second stage is the decomposition of the basic sulphate to the oxide; that is not relevant here. The initial decomposition temperature occurs in the temperature range 782 - 810 °C with a flowing atmosphere of inert gas; using a stationary atmosphere of Ar, the initial decomposition temperature is shifted to 890 °C.

Previous high-temperature phase diagrams involving $La_2(SO_4)_3$ are the systems $La_2(SO_4)_3$ - Rb_2SO_4[83] and $La_2(SO_4)_3$ - Cs_2SO_4.[84] In both these cases two unstable double salts are formed, one undergoing incongruent melting, the other, solid-state decomposition.

Pure Ag_2SO_4 exists in two crystalline forms, (I) and (II) which possess orthorhombic and Na_2SO_4—(I) structures respectively.[85] A number of studies have revealed that the (I)→(II) transition occurs in the temperature range 412 - 430 °C and that fusion takes place between 643 - 661 °C.[26,68,69,86,87]

Ag_2SO_4 is stable as a liquid until around 900 °C where decomposition proceeds as follows:

$$Ag_2SO_4(l) \rightleftharpoons 2Ag(s) + SO_2(g) + O_2(g) \qquad (3.2.2)$$

3.2.2 Materials

$La_2(SO_4)_3$ was obtained by dehydration of Aldrich Gold label $La_2(SO_4)_3.9H_2O$ (99.999 %) by heating at 400 °C for 48 h. This material was cooled under vacuum, finely ground, and treated again in the same manner. Complete dehydration was shown by the absence of O-H bands in the infra-red spectrum of the final material. BDH Ag_2SO_4 (99 %) was finely ground but required no further treatment. Mixtures of total mass 200 mg were prepared by grinding the salts together for 10

min under a flowing atmosphere of dry N_2 (to prevent excessive absorption of moisture). The entire sample was transferred to the quartz tube which was evacuated to 0.01 torr and the contents were then heated to 150 ^{o}C for 2 h prior to sealing. This tube was placed in the sample well of the DTA block and an identical evacuated quartz tube (but containing no reference material) was placed in the reference well. Quartz containers of approximate volume 0.3 cm^3, length 2 cm, and wall thickness 1 mm were used.

3.2.3 Apparatus

The DTA apparatus used in this study has been described in Section 3.1.2 and temperature control was provided by the Stanton Redcroft LVP CC220 temperature programmer using ramp rates of 1 - 12 K min^{-1} (6 K min^{-1} being typical).

Direct observations of samples at high temperatures were made using the custom-built optical furnace described in Section 3.1.2.6.

3.2.4 Results

The phase diagram obtained by DTA is shown in figure 3.9 and its main features are described below. The diagram records the transitions obtained on heating, at rates of 6 K min^{-1}, except the right-hand liquidus line which was obtained on cooling. A selection of DTA thermograms is shown in figure 3.10.

In presenting DTA thermograms, the convention followed by the present author is that recommended by ICTA where an exotherm is indicated by an upward deflection and an endotherm by a downward deflection.

Figure 3.9 Phase diagram of the system Ag_2SO_4 - $La_2(SO_4)_3$

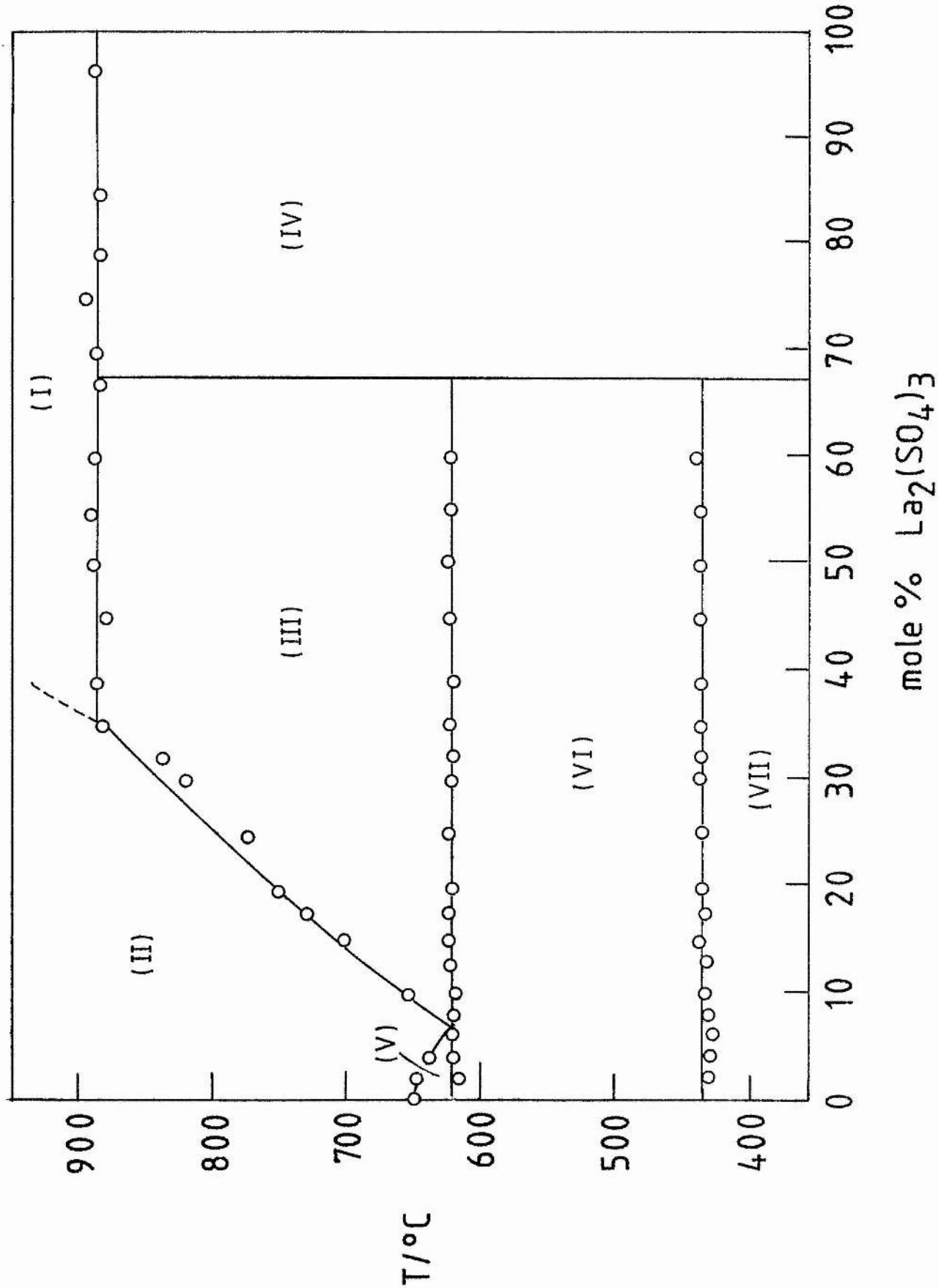

Legend for figure 3.9. Phase diagram of the system Ag_2SO_4 - $La_2(SO_4)_3$.

(I)	L	+	1
(II)	1		
(III)	2LA	+	1
(IV)	2LA	+	L
(V)	A(II)	+	1
(VI)	A(II)	+	2LA
(VII)	A(I)	+	2LA

Where the above symbols have the following meaning :

1	=	liquid
L	=	$La_2(SO_3)_4$
2LA	=	$2La_2(SO_4)_3.Ag_2SO_4$
A(I)	=	Ag_2SO_4-(I)
A(II)	=	Ag_2SO_4-(II)

These abbreviations will also apply to the remainder of figure 3.10

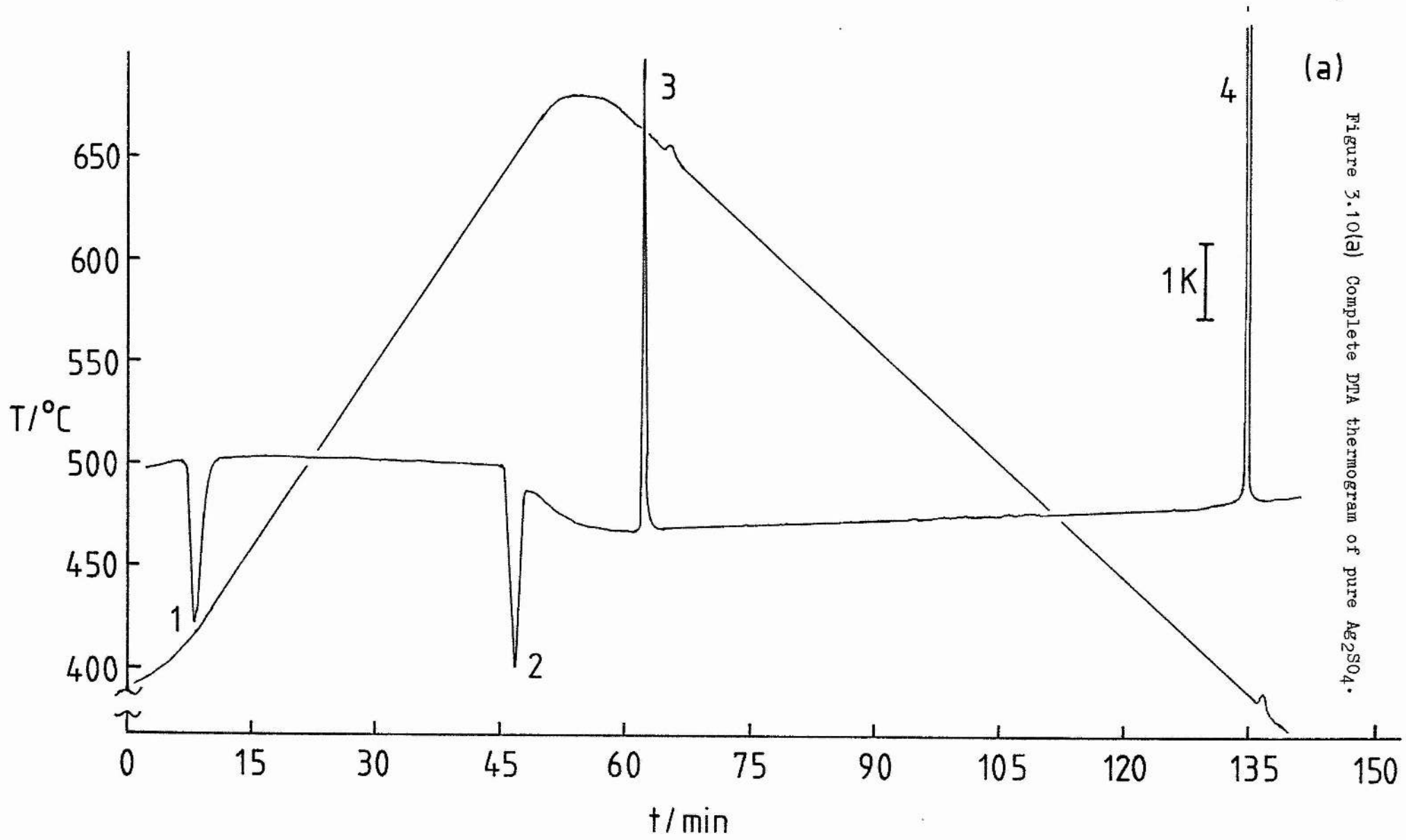

Figure 3.10(a) Complete DTA thermogram of pure Ag_2SO_4.

Legend for figure 3.10(a) Complete DTA thermogram for pure Ag_2SO_4, showing the temperature-time traces for the sample (sloping line). 1) A(I) ⟶ (II) polymorphic transition (433 °C, peak temperature). 2) A(II) ⟶ A(1) (665 °C), 3) A(1) ⟶ A(II) (652°C), 4) A(II) ⟶ A(I) (392 °C). Peaks 1) & 2) were obtained on heating at 6 K min^{-1}. Peaks 3) & 4), obtained on cooling at 4 K min^{-1}, exhibit supercooling as indicated by the peaks in the temperature-time trace.

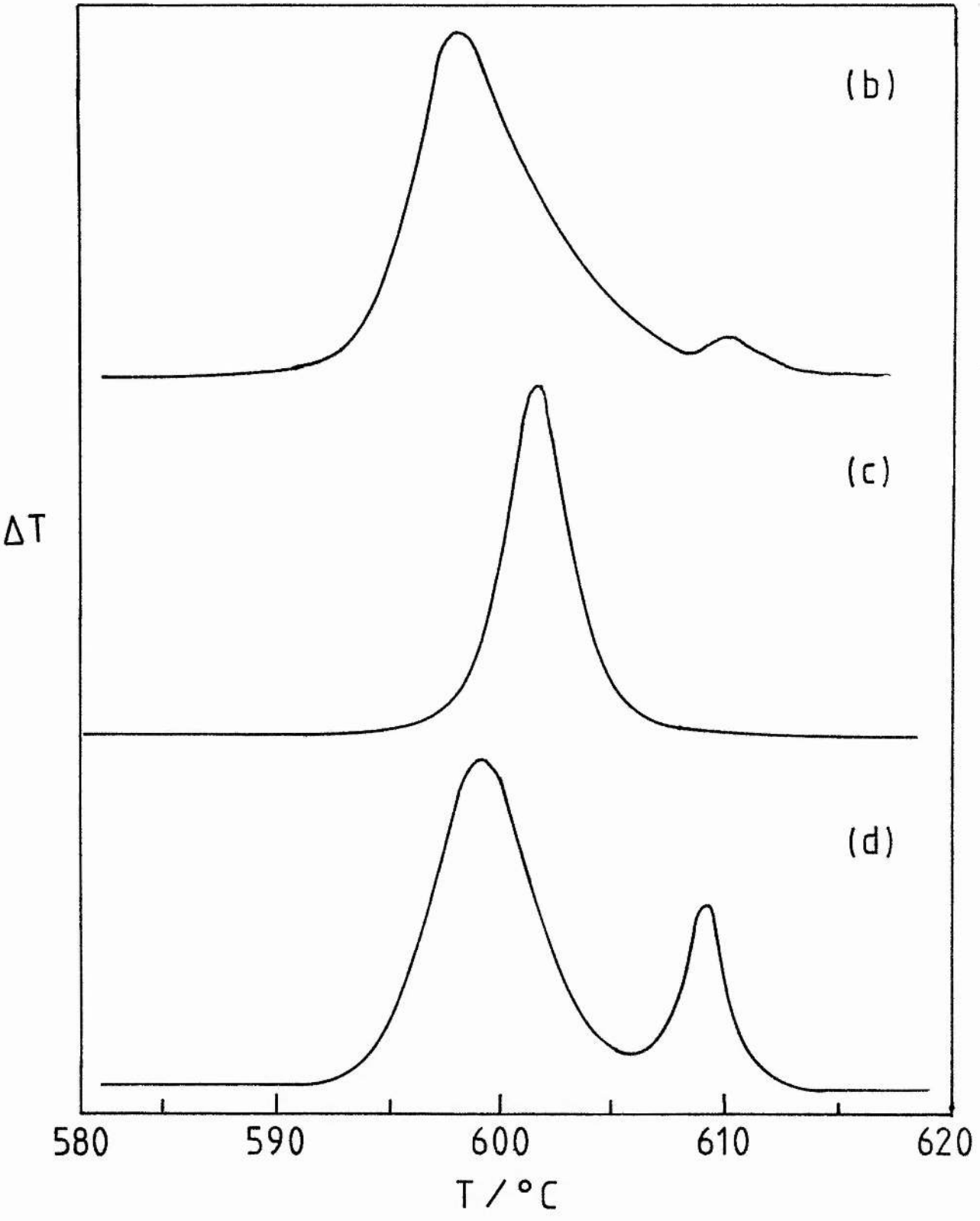

Figure 3.10(b-d) DTA thermogram showing the positions and intensities of the exotherms associated with the eutectic transition , obtained on cooling various mixtures at a rate of 6 K min^{-1}, (b) 10 mole%, (c) 8 mole% and (d) 6 mole% $La_2(SO_4)_3$.

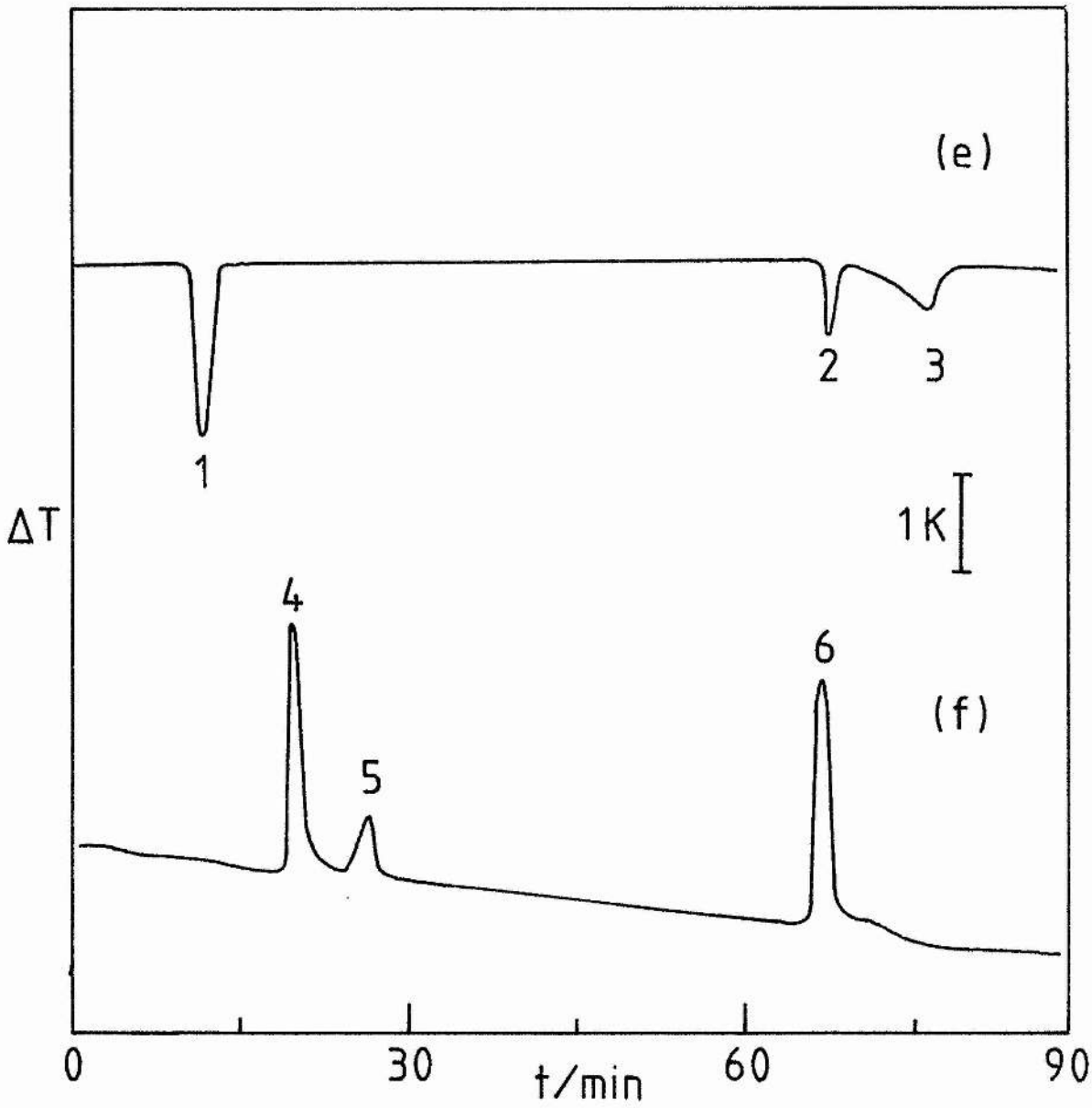

Figure 3.10(e-f) DTA thermogram for a 3 mole% $La_2(SO_4)_3$ mixture. (e) heating 6 K min^{-1}, 400-700 °C : 1) A(I) ⟶ A(II) (431 °C), 2) eutectic transition, A(II) + 2LA ⟶ l , (617 °C), 3) liquidus curve (647 °C, cf figure 2.7(b)). (f) cooling 6 K min^{-1}, 700-300 °C : 4) liquidus (637 °C), 5) eutectic ,l ⟶ A(II) + 2LA ,(589 °C), 6) A(II) ⟶ A(I) (401 °C).

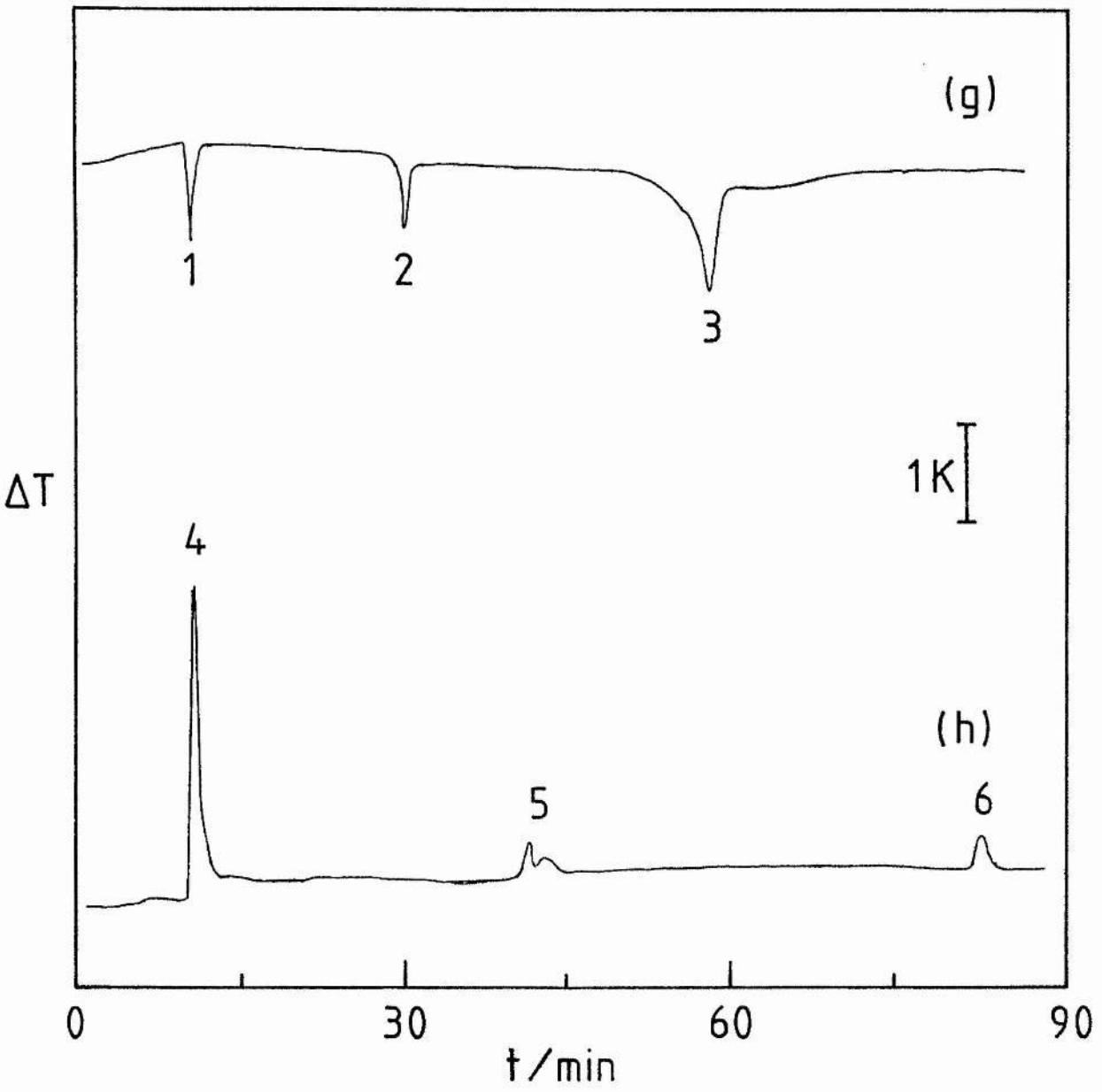

Figure 3.10(g-h) DTA thermogram for a 45 mole% mixture. (g) heating 5 K min^{-1}, 400-950 °C : 1) A(I) ⟶ A(II) (430 °C) , 2) eutectic (619 °C), 3) incongruent melting, 2LA ⟶ L + 1, (879 °C) . (h) natural cooling, 950-350 °C : 4) incongruent melting reverse reaction, 1 + L ⟶ 2LA , (843 °C), 5) eutectic (604 & 593 °C), 6) A(II) ⟶ A(I) (412 °C).

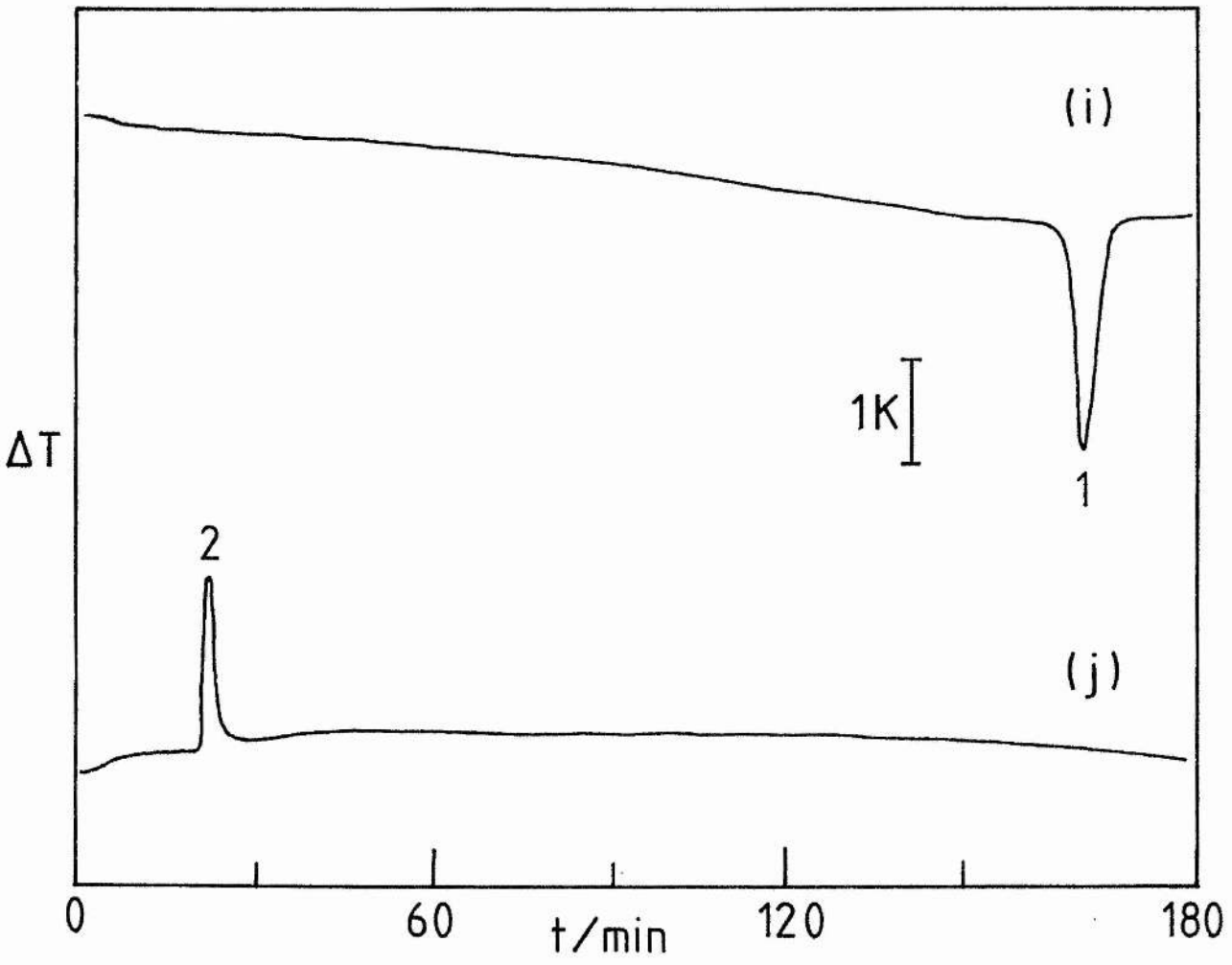

Figure 3.10(i-j) DTA thermograms for a 67 mole% mixture. (i) heating 3 K min^{-1}, 400-950 °C : 1) incongruent melting (875 °C). (j) cooling 3 K min^{-1}, 950-350 °C : 2) reverse incongruent melting 847 °C). Note the complete absence of all other transitions.

The morphological (I) ⟶ (II) transition of Ag_2SO_4 occurs at 433 ± 3 °C on heating but the reverse reaction undergoes supercooling and occurs at 407 ± 6 °C (figure 3.10(a). As shown in figure 3.10(e-h), this transition is evident on both heating and cooling cycles at all compositions in the range 1-61 mole% (all compositions are expressed as mole% $La_2(SO_4)_3$). Pure Ag_2SO_4 melts at 665 °C. A double salt, $2La_2(SO_4)_3.Ag_2SO_4$, is formed and this melts incongruently at 878 ± 6 °C over the composition range 34-95 mole%. On cooling the reverse reaction exhibits hysteresis and occurs at 844 ± 5 °C (see figure 3.10(g-j)).

A eutectic of composition 8 mole% is formed between the double salt and Ag_2SO_4. This is detected at 618 ± 3 °C on heating mixtures in the composition range 1-61 mole% (see figure 3.10(e-h)). As shown in figure 3.10(b-d), however, this transition is evident on cooling as a doublet and this feature will be discussed further in Section 3.2.5.

3.2.5 Discussion

Powder X-ray diffraction patterns of heated and unheated mixtures (67 mole%) were obtained using a Philips 1040 diffractometer and are shown in figure 3.11 as evidence of double salt formation.

One complication is that $La_2(SO_4)_3$ obtained by dehydration of the nonahydrate is not isolated in its most stable crystalline form. The anhydrous material, when examined by cross-polar microscopy[25] had the appearance of a glass. However, if some Ag_2SO_4 is added to the

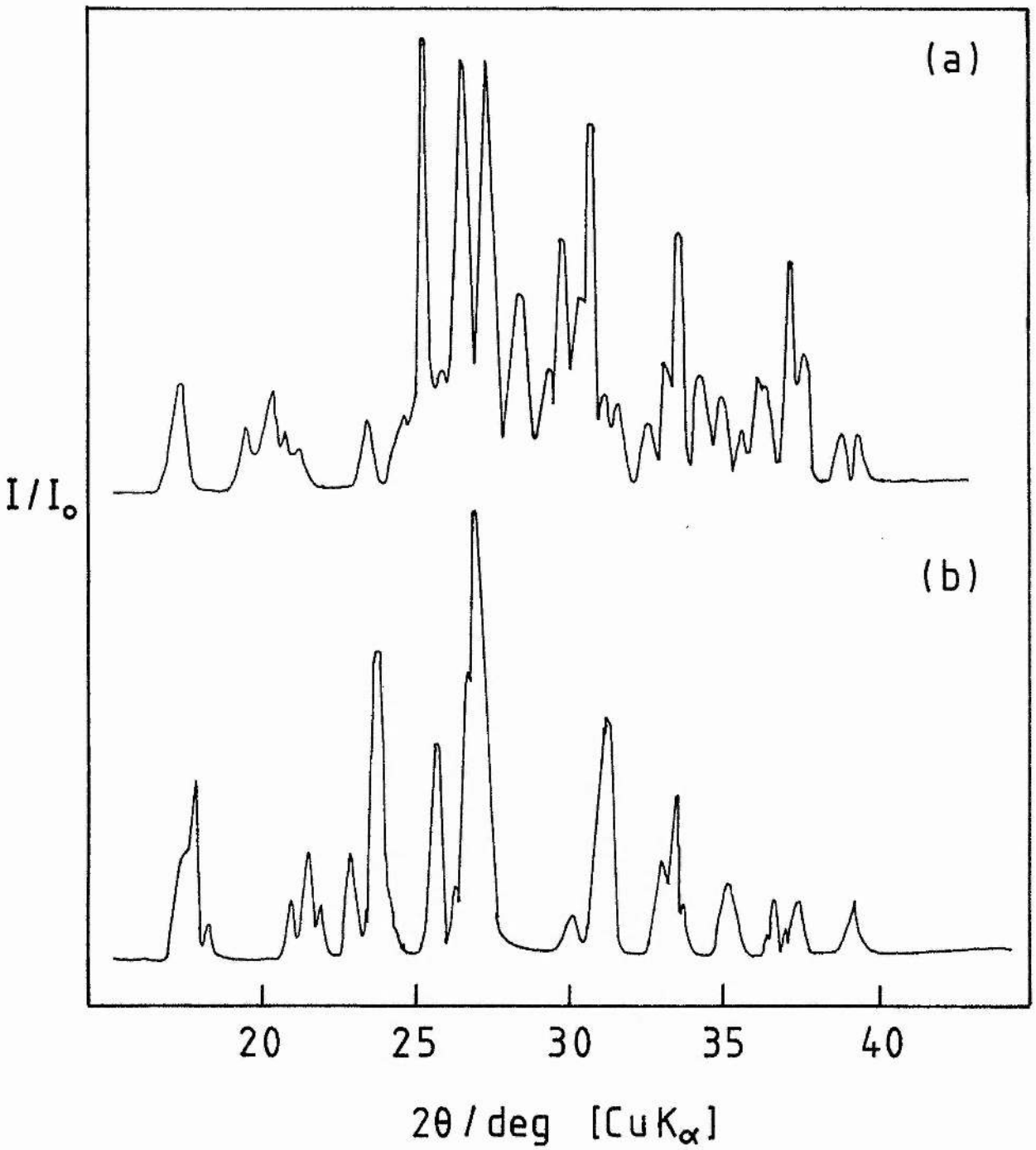

Figure 3.11 XRD patterns of (a) 2LA, and (b) an unheated mixture of the same overall composition.

$La_2(SO_4)_3$ and this mixture (96 mole%) is then heated to above the incongruent melting point and held there for 170 h before being slowly cooled (< 1 K min^{-1}), the particles assume a regular crystalline appearance. Under the cross-polars these exhibit extinction which implies a non-cubic structure. The X-ray diffraction pattern is also slightly modified. Similar behaviour has also been observed for $BeSO_4$.[26] The unheated sample of figure 3.11(b) is a 67 mole% mixture of recrystallised $La_2(SO_4)_3$ and Ag_2SO_4. This mixture was maintained at 1000 °C for 240 h then cooled at a rate of 0.6 K min^{-1} to provide a sample whose X-ray diffraction pattern is shown in figure 3.11(a). The formation of the double salt is indicated by other observations.

Both eutectic and the Ag_2SO_4 morphological transition terminate at 61 mole% where though very weak, they persist even after five heating/cooling cycles. Any double salt must therefore lie at a composition greater than 61 mole%. Allowing for the fact that under the above experimental conditions Ag_2SO_4 cannot be detected in mixtures more dilute than 5 mole% Ag_2SO_4, this puts the composition of the double salt at approximately 67 mole%. Another indication is the appearance, on first heating only, of an exotherm at 615 ± 1 °C seen with mixtures of composition 8-95 mole%. As shown in figure 3.12 the magnitudes of the exotherm and of the eutectic endotherm, which immediately follows it, vary with composition, the endotherm being completely swamped at compositions greater than 40 mole%. Thermogravimetric analysis (TGA) showed that there was no weight loss associated with this exotherm.

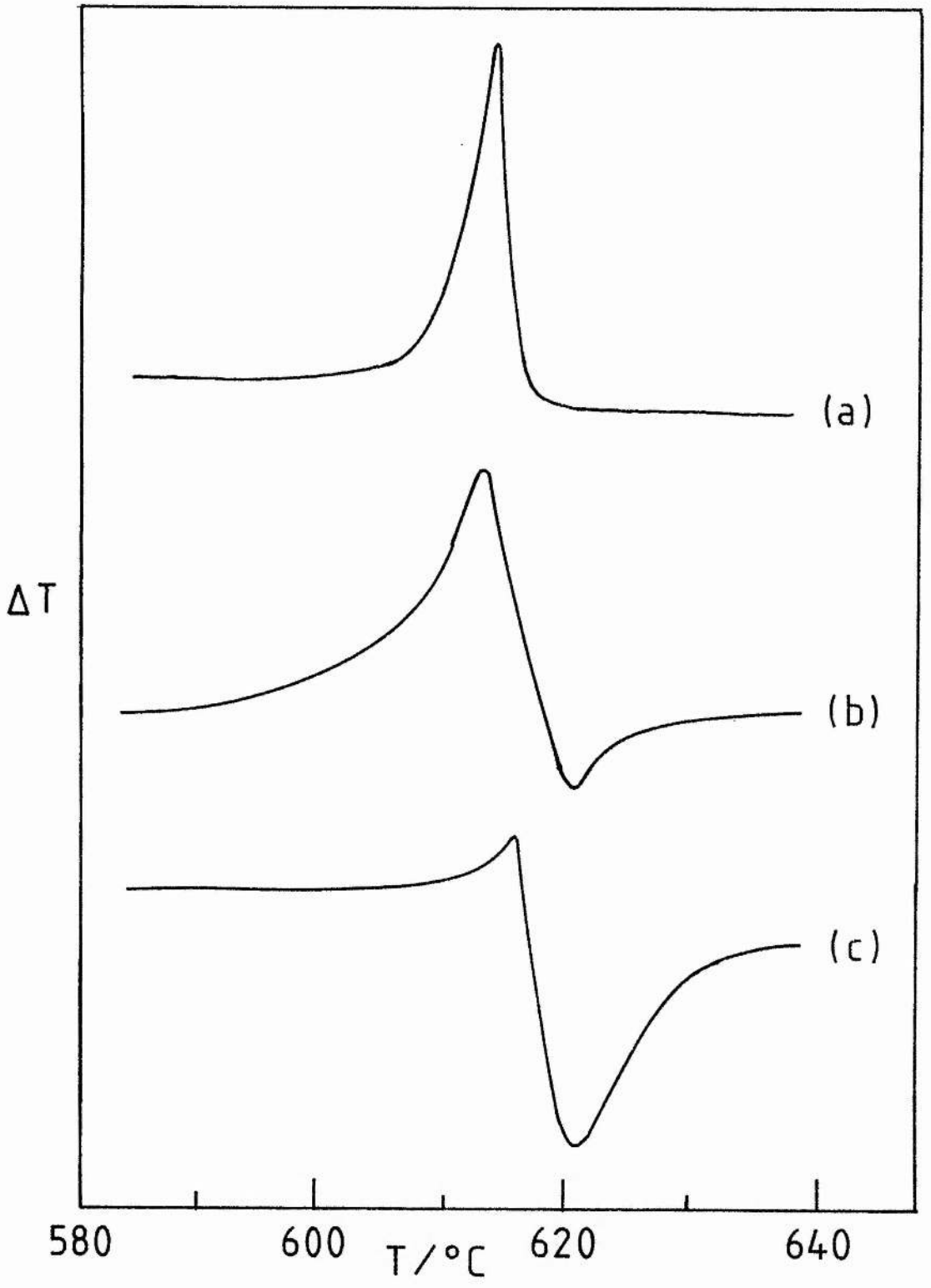

Figure 3.12 DTA traces showing the variation of the relative magnitudes of exotherm and eutectic endotherm obtained on the first heating of mixtures of composition 40 mole% (a),35 mole% (b) and 9 mole% (c).

One possible explanation for this exotherm is that heat is evolved when the double salt is formed and the intimate association with the eutectic tends to suggest that liquid plays a mechanistic role in the formation of the double salt. The exotherm is also observed at compositions greater than 67 mole%, a region where (in the context of the present phase diagram) liquid would not be expected. This effect may be explained by supposing that the system is in a metastable state at this temperature, and that the eutectic liquid is formed in order to promote formation of the double salt and hence bring the system back to its equilibrium state. This is in accordance with the observation that no such transition is seen in this temperature range in subsequent heating or cooling cycles.

As stated previously two exothermic heat effects are associated with the eutectic transition on cooling, (figure 3.10(b-d)).

At 606 $\pm$ 5 ^{o}C there is a small peak, the intensity of which varies little with composition. At 595 $\pm$ 5 ^{o}C the larger of the two peaks is detected. The magnitude of this exotherm does vary with composition, being most intense between 4 and 13 mole% and completely engulfing the high temperature transition between 7 and 9 mole%. This "splitting" is observed at cooling rates of between 1 and 6 K min^{-1} and the difference of 10 ^{o}C is always maintained.

However, when a sample of 13.5 mole% was heated to above the eutectic temperature and slowly cooled (< 1 K min^{-1}) until the first transition was reached and allowed to equilibrate there for 30 min or more, the larger low-temperature transition was not detected when cooling was resumed.

A further attempt to investigate this apparent kinetic effect was made using the optical furnace previously described. Mixtures in the range 0-80 mole% were examined. On heating, the eutectic transition is characterised visually by a colour change from white to intense yellow as liquid is formed. This is apparent in the composition range 4-55 mole%. The effect is observed over the stated composition range but the colour intensity is dependent on the composition of the mixture relative to that of the eutectic. On cooling, a two-stage process is observed. Again taking 13.5 mole% as an example, as the sample is cooled towards the eutectic, solid is seen floating on a clear yellow liquid; but at 605 ^{o}C there is a sudden burst of needle-like crystals spreading throughout the yellow liquid. Further cooling causes yet more crystallisation until finally at 595 ^{o}C the remaining yellow colour suddenly disappears leaving a completely white solid. If the sample is heated to above the eutectic, cooled slowly (< 1 K min^{-1}) until the burst-crystallisation occurs and held steady at this temperature (604 ± 1 ^{o}C) then complete conversion of the yellow medium to the white solid takes place in 30 min. This confirms the kinetic effect inferred from DTA and gives some physical evidence for the nature of the process which is occurring.

The splitting effect was also reproduced in a limited number of flowing gas experiments where the salts were contained in Pt cups. Overall, the flowing gas experiments gave similar, but less precise results to those carried out with sealed tubes. The optical furnace gave valuable confirmation of other DTA interpretations, since it permitted direct observation of other phase changes such as incongruent melting.

The above DTA results indicate the formation of only the one double salt; this is in contrast to the systems cited above which each contain two double salts.

3.3 The System Silver Sulphate - Cadmium Sulphate

The phase diagram of the binary system Ag_2SO_4-$CdSO_4$ presented here was studied by DTA and X-ray diffraction.

There have been a limited number of studies on binary sulpate systems which involve $CdSO_4$. A series of binary systems by G. Calagini and D. Marotta in 1913, include the systems Li_2SO_4 - $CdSO_4$ K_2SO_4 - $CdSO_4$ and Na_2SO_4 - $CdSO_4$.[8] The last two systems do not appear to obey the phase rule and show no polymorphic transitions for $CdSO_4$. They do, however, indicate the formation of a number of unstable double salts; a double salt of stoichiometry $3CdSO_4.X_2SO_4$ (X= Na,K) occurs in both instances. While there is some doubt as to the accuracy of these diagrams, the formation of double salts possessing these stoichiometries was confirmed by later work by Bergman and Bakumskaya who studied a number of ternary systems involving these components.[8]

The only previous work to be reported for the system Ag_2SO_4 - $CdSO_4$ is a binary section taken from a quaternary system[88] which appears in Levin.[8] This shows a eutectic at 62 mole% (all compositions are expressed as mole% of Ag_2SO_4) and 583 ^{o}C. The eutectic horizontal is shown at compositions in the range 0-80 mole% at which point a region of solid solution begins. A maximum in the silver sulphate-rich liquidus curve is indicated at 671 ^{o}C and 90 mole%, and is interpreted as being a maximum melting solid solution. The other liquidus curve is shown only as far as 800 ^{o}C, and furthermore there is no evidence of any polymorphic transitions, an

observation which is at variance with existing DTA studies on $CdSO_4$.[89 - 93] These studies show two high temperature polymorphic phase transitions, (I)→(II) and (II)→(III) which occur in the temperature ranges 750-843 °C and 830-897 °C respectively. A high-temperature X-ray diffraction study[94] has indicated the respective transition temperatures as being 754 ± 12 °C and 820 ± 13 °C and in addition has shown the structures of the three modifications, (I), (II) and (III) to be orthorhombic ($HgSO_4$ structure), orthorhombic ($CrVO_4$ structure) and hexagonal ($NaKSO_4$ structure) respectively.

Pure $CdSO_4$ undergoes decomposition as follows:

$$3CdSO_4(s) \rightleftharpoons 2CdO.CdSO_4(s) + 2SO_2(g) + O_2(g) \qquad (3.3.2)$$

The temperature of this decomposition begins in the temperature range 780 - 820 °C.[82,95] The basic oxide, $2CdO.CdSO_4$, undergoes further decomposition to CdO.

Several workers have observed transitions at temperatures around 1010 °C, and this has been attributed to formation of a eutectic between cadmium sulphate and the basic oxide.[89,92]

The high-temperature transitions of Ag_2SO_4 have been discussed in Section 3.2.

3.3.1 Materials

Reagents used were BDH Analar Ag_2SO_4 (99 %) while $CdSO_4$ was obtained by heating Aldrich Gold Label $CdSO_4.H_2O$ (99.999 %) to 250 °C for 48 h. Mixtures were prepared by gently grinding the salts together for 5 min under $CHCl_3$ (Fisons A.R. grade 99.9 %). Any remaining solvent was removed by heating at 100 °C for 30 min before transferring mixtures to the quartz ampoules. Immediately before evacuating and sealing the ampoules, samples were held at 400 °C for 1 h. Sample masses of 100-200 mg were used throughout.

3.3.2 Apparatus

The DTA apparatus used in this study was essentially as described in Section 3.1.2. In the present study the Control and Readout LTD 802KB/407/505 temperature programming system was used.

3.3.3 Results

The phase diagram determined by DTA (figure 3.13) records the average peak temperatures of transitions obtained on heating at a rate of 6 K min^{-1}, taken over multiple heating/cooling cycles. A selection of DTA thermograms is shown in figure 3.14.

Figure 3.13 Phase diagram of the system Ag_2SO_4 - $CdSO_4$

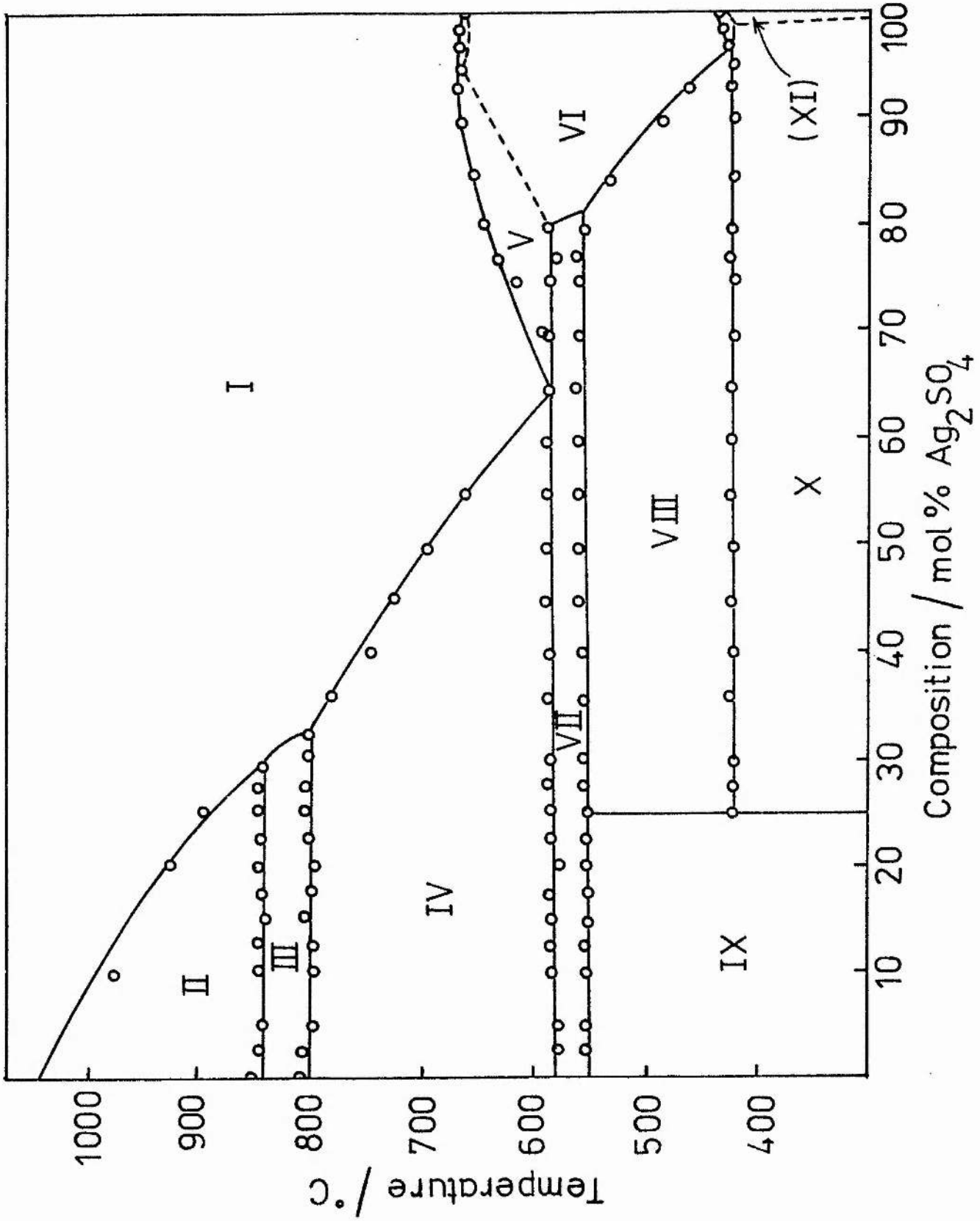

Legend for figure 3.13. Phase diagram of the system Ag_2SO_4 - $CdSO_4$.

(I)	l		
(II)	C(III)	+	l
(III)	C(II)	+	l
(IV)	C(I)	+	l
(V)	β	+	l
(VI)	β		
(VII)	C(I)	+	β
(VIII)	3CA	+	β
(IX)	3CA	+	C(I)
(X)	3CA	+	α
(XI)	α		

Where the above symbols have the following meaning :

l	=	liquid
C(I)	=	$CdSO_4$-(I)
C(II)	=	$CdSO_4$-(II)
C(III)	=	$CdSO_4$-(III)
3CA	=	$3CdSO_4 . Ag_2SO_4$
α	=	solid solution (I)
β	=	solid solution (II)

These abbreviations will apply to all remaining figures in this Chapter.

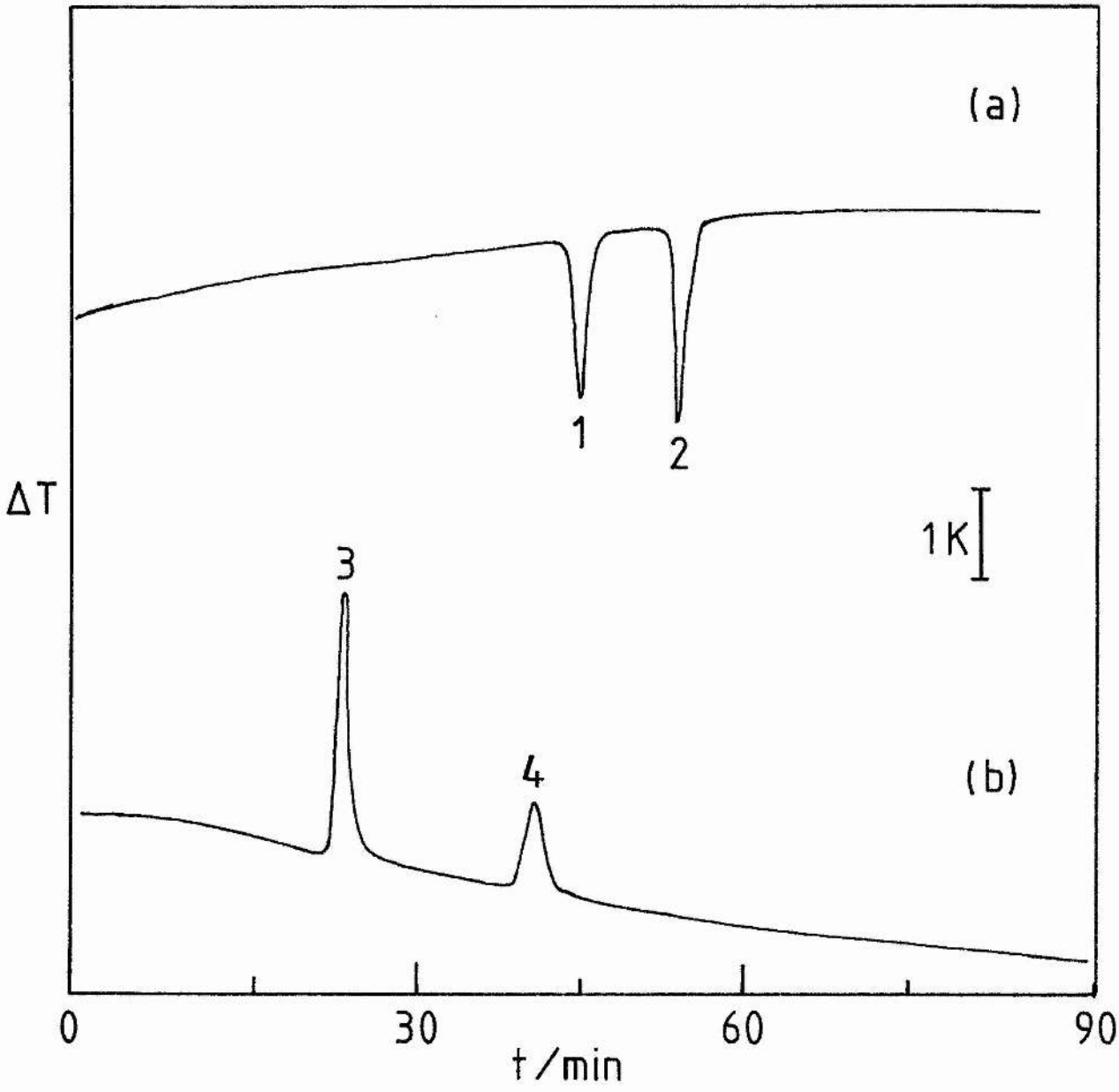

Figure 3.14(a-b) DTA thermogram of pure $CdSO_4$, over the temperature range 510-1030 °C. (a) heating 6 K min^{-1}: 1) C(I) ⟶ C(II) (804°C), 2) C(II) ⟶ C(III) (854 °C). (b) cooling 6 K min^{-1}: 3) C(III) ⟶ C(II) (837 °C), 4) C(II) ⟶ C(I) (650 °C).

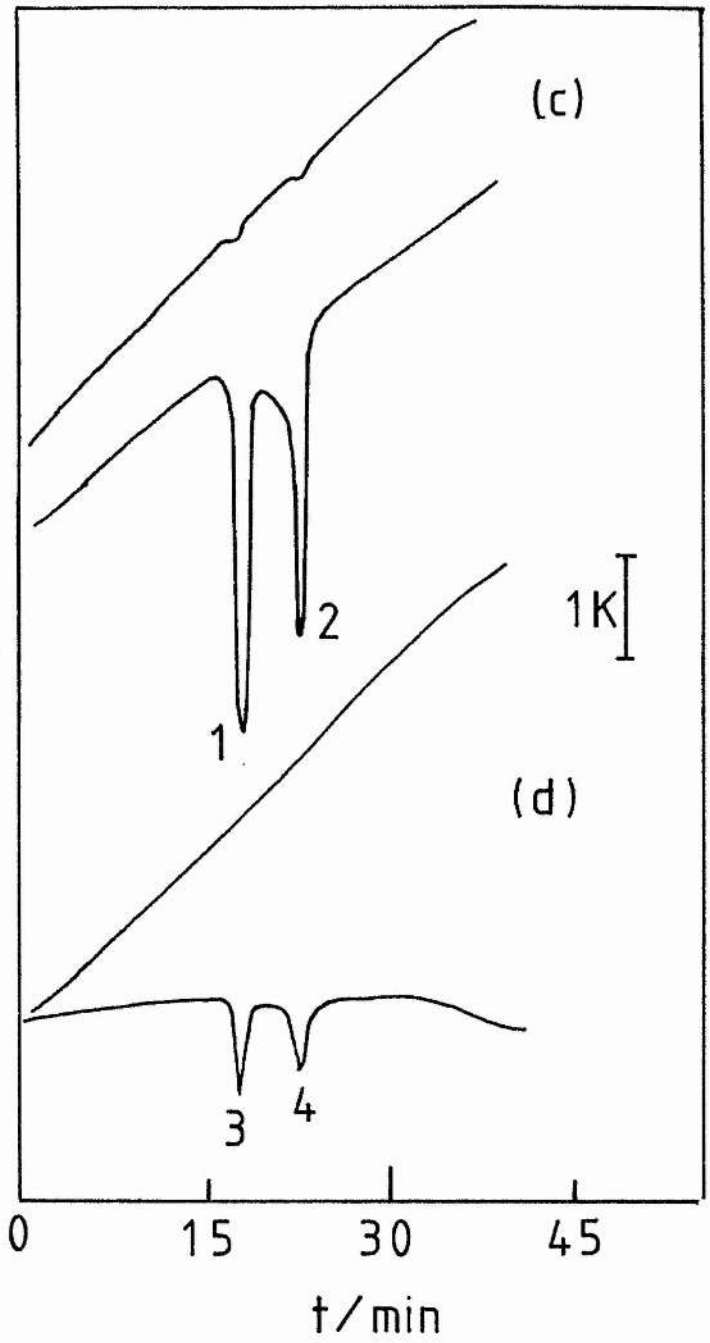

Figure 3.14(c-d) DTA thermogram of a 15 mole% Ag_2SO_4 mixture, 400-650 °C. (c) open quartz cups with thermocouple in contact with sample, heating 6 K min^{-1}: 1) 3CA $\longrightarrow$ C(I) + β (551 °C), 2) eutectic, 3CA + β $\longrightarrow$ 1, (582 °C). (d) sealed ampoule conditions, heating at 6 K min^{-1} : 3) 3CA $\longrightarrow$ C(I) + β (551 °C), 4) eutectic (582 °C). The upper trace in each pair, (c) & (d), is the T signal. In the case of (c), the higher sensitivity is apparent in the plateaux in the T signal. The difference in transition temperatures between (c) & (d) is neglegible.

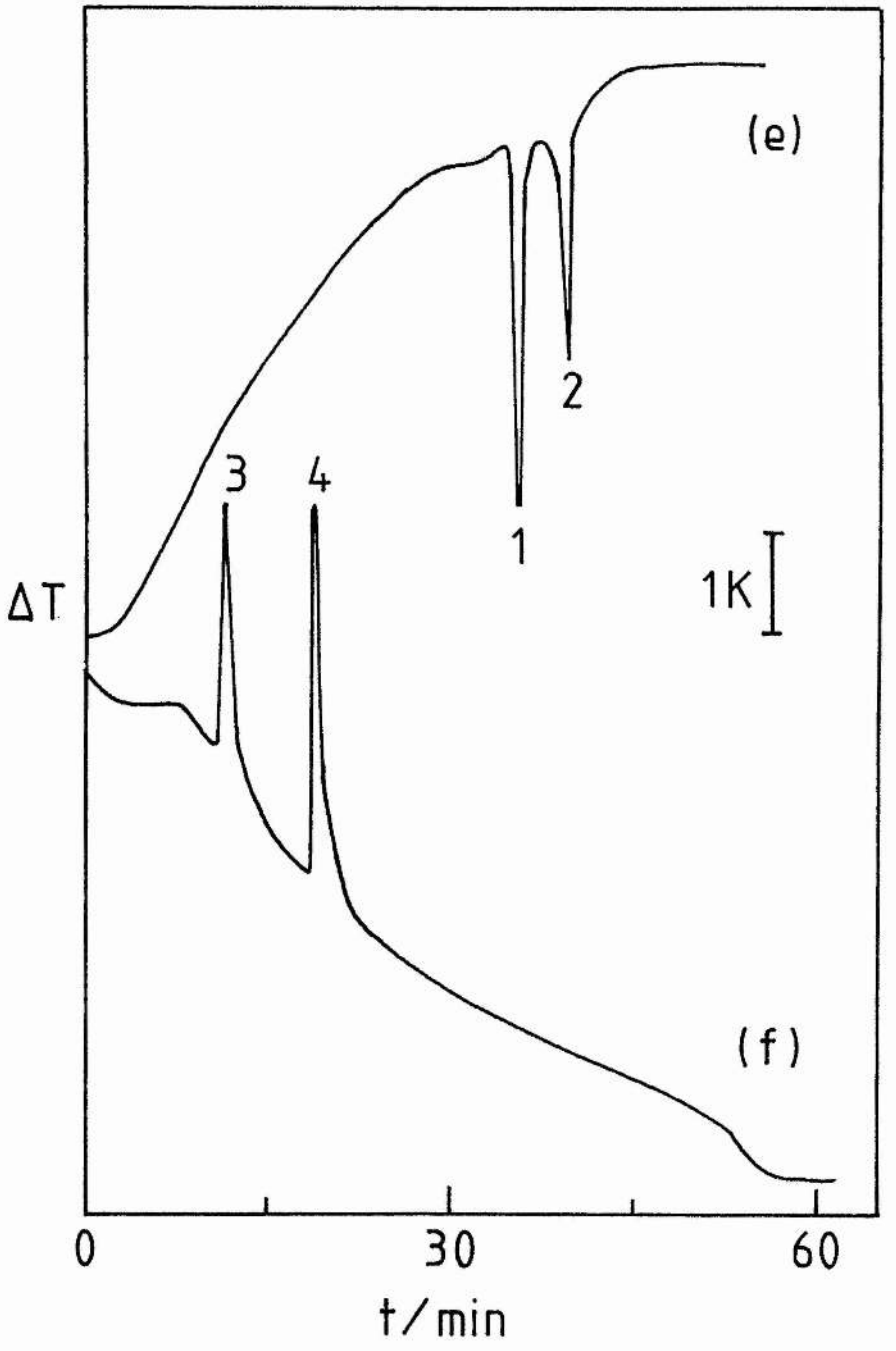

Figure 3.14(e-f) DTA thermogram of a 25 mole% mixture, 300-600 °C, run in an open quartz cup with thermocouples embedded in the sample. (e) heating 6 K min^{-1} : 1) 3CA $\longrightarrow$ C(I) + β (552 °C), 2) eutectic (585°C). (d) cooling 6 K min^{-1} : 3) eutectic (579 °C), 4) β + C(I) $\longrightarrow$ 3CA (530 °C). Supercooling during transition 3) is much less pronounced than during 4).

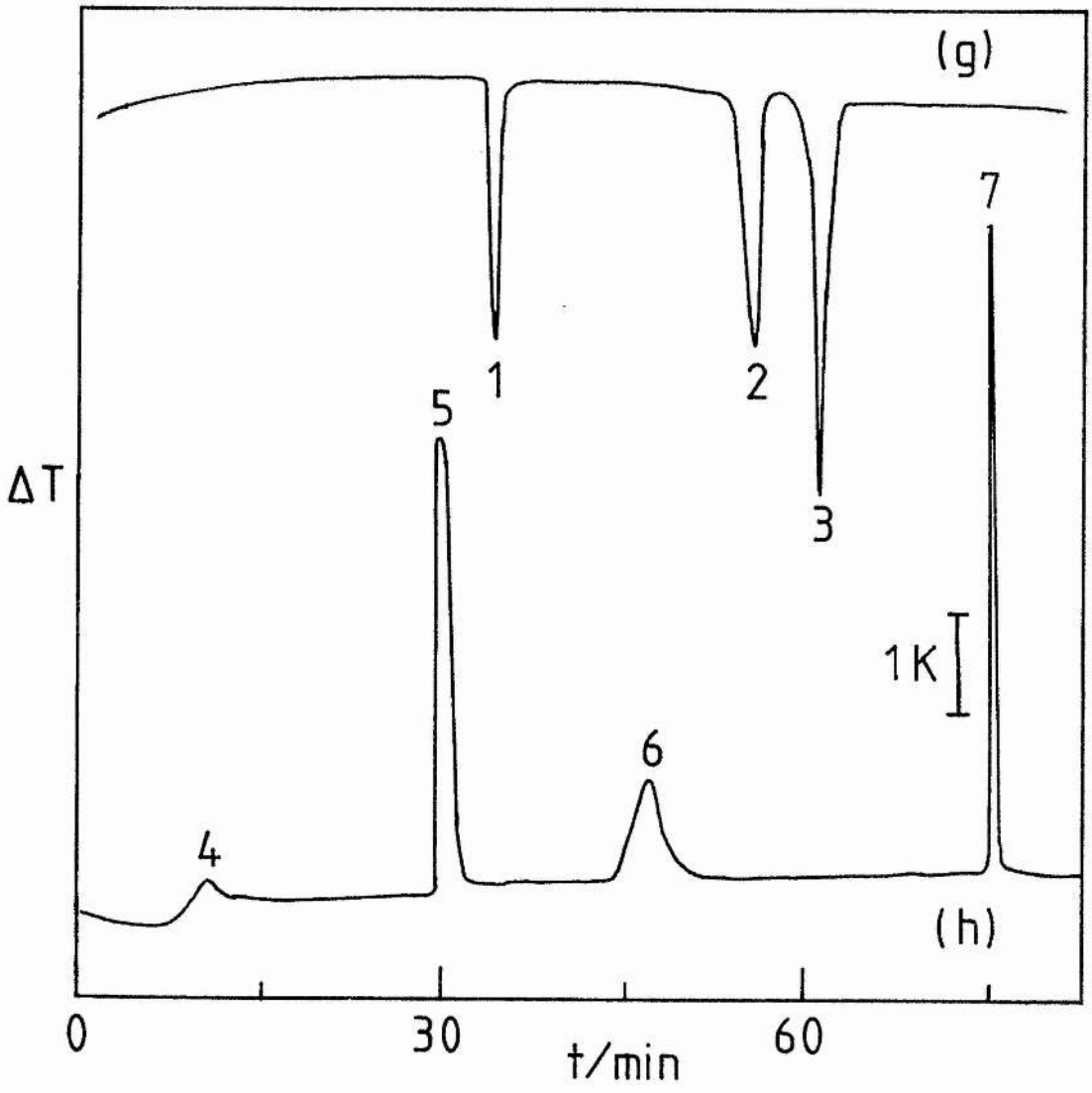

Figure 3.14(g-h) DTA thermogram of a 50 mole% mixture under sealed tube conditions , 300-700 °C. (g) heating 6 K min^{-1}:
1) $\alpha \longrightarrow \beta$ (417 °C), 2) 3CA $\longrightarrow$ C(I) + β (557°C), 3) eutectic (586 °C). (h) cooling 6 K min^{-1} : 4) C(I)-liquidus (678 °C), 5) eutectic (578 °C), 6) β + C(I) $\longrightarrow$ 3CA (532 °C),
7) $\beta \longrightarrow \alpha$ (377 °C).

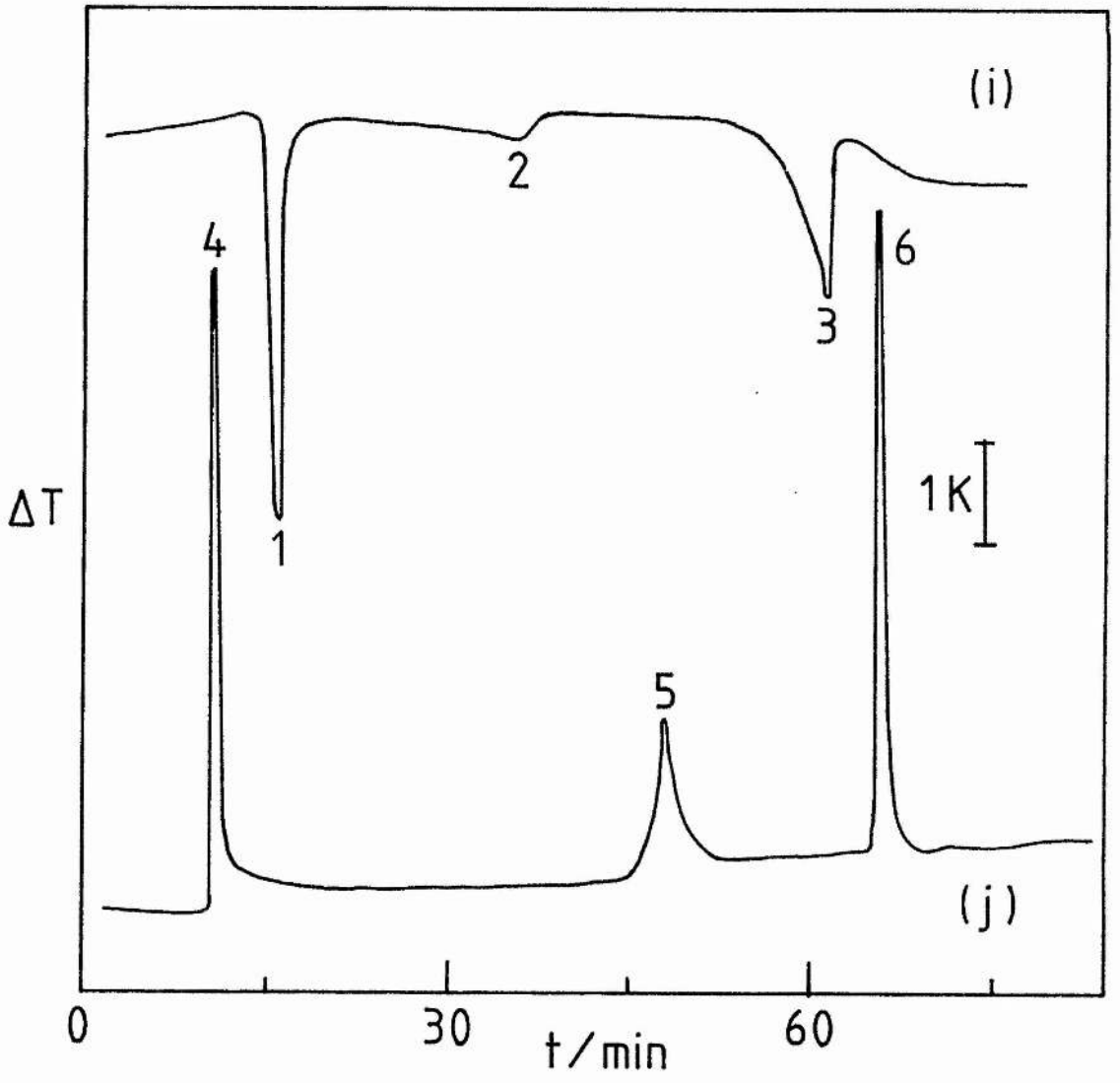

Figure 3.14(i-j) DTA thermogram of a 84 mole% mixture under sealed tube conditions, 300-700 °C. (i) heating 6 K min^{-1} : 1) $\alpha \longrightarrow \beta$ (416 °C), 2) 3CA $\longrightarrow \beta$,solidus (530 °C), 3) β -liquidus (646 °C). (j) cooling 6 K min^{-1} : 4) β-liquidus (638 °C), 5) $\beta \longrightarrow$ 3CA, solidus (467 °C), 6) $\beta \longrightarrow \alpha$ (393 °C).

The morphological (I) ⟶ (II) transition of $CdSO_4$ is observed at 797 ± 5 °C on heating (744 ± 5 °C on cooling) over the composition range 0-29 mole%, while the transition, (II) ⟶ (III), occurs at 838 ± 2 °C (825 ± 7 °C), 0-32 mole% (figure 3.14(a-b),(g-i)). The eutectic horizontal occurs at 585 ± 2 °C (576 ± 3 °C) throughout the range 1-80 mole% (figure 3.14(c-i)), the eutectic composition itself being 64 mole%. Two regions of solid solution, corresponding to the (I) and (II) forms of Ag_2SO_4 are apparent. The low-temperature solid solution, α, appears over a composition range so narrow that the sub-solidus curve cannot be detected, but forms a eutectoid at 97 mole% with the high-temperature solid solution, β. The transition temperature of the eutectoid horizontal is 419 ± 2 °C (395 ± 10 °C) over the composition range 1-98 mole% (figure 3.14(g-i)). Solidus curves for the β phase could not be detected despite making "in situ" visual observations using the optical furnace described in Section 3.1.2.6. The maximum on the liquidus curve at 670 °C, 95 mole%, implies a maximum-melting solid solution. The double salt, $Cd_3Ag_2(SO_4)_4$, (or $3CdSO_4.Ag_2SO_4$), undergoes solid-state decomposition at 554 ± 3 °C, the reverse reaction exhibiting considerable supercooling (491 ± 9 °C), (see figure 3.14(c-h)). The composition of the double salt is indicated by the absence of the eutectoid horizontal at compositions < 25 mole%, this value being determined by use of the very sensitive direct-contact thermocouple arrangement of figure 3.6(b), which proved capable of detecting small quantities of Ag_2SO_4 (< 1 mole%), (see figure 3.14(c-f)). Additional evidence is provided by XRD. Figure 3.15(b) shows the characteristic pattern of the compound while 3.15(a) shows that of the unheated 25 mole% mixture.

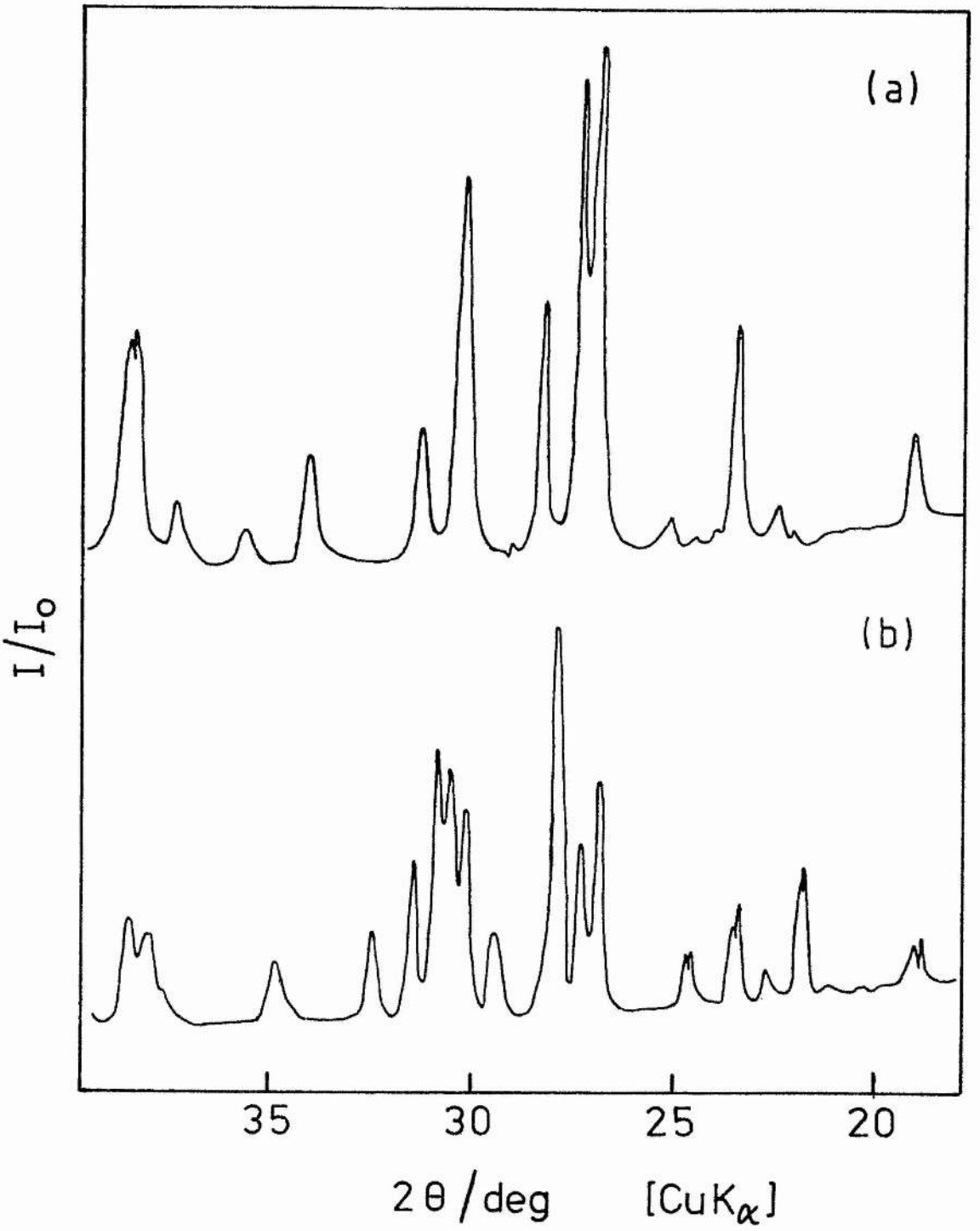

Figure 3.15 XRD patterns of (a) an unheated 25 mole% mixture, and (b), a heated mixture of the same composition. Therefore (b) shows the XRD pattern of 3CA.

No transitions relating to the liquidus curve were apparent between 0 and 10 mole%, nor in pure $CdSO_4$ itself, over the temperature range 860-1030 °C (see figure 3.14(a-b)). Melting must therefore occur above this temperature and from the present study this is estimated to be approximately 1040 °C, which is the value to which the liquidus curve is extrapolated on the present diagram (Margulis[92] extrapolates the melting point to 1130 °C). No transitions relating to the eutectic, CdO - $2CdO.CdSO_4$ were observed.

3.3.4 Comments

The transition temperatures for $CdSO_4$ obtained in the present work fall into the middle range of the literature values, being closest to those of Margulis[91] who reported temperatures of 787 °C and 837 °C for the (I) ⟶ (II) and (II) ⟶ (III) transitions respectively. Because the conditions employed in the high-temperature X-ray study closely approach those of equilibrium, the spread of DTA data around those values underlines the importance of the kinetics of phase transitions and the effect of differing techniques of preparation and pretreatment of materials. The present diagram reinforces the results of the earlier study by Dombrovskya,[8,88] particularly with regard to the values for the composition and temperarure of the eutectic and also the temperature of the maximum in the Ag_2SO_4-liquidus curve. The stoichiometry of the double salt formed in this system is common to the other systems mentioned above[8].

In order to obtain equilibrium transition temperatures and enthalpies of transition, the high-temperature drop calorimeter study was proposed, and this work is described in Chapter 4.

3.4 Conclusions

The phase diagrams presented in Sections 3.2 and 3.3 are, like most high-temperature diagrams, approximations in which the accuracy is limited by the interference of kinetics. Supplementary techniques have been introduced when the principal technique (DTA) has been inadequate in this respect: the optical furnace and the drop calorimeter (Chapter 4). In other instances where DTA has proved to be inadequate, eg in determining the solidus curve in the system $CdSO_4$ - Ag_2SO_4, a technique such as hot-stage microscopy would have yielded more information.

4 DROP CALORIMETRY

4.1 Introduction

The aim of calorimetry is to provide information on the thermodynamics of chemical processes. This is most easily accomplished by making direct measurements of the energy change within a system as a consequence of a chemical reaction (eg heat of combustion, solution, mixing etc) or by combining thermodynamic data (eg Gibbs Functions) from measurements made on pure substances to yield the energy changes for a postulated chemical reaction, or one which may not be measured directly.

In the present work, the objective is to obtain high-temperature thermodynamic data for pure metal sulphates in the solid-state, and all subsequent discussions will be restricted to this type of system. The results of such work directly yield data on heat capacities and enthalpies of transition. If low-temperature data are available and the two sets can be matched with a good degree of accuracy, then high-temperature Gibbs functions of the substance may be obtained.

Before looking at calorimeters in greater detail, some thermochemical background relevant to non-reacting systems is discussed.

As mentioned above, calorimeters measure changes in the heat content of a substance, which at any given temperature T and at constant pressure, is known as the molar enthalpy (H_T^o) and this possesses an absolute value which cannot be measured. Changes in enthalpy are therefore measured with respect to a specific temperature, generally 298.15 K, at which the substance exists in some standard state, usually the most stable crystalline form, at 1 atm pressure. The enthalpy difference or increment of the substance of the system at T > 298.15 K is:

$$\Delta H = H_T^o - H_{298.15}^o \qquad (4.1.1)$$

The superscript (^{o})indicates that some standard state has been selected.

If a substance is cooled from temperature T to 298.15 K, the heat evolved is given by equation (4.1.1)

C_p is the molar specific heat capacity at constant pressure, and it may be defined as the quantity of energy, dq, required to raise the temperature by an infinitesimally small amount, dT. At constant pressure $dq \equiv dH$ and so:

$$C_p = dH / dT \qquad (4.1.2)$$

If C_p is expressed as a function of T then equation 4.1.2 allows evaluation of enthalpy increment over the relevant temperature range.

$$H_{T_2} - H_{T_1} = \int_{T_1}^{T_2} C_p dT \qquad (4.1.3)$$

If the substance undergoes transitions, eg at temperature T_t, then these must be taken into account:

$$H_T^o - H_R^o = \int_{T_R}^{T_t} C_p dT + \Delta H_t + \int_{T_t}^{T} C_p dT \qquad (4.1.4)$$

Where subscript R refers to some initial or reference state. In thermodynamic tables enthalpy is generally expressed as $H_T^o - H_{298.15}^o$. The change of entropy, dS, occurring during a reversible process at constant temperature is:

$$dS = dH / T \qquad (4.1.5)$$

Then from (4.1.2)

$$dS = C_p dT / T \qquad (4.1.6)$$

Integration of (4.1.6) allows the entropy of the system at temperature T to be calculated:

$$S_T^o - S_R^o = \int_{T_R}^{T} (C_p / T) dT \qquad (4.1.7)$$

S_R^o is the standard entropy at the reference temperature. From the Third Law of thermodynamics, the entropy of a perfectly crystalline substance is taken to be zero at 0 K, so absolute entropies may be obtained from heat capacity measurements made to temperatures of

around 4 K and extrapolated to 0 K.

From the Gibbs equation,

$$G^{\circ} = H^{\circ} - TS^{\circ} \qquad (4.1.8)$$

the following equation may be derived:

$$-(G_T^{\circ} - H_{298.15}^{\circ})/\ T = S_T^{\circ} - (H_T^{\circ} - H_{298.15}^{\circ})/\ T \qquad (4.1.9)$$

The term on the left-hand side of the equation is called the Free Energy Function (fef). The change in the standard Gibbs function at any given temperature T, may be calculated from a knowledge of the fefs of the pure compounds since:

$$\Delta G_T^{\circ} = -T\Delta fef + \Delta H_{298}^{\circ} \qquad (4.1.10)$$

where $\Delta fef = \Sigma fef(products) - \Sigma fef(reactants)$

and

$$\Delta H_{298}^{\circ} = \Sigma \Delta_f H^{\circ}(products) - \Sigma \Delta_f H^{\circ}(reactants)$$

Where $\Delta_f H^{\circ}$ refers to the standard heat of formation of products or reactants at 298.15 K.

In the JANAF tables,[11] values of C_p, S°, fef, $(H_T^{\circ} - H_{298}^{\circ})$, and $\Delta_f H^{\circ}$ and $\Delta_f G^{\circ}$ are given for each temperature increment.

The high-temperature Gibbs function relative to a standard state may be calculated, since $G^{o}_{T} - G^{o}_{298.15} = -T\Delta fef$, and this manipulation allows the Gibbs function curves found in Section 1.2.2 to be calculated.

4.2 Calorimeters

This discussion is limited to the types of calorimeters normally used to obtain heat capacity data, in the temperature range 300 - 1500 K. There are two principal designs which are commonly used for this purpose: the Adiabatic and the Drop Calorimeter. The latter is the most widely used and is also the type used in this present work. Therefore it will be fully described in Section 4.3.

Calorimeters suitable for studying other types of high-temperature reactions are reviewed by Kubaschewski and Alcock.[103]

4.2.1 Adiabatic Calorimeter

In this design, shown in schematic form in figure 4.1, there is no exchange of heat between the calorimeter and its surroundings. The calorimeter is maintained at the desired temperature prior to any measurements being made. Heat interchange with the surroundings is minimised by enclosing the calorimeter within a heated adiabatic shield, the temperature of which is accurately controlled to within ±

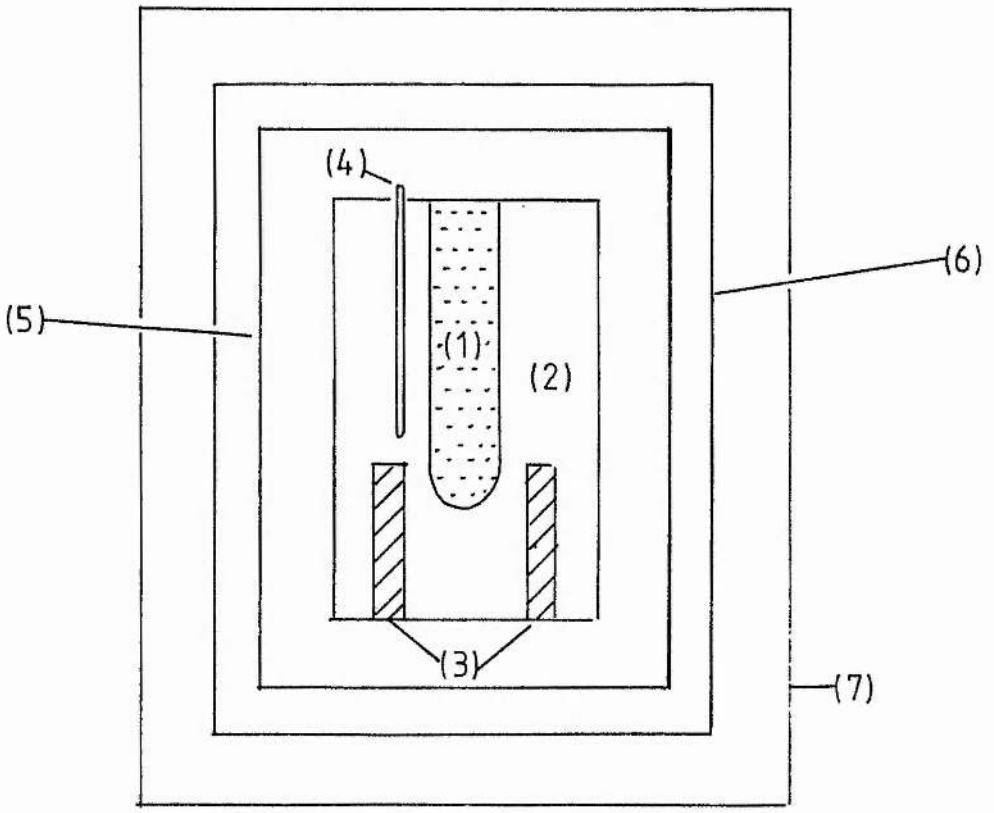

Figure 4.1 Schematic representation of an Adiabatic calorimeter. (1) sample, (2) calorimeter, (3) heaters, (4) thermocouple, (5) adiabatic shields, (6) heated inner shield, (7) outer guard.

0.1 K of the calorimeter temperature. The adiabatic shield is itself surrounded by an inner guard which is kept to within $\pm$ 0.5 K of the shield temperature.

In the design of West and Ginnings,[96] the calorimeter and shield are made of silver and has a maximum operating temperature of 800 K. The calorimeter described by Dench[97] may be used to 1700 K, the calorimeter vessel and shields being constructed from tantalum and the entire assembly contained within a water-cooled vacuum furnace. Temperatures are monitored using Pt-Pt/Rh thermocouples.

An adiabatic calorimeter may be operated in two ways: by continuous heating or intermittent heating. Using the former method the calorimeter and shield are simultaneously heated under constant power input (at a rate of 0.5 K min^{-1}). The calorimeter temperature is recorded as a function of time so allowing the average heat capacity of the calorimeter plus sample to be calculated for any given period. By performing a similar procedure for the empty calorimeter, the heat capacity for the sample alone may be calculated.

Using the intermittent heating method, the calorimeter temperature is measured at equilibrium with no power input. A constant current is then applied for a precisely known period of time and the final temperature of the calorimeter measured, thus allowing the heat capacity of the sample to be determined.

For high-temperature thermodynamic data to be of maximum value they should be used in conjunction with low-temperature thermodynamic data (4 - 300 K). The method used almost exclusively in this temperature range is low-temperature adiabatic calorimetry.[98] The design is essentially the same as that of high-temperature adiabatic calorimeters except that a cryostat bath is necessary to provide a low working temperature and the calorimeter must be operated under a high vacuum (< 10^{-6} torr) to minimise heat loss by conduction.

4.2.2 Drop Calorimeter

This type of calorimeter was first described by Southard (1941)[99] and is shown in figure 4.2. It is variously known as an Isoperibol, Aneroid, Isothermal Jacket, or simply a Copper Block calorimeter.

The sample is contained in a capsule which is suspended in the hot zone of a furnace and held at temperature T, the temperature of interest, and allowed to reach thermal equilibrium. The calorimeter shutter is then opened and the sample is allowed to fall into the copper block. The shutter is closed and the temperature rise measured using a very precise thermometer, eg a quartz thermometer or a platinum resistance thermometer with a Mueller resistance bridge. During the period of temperature rise the calorimeter jacket is held at constant temperature, generally around 298.15 K (with a precision better than $\pm$ 0.005 K). Heat interchange between the block and jacket is minimised by keeping the temperature rise low (< 5 K), by having

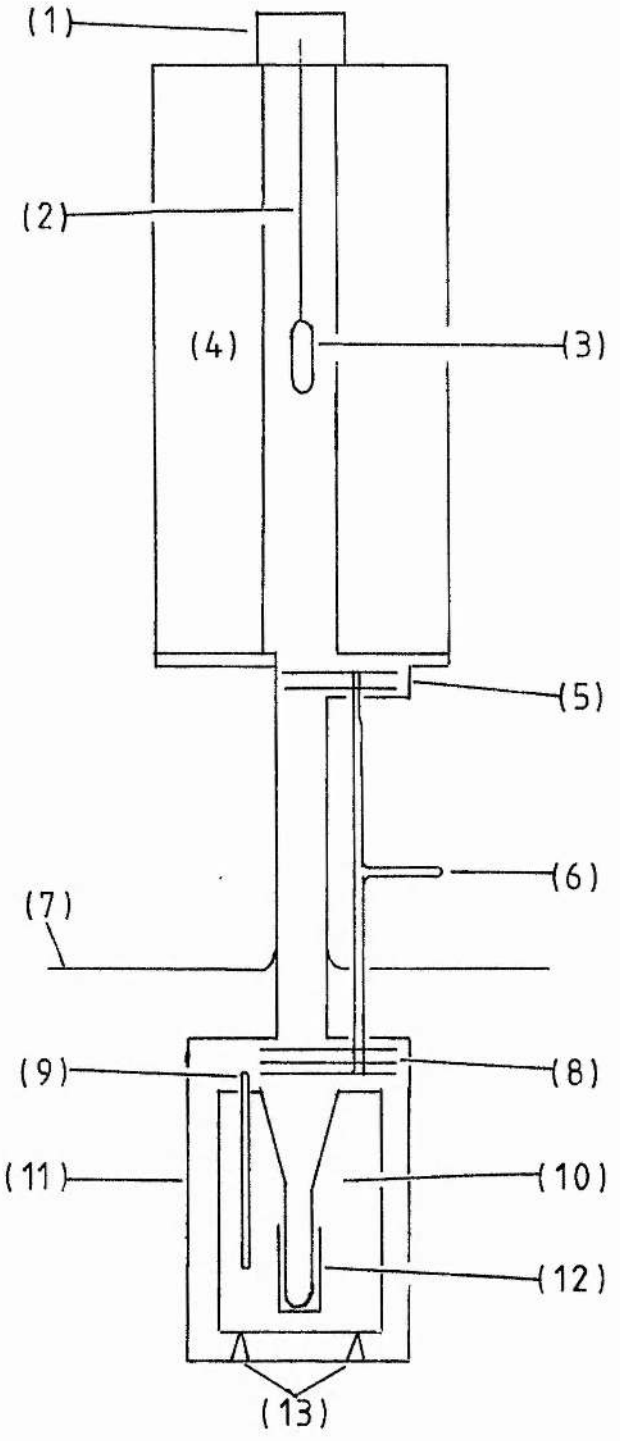

Figure 4.2 Drop calorimeter (after Southard[99]). (1) drop mechanism, (2) drop wire, (3) capsule, (4) furnace, (5) water-cooled shutter, (6) shutter mechanism, (7) isothermal water-bath, (8) lower shutter, (9) temperature sensor (eg. resistance thermometer or quartz oscillator probe, (10) copper block, (11) isothermal jacket, (12) heater, (13) knife-edge block supports.

the surfaces of jacket and block highly polished, and by either filling the gap between the block and the jacket with a gas of low thermal conductivity (eg CO_2), or by evacuation.

The heat capacity of the block assembly around its operating temperature is known as the calorimeter constant, K_b, and is determined by measuring the temperature rise of the block on supplying known quantities of heat, either by input of electrical energy or by dropping a standard calibrant, eg synthetic sapphire, for which the high-temperature heat capacity is accurately known. The heat capacity of the empty capsule must be determined from a separate series of experiments. Possible sources of heat leak must also be accounted for.

4.2.3 Comparison Between Adiabatic and Drop Calorimeters

The drop method described above requires a relatively simple apparatus since the calorimeter is maintained at room temperature. Consequently the sophisticated shields used in the adiabatic calorimeter are unnecessary. In most drop calorimeters simple tubular resistance furnaces are used to maintain the sample at the required temperature with an accuracy and precision as good as that obtained by an adiabatic calorimeter. At very high temperatures (1700 - 3000 K) the problem of radiation loss from an adiabatic calorimeter is so great that the use of the drop method prevails. A drop calorimeter operating in this temperature range has been described by Leibowitz et al.[101] At temperatures just above ambient (300 - 400 K) thermodynamic

data obtained by the drop method are imprecise due to the insensitivity of the calorimeter on undergoing a small temperature change.

It is intrinsic in the drop method that the sample returns to its ground state after the drop (equation 4.1.1); therefore it is not possible to use this method on substances which undergo quenching. This applies particularly to measurements made on liquid materials but may also apply to solid-state transformations.

If the degree of quenching cannot be determined by physical analysis (eg X-ray diffraction) then it will be evident as scatter in the results and the drop method has to be abandoned in favour of adiabatic calorimetry. One interesting way of avoiding this problem was put forward by Tamura et al,[102] who turned the conventional drop method on its head. The sample (BeF_2) was suspended in a thermostat at 298.15 K and dropped into one cell of a Calvet twin calorimeter, which was set to the temperature of interest (400 - 1100 K). Using this procedure, which the authors termed Transposed Drop Calorimetry, the enthalpy of fusion was determined without the complication of vitrification which occurred when the conventional dropping technique was used. Good use was made of of an existing calorimeter which was not particularly suited to heat capacity measurements. However construction of the Calvet calorimeter is itself more complex than that of the copper block type and the latter type would normally be used.

4.3 Experimental : Calorimeter Design

4.3.1 Introduction

The limitations of time (one year to design and redesign the apparatus, have it constructed, calibrate it, and use it to obtain experimental data on compounds of interest) required the chosen design to be simple yet to compromise little in the accuracy and precision of the results.

The design was, to some extent, dictated by existing equipment; namely the quartz thermometer, the temperature probes, and the high-precision thermostat bath. These, while being eminently suitable in many respects, did impose some compromises.

The final design was inspired by the simplicity of the system described by Conard et al.[104] However, the state-of-the-art design of Fredrickson[105] indicated a number of possible improvements and the review by Douglas and King[106] provided a particularly useful general background.

The completed drop calorimeter is outlined in figure 4.3 whilst the entire system (measuring devices, data acquisition system, furnace controller and calorimeter) are shown schematically in figure 4.4.

Figure 4.3 The drop calorimeter used in this work.

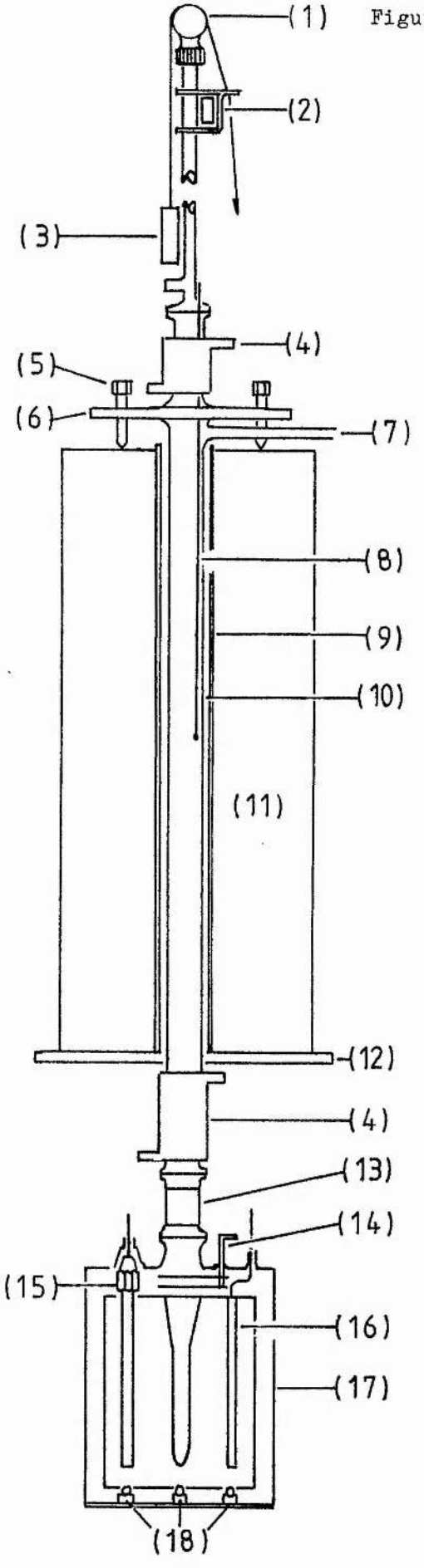

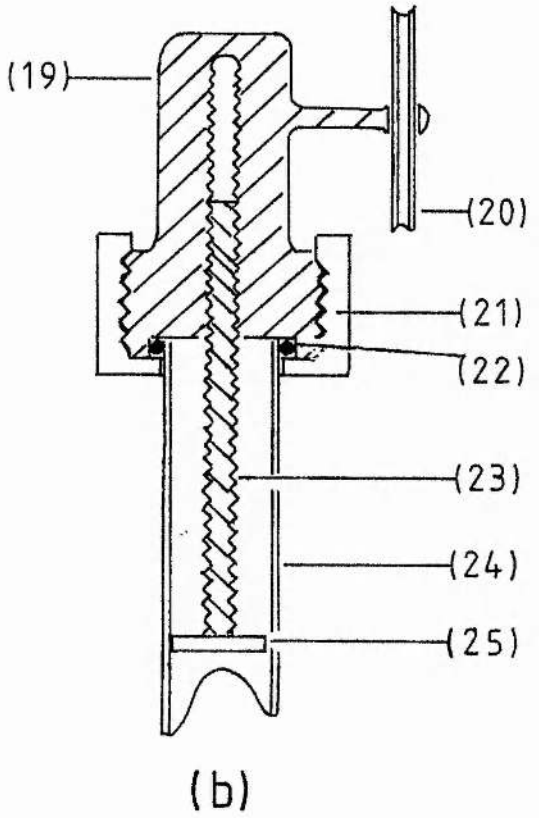

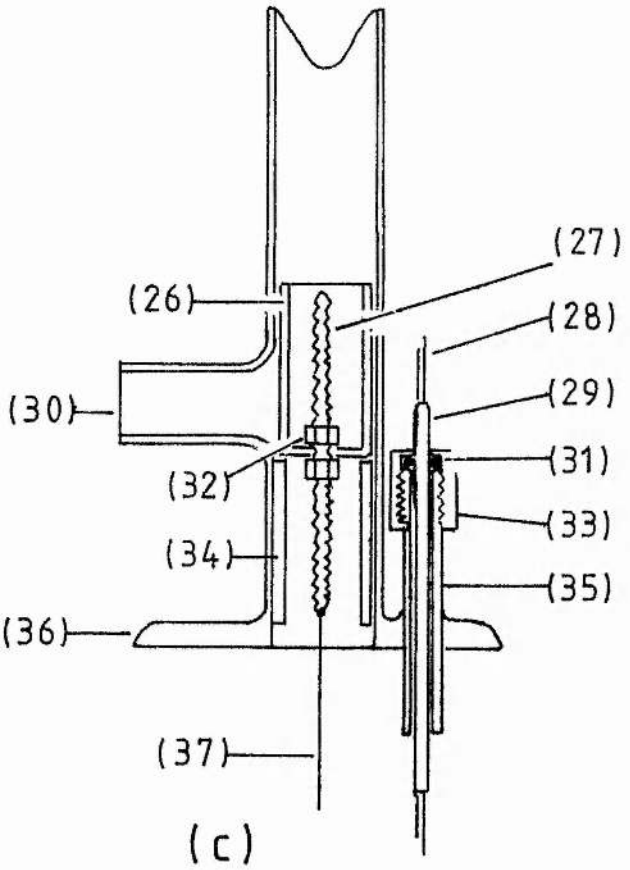

Legend for figure 4.3 The drop calorimeter used in this work.

(a) overall view of the drop calorimeter :

(1) pulley
(2) electromagnet & carriage
(3) carriage counterweight
(4) cooling jackets
(5) height-adjuster screws
(6) brass tripod-support
(7) outlet to vacuum oil-pump
(8) sample thermocouple
(9) ceramic furnace core
(10) stainless steel work-tube
(11) furnace body
(12) lower water-cooled baffle
(13) pyrex inspection window
(14) shutter mechanism
(15) quartz oscillator probe
(16) calibration heater
(17) isothermal brass jacket
(18) copper block supports

(b) pulley head, detail :

(19) brass pulley-head
(20) pulley wheel
(21) brass collar
(22) '0'-ring
(23) drop-height adjuster
(24) stainless steel drop-tube
(25) drop-height adjuster-plate

(c) drop-tube flange, detail :

(26) iron drop-weight
(27) suspension wire adjuster
(28) sample thermocouple
(29) 2-bore alumina rod
(30) e/magnet carriage stop
(31) '0'-ring
(32) adjuster-nut
(33) "Swagelock" fitting
(34) drop-weight stop
(35) thermocouple feed-through
(36) drop-tube flange
(37) suspension wire

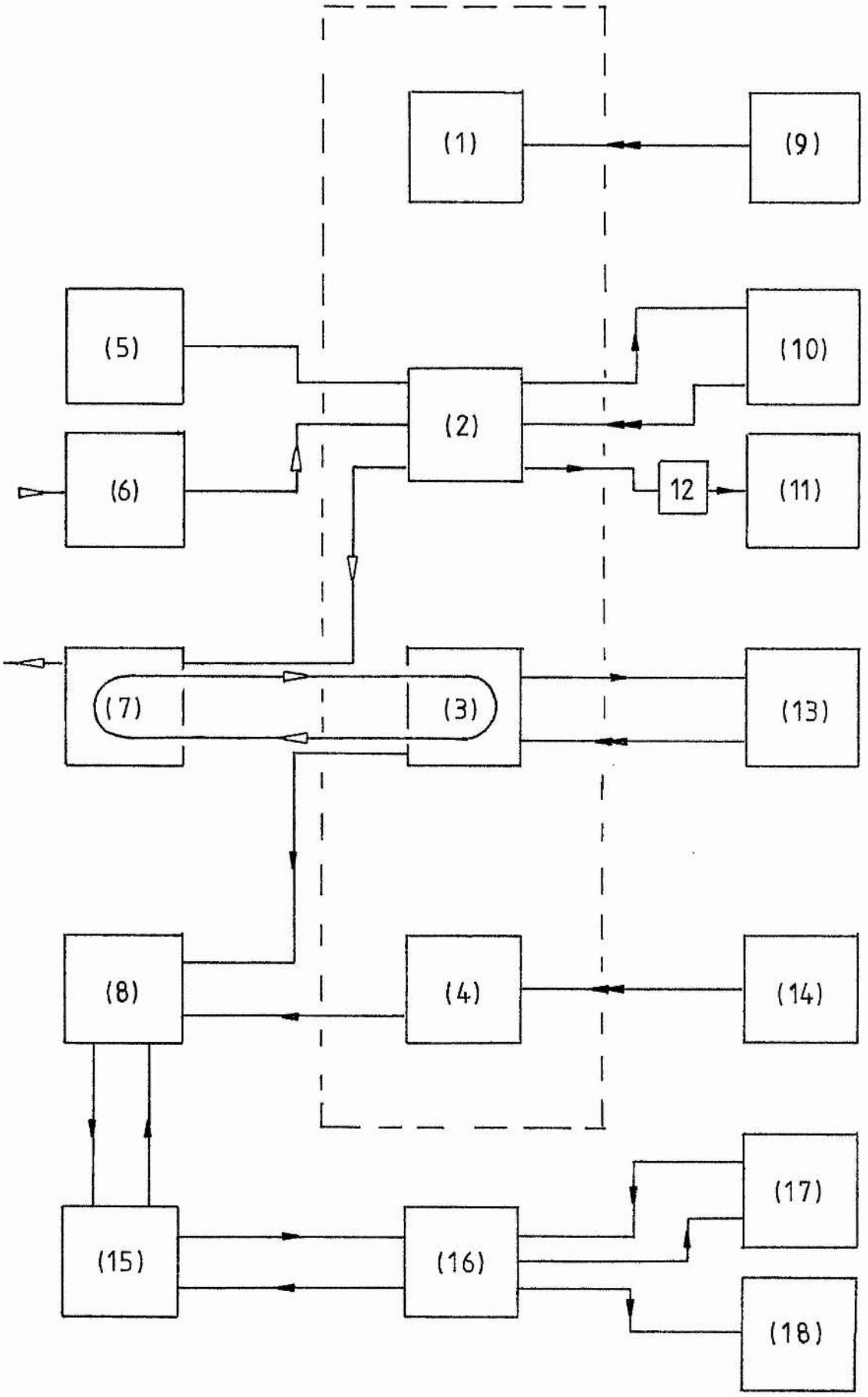

Figure 4.4 Schematic depiction of the drop calorimeter and associated systems.

Legend for figure 4.4 Schematic depiction of the drop calorimeter and associated systems.

(1) drop-weight electromagnet

(2) furnace

(3) LKB precision thermostat water-bath

(4) calorimeter

(5) rotary oil pump

(6) water-cooler

(7) Grant thermostat bath, showing the water-recirculating loop to the LKB bath

(8) HP 2801 A, quartz thermometer

(9) electromagnet power supply

(10) Stanton-Redcroft temperature programmer

(11) Solartron 7045 digital voltmeter

(12) thermocouple cold-junction (ice/water)

(13) LKB proportional controller

(14) custom-built heater calibration unit

(15) custom-built interface unit

(16) BBC microcomputer

(17) Cumana disc-drive

(18) visual display unit

—▶— represents flow of data

—▶▶— represents flow of regulated current

—▷— represents flow of water

Components enclosed within the dotted box are the primary calorimeter components.

For ease of discussion the system is broken down into various components which are described separately, with aspects of design rationale. References are made to literature where appropriate, together with any possible improvements.

4.3.2 Furnace

The furnace was similar in specification to that described by Conard et al[104] being of the straight-wound resistance type. The core was an alumina tube 60 cm long and 6.2 cm od. It was evenly wound with Kanthal A wire (17 SWG), having a resistance of 40Ω at 20 °C, including connections. The windings were covered with alumina cement and the core was gradually heated over a period of three days until the cement was dry and had no obvious cracks. Insulation was provided by encasing the core within Kanthal M.I.28 insulating bricks to a depth of three bricks all round. This assembly was enclosed within stainless steel sheeting. A stainless steel work-tube, 3.8 cm od and 112 cm long was held in position over the furnace on a brass tripod to which it was welded. The feet of the tripod provided adjustment to facilitate vertical alignment of the work-tube. The work-tube was terminated at each end by Edwards vacuum flanges which work by compressing an O-ring between two mating flanges. Stainless steel tubing attached the work-tube and hence the entire calorimeter to a rotary oil pump which maintains a vacuum < 0.1 torr.

The furnace body rested on a heavy-duty steel frame. Between the top of the brass plate and the top flange was a double-wound copper cooling-coil. At the bottom of the furnace, also making contact with work-tube there was a large circular copper cooling-coil. Finally between this and the bottom flange was a brass cooling-jacket which allowed direct contact between the flow of water and the work-tube. Water from the mains supply flowed through a water-cooler at the rate of 1.2 l min^{-1}. It emerged from the cooler at a temperature of around 3 K less than mains supply. The water travelled first through the cooling-jacket then to the large copper coil and finally passed through the top cooling-coil. This arrangement prevented heat conduction to the calorimeter, which was further reduced by a short length of pyrex tubing (4.0 cm od) connecting the calorimeter jacket to the work-tube.

The furnace was found to have a hot zone of length 6 cm (uniform to $\pm$ 1 K at 1000 - 1200 K) the centre of which was located 45.2 cm below the face of the drop-tube flange.

Furnace temperature was regulated using the Stanton-Redcroft LVP programmer described in Section 3.1, which provides isothermal control with a stability better than $\pm$ 0.5 K.

The temperature of the sample suspended in the furnace was measured using a Pt/Pt-13%Rh thermocouple which ran through a two bore alumina rod, held in place by a vacuum-tight fitting which fed through the drop tube flange. The thermocouple (length 150 cm) was continuous

as far as the cold-junction where it was soldered to copper-conductor wire. The cold junction fitted tightly into a glass finger filled with liquid paraffin which was placed in an ice-water bath, which was stirred 10 minutes before the sample was dropped.

The thermocouple emf was read from a Solartron 7045 digital voltmeter and the emfs may be interpreted using the IPTS-68 tables.[80]

4.3.3 Calorimeter

The calorimeter (shown in figure 4.3) consisted of a copper block, 10 cm in diameter, 16 cm high. The capsule fitted snugly into a recess 14 cm deep, the sides of which were angled at 30 ^{o} to the vertical to allow the sample to fall more easily. Two wells, 180 ^{o} apart with their centres 3.5 cm from the calorimeter centre and 14 cm deep, accommodated the quartz probe and the calibration heater. The well for the heater was 0.7 cm in diameter. The heater consisted of a coil of insulated constantan wire which was inserted in the well. This was filled with molten Wood's metal thus providing extremely good thermal contact with the block.

The height of the block was dictated by the length of the available quartz probes. The block was supported by three small glass balls 0.3 cm in diameter which rested on brass stubs on the bottom of the calorimeter jacket. A gap of approximately 1 cm was kept between the surface of the block and the calorimeter can which were both chromium plated in order to reduce heat losses by radiation.

The lid of the jacket had a number of chimneys to allow the heater wire and probe lead to exit. These were made vacuum-tight with Araldite adhesive. The lid also supported the shutter mechanism which consisted of two aluminium plates with narrow slits just large enough to accommodate the drop wire. Forcing the two remote levers together caused the shutters to close over the centre of the calorimeter well, while forcing the levers apart had the opposite effect. The shutters were situated in the gap immediately above the block.

The lid itself fitted inside the jacket against a flange sited at the top of the jacket. A heavy brass ring screwed along a thread on the outside of the jacket, compressing an 'O'-ring which was situated between the lid and flange thus giving a vacuum-tight seal. Further compression was achieved by tightening six screws, which were evenly spaced around the top of the ring.

4.3.4 Precision Thermostat Bath

An LKB 7600A Precision Thermostat Bath/Proportional Controller was used. The calorimeter jacket was totally submerged in water, the level of which reached the flange at the top of the jacket. The calorimeter jacket did not rest on any part of the water bath and thus its mass was borne by the brass tripod. This was done in order not to impede the stirring action on which precise temperature control depended.

The bath temperature was controlled in much the same way as the furnaces described in Chapter 3. The sensor used in this instance was a thermistor which was located near the bottom of the container. The bath vessel (volume 6 l) had windings along its entire length. A steady temperature was maintained by a proportional control unit, on which the desired temperature was set. The temperature control is claimed to be ± 0.001 K over 48 hours, the temperature rising 0.001 K per K change in ambient temperature. In fact, over the duration of an experiment, 2-4 h, the bath temperature was maintained with a precision of ± 0.0005 K. In order to control the temperature with such precision, the bath temperature had to be 10 K above ambient. However, the calorimeter was operated in a small room with a furnace and water-cooler running continuously and therefore this was not possible; the ambient temperature rose to bath temperature (298.15 K) even with the room's refrigerant unit operating continuously.

It was necessary to pump water through the cooling jacket of the bath. This was done using a Grant thermostat bath which circulated the water through a loop. This thermostat bath itself required to be force-cooled, as otherwise it also eventually reached ambient temperature. Cooling was achieved by allowing the cooling-water emerging from the various furnace cooling jackets to pass through a double coil of plastic tubing which was placed in the small thermostat bath. The most satisfactory setting of this thermostat bath was 296 K.

The temperature of the precision water-bath was measured using a second quartz probe.

4.3.5 Drop Mechanism

This problem has previously been tackled in a number of ways. Perhaps the most sophisticated system is that described by Fredrickson[105] where the capsule was suspended on a thin wire which was attached to a magnetic weight positioned in a drop tube. The weight, in turn, was suspended by a metal tape wound on the drum of an eddy current brake. When the current to the brake was removed the weight was released and as it approached the calorimeter it passed through a sensor coil. The current induced in the sensor coil activated the eddy current brake and this allowed the capsule to decelerate smoothly as it fell into the calorimeter block. The operation is very reproducible and the sample accelerated to almost the maximum possible rate.

At the other extreme, the sample may be suspended within a furnace on a thin platinum filament strung across heavy duty platinum electrodes. A current is passed through the filament, which melts, thus allowing the sample to fall freely.[107] In the calorimeter of Conard et al,[104] the capsule was attached to a suspension wire (Pt-13%Rh) the top of which had a bead that rested on a slit in a glass rod. On pulling the rod the wire slipped from the slit, allowing the capsule to fall freely.

Similar dropping techniques are used in a number of designs; however, while the sample drops freely, it is not easy to retrieve the capsule without dismantling at least part of the apparatus.

With the present calorimeter it was decided to make easy retrieval (and changing) of the sample a priority, but without compromising on the drop rate or reproducibility of the dropping procedure.

The capsule was attached by a length of Pt-13%Rh wire, 0.05 mm diameter, to a hollow iron weight, 1.7 cm diameter, 2.5 cm long and 20 g mass. The weight was free to move throughout the height of the tube. A hollow brass ring near the bottom of the tube prevented the weight falling into the furnace, while an adjustable screwed rod which accurately set the drop height was inserted at the top of the tube. An electromagnet, 5 cm in diameter and energised by a 12V, 1A power supply, was mounted on a carriage and this slid freely along the length of the drop tube. The bottom of the carriage came to rest on a right-angled port protruding from the tube. A thick copper cable ran through the carriage, one end being attached to a brass ring, the other to a large counterweight which ran over a pulley attached to the top of the drop-tube by an 'O'-ring and collar. The pulley also housed the drop height adjuster.

With this arrangement the electromagnet was always pulled to the top of the drop tube and stopped by the pulley head. To drop the sample the magnet was de-energised and because the entire calorimeter was operated under vacuum, neither the capsule nor the drop-weight suffered air turbulence during the descent and hence the capsule dropped absolutely vertically. To retrieve the capsule the calorimeter was let up to air, the magnet was energised and pulled down until it caught the weight. The magnet was then carefully released pulling the weight and hence the sample back to position. It is important that this last operation be carried out at atmospheric pressure since if the magnet "loses" the weight, then descent of the capsule will be slow. Raising the weight under vacuum causes the capsule to oscillate and magnet failure at this point would probably result in a broken capsule. At worst this would necessitate dismantling and cleaning the calorimeter. Even if the capsule itself remained intact but the drop-wire broke, the calorimeter would have to be removed from the water bath and the capsule retrieved using tweezers. If the glass hook was broken, a glass or metal tube (1 cm od) with the inside rim thickly coated with Araldite resin could be carefully inserted into the well and attached to the top of the capsule. The adhesive would then be allowed to set and the tube removed with the capsule attached to it. Any fragments of glass could be removed using a blob of "Blutack" on a glass rod.

Under normal circumstances the sample is left in the furnace for up to two hours to equilibrate before dropping and any motion is damped-out during this time.

Appendix 1 contains formulae to enable the calculation of the drop wire length and the height-adjuster distance.

4.3.6 Temperature Measurement

Temperature measurement was made using a Hewlett Packard 2801A Quartz thermometer and two 2850C type probes. One probe, serial number 743-5, was inserted in the calorimeter block, while probe 704-41 was placed in the water bath. A portion of the armoured cable between the top of the probe and the calorimeter chimney was removed to prevent heat leakage. The exposed cable was covered in Araldite to vacuum seal it. This was the only modification made to this device.

The probes were calibrated using a procedure outlined in the operating manual. The probe was placed in an ice-water mixture contained in a Dewar. The scale-factor thumbwheel switches on the back of the instrument were set (9220 for 743-5 and 9281 for 704-41) and the fine-zero potentiometer adjusted until the display read zero. The probe was then removed from the bath and allowed to come to ambient temperature before being once more immersed in the bath. This was repeated several times for each probe until no further adjustment was required. The accuracy of this calibration is stated as $\pm$ 0.01 K

with a precision of ± 0.0001 K which is adequate for present purposes.

A correction for non-linearity of frequency with temperature has to be added to the display reading and this is given in the calibration charts provided for each probe; for both probes this value is - 0.01 K in the temperature range 290 - 300 K with the trim switches set as above. Consequently the bath temperature was set so that the display read approximately 25.01 ^{o}C, which is equivalent to 298.15 K, and the former temperature reading should be entered in the appropriate calculations.

The thermometer unit had outputs to a Hewlett-Packard printer and to a remote switching device and these were used to interface the thermometer to the microcomputer. This required an additional piece of custom-built circuitry. The output from the thermometer was standard BCD (Binary Coded Decimal) format; however, the output level is high, 35 V for binary "0", 0 V for a "1". The standard TTL levels on which the microcomputer operates are +5 and +1 volts respectively. The interface unit however, translated the voltage level from the thermometer to the TTL levels used by the BBC microcomputer. The level was shifted using opto-isolators and additional buffering was provided to clean up the signal. This signal was then fed to PIAs (Peripheral Interface Adaptors) which sent data to the 1 MHz bus on the microcomputer.

For a useful introduction to micro-processor control systems see reference 108.

4.3.7 Data Acquisition

This was built around a BBC model "B" microcomputer. A Cumana 40-track disk drive with 5.25 inch floppy disks was used for permanent data storage (each disk storing up to 100 kbytes of information after formatting). Video output was to a Zenith green-screen monitor.

The microcomputer is built round the 8-bit 6502 processor. It has 32 kbytes of Random Access Memory (RAM) and supports high-resolution graphics. The present machine was fitted with the OS 1.2 operating system and Acorn DFS (Disk Filing System). The latter specified the disk format as single-density. The machine featured a number of useful standard interfaces including serial interfaces, a parallel printer-port, disk port and the 1 MHz bus mentioned above.

This computer uses the BASIC language and the interpreter supplied with the machine provides a very fast sophisticated implementation of the language. This dialect of BASIC is highly structured particularly with the provision of named procedures, eg PROCname (X,Y,Z), which is similar to CALL-ing a subroutine in FORTRAN. Programmes can also be written in mixed BASIC/assembly language (a fast low-level language).

4.3.7.1 Using the Microcomputer System

The system used a master disk containing the important programmes in conjunction with slave disks on which data-files were stored for subsequent retrieval. The Drop Calorimeter Master Disk was inserted in the drive and the system "booted" by holding down the SHIFT key and pressing the BREAK key simultaneously. The master disk contained a suite of three principal programmes: HP, DISPLAY and DELTA_T, for data acquisition, display (graphics and "screen dump") and data fitting/calculations respectively. Also on disk were utilities; FORM40 for formatting blank disks (see reference 109) and EPSON which configures the microcomputer for use with an Epson parallel—printer. This latter programme was automatically run on booting since programme DELTA_T has a printer option included. Also on the master-disk was the programme !BOOT which was run on auto-boot; this configured the user-defined keys and chained the programme MENU which allowed the desired programme or utility to be selected.

All programmes were written in BASIC or BASIC/assembler with the exception of !BOOT. The present author has designed the system to work on a menu-driven basis and thus very little knowledge of even simple BASIC or operating system commands is required.

Once the required item from the main menu has been selected, the user is prompted to insert the disk to which data is to be written or from which data are to be read. The author has assumed that the user wishes to keep data files relevant to one particular series of results on the one disk, especially since each disk will hold only 20-25 data

files. Each temperature reading constitutes 6 bytes of disk space and so the space used per file = no.of points x 6 and is usually 4-6 kbytes. Whenever a disk changeover is required this is indicated by an on-screen prompt.

Data-disks must be formatted before use (details of the formatting procedure are described elsewhere[109]) but the formatting programme (FORM40) can be selected from the main menu. After completing data-acquisition it is recommended that the newly created data-file be "backed up" onto another disk. This is accomplished using the command *COPY0 0 <FILENAME>. Again this can be invoked from the main menu complete with on-screen instructions for use.

4.3.7.2 Programmes

HP This programme, author J.R. Bews, collects data from the quartz thermometer which it prints on screen and places in an area of the computer's memory (buffer). If the buffer overflows or the user terminates data-acquisition by pressing the ESCAPE key, data are written from the buffer to disk in real-number format (6 bytes) using BASIC file commands. Information on the sample, furnace temperature, water-bath temperature, number of data points, and sampling interval is also written to disk. This programme is written principally in assembly language, for greater speed and easier manipulation of the computer's registers.

DISPLAY This programme, written in BASIC by the present author, reads data from a disk-file and displays them either on high-resolution graphics or gives a screen dump of data (format 25 rows by 4 columns). It is useful for verifying data.

DELTA_T This BASIC programme, which was also written by the present author, is listed in Appendix 2 and may be briefly described as follows. Data are read from disk (PROCread_file) into an array and are sorted (PROCtmaxmin) to find the data-point at which the temperature, T_o, begins to rise markedly (> 0.0005 K in 10 s); the corrected temperature rise is then computed using Newton's Law of cooling, according to the method of Rossini[110] and described specifically for a copper block calorimeter by Stout et al.[111] This procedure is outlined below.

Newton's Law of cooling is:

$$dT / dt = k(T_i - T_B) \qquad (4.3.1)$$

Which is expanded and rearranged to give:

$$\theta_i = k((T_i + T_{i-1}) / 2 - T_B)(t_i - t_{i-1}) \qquad (4.3.2)$$

Where θ_i is the temperature correction,(K); k is Newton's Law heat exchange coefficient(s^{-1}); T_i is the temperature of the calorimeter block; T_B is the temperature of the water bath, ie the surroundings (K); t is time (s); and i is the index for sequential data points.

Equation 4.3.2 is used to calculate the temperature correction θ_i, due to heat exchange between the calorimeter block and the isothermal jacket over the time interval between two sequential temperature readings which is usually 10 s.

At any given data point (T_n, t_n) the total accumulated temperature correction ΔT_n is:

$$\Delta T_n = \sum_{i=1}^{n} \Theta_i \qquad (4.3.3)$$

Integration of equation (4.3.1) gives

$$\ln(T_i - T_B) = k(t_i - t_f) + A \qquad (4.3.4)$$

Where t_f is the time of the final measurement. $A = \ln(T_f - T_B)$, which is a constant and T_f is the calculated final temperature for the experiment. Equation (4.3.4) is therefore of the form:

$$y = mx + c \qquad (4.3.5)$$

The values for k and A may be obtained for each experiment by fitting the data at the end of the experiment to an equation of form (4.3.5) by the method of least-squares. See figure 4.5 for an illustration of a typical temperature profile.

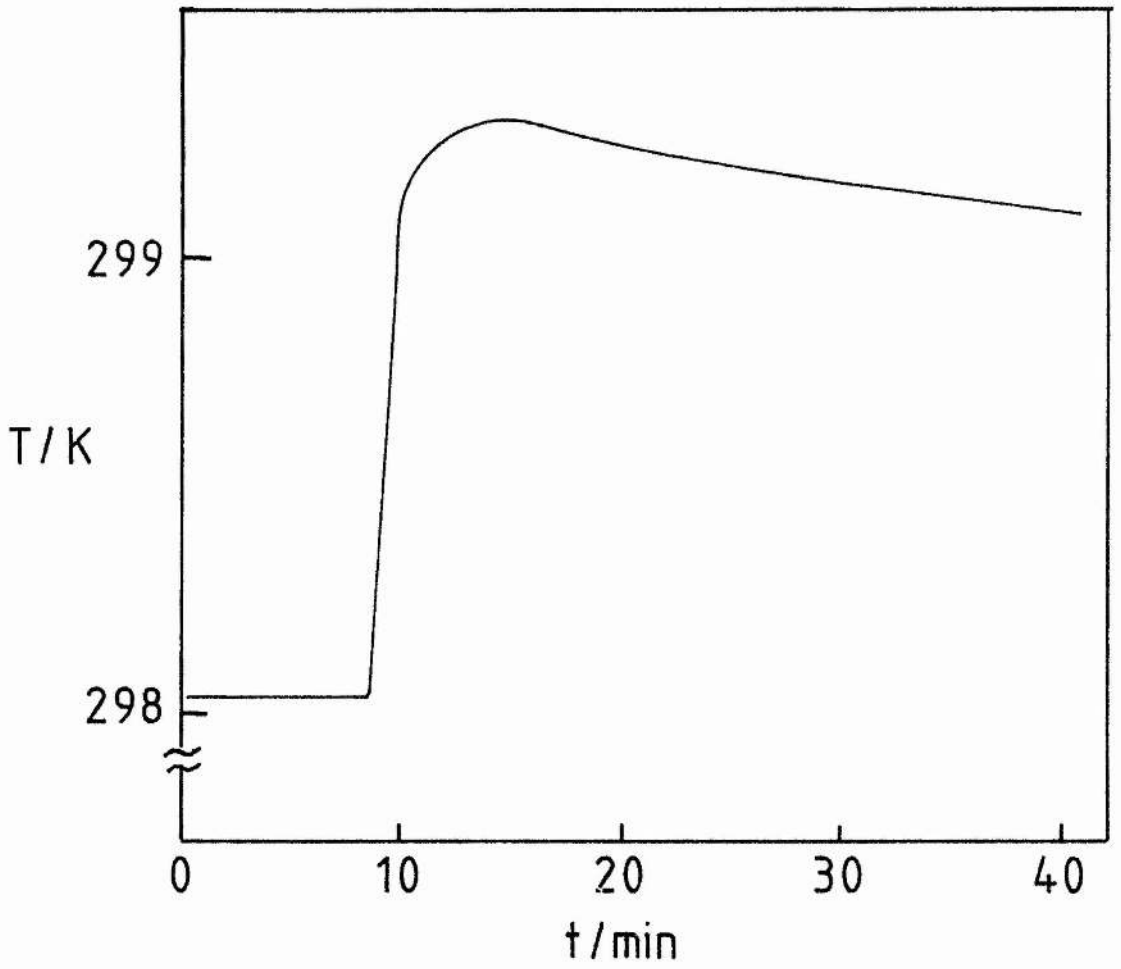

Figure 4.5 A typical temperature-time trace for a drop, where T is the block temperature.

The calculated final temperature T_f is:

$$T_f = T_B + \exp(A) \qquad (4.3.6)$$

A section of the programme (PROCcalkA) calculates a least-squares value (PROCleast_squares) for k and A, based upon the four last data-points - initially in 10 s increments (PROCgrad_icept.) - and equation (4.3.4). It uses these values of k and A to extrapolate back a further two data points and the calculated value for T_i at this point is compared to the actual value; if the difference between the two is less than 0.00015 K then that value of T_i is included in the least-squares calculation and new values for k and A are computed. This procedure is repeated until the difference between the two values exceeds 0.00015 K and the immediately preceding values of k and A are stored. The initial increment between four final points is 10 s; this is increased in steps of 10 s to a final value of 100 s and the k value with the highest correlation coefficient is used in equations (4.3.2) and (4.3.6). It was found that k was generally in the range $3 - 4 \times 10^{-5}$ s^{-1}.

PROCdelta_t calculates θ_i and T_F. The corrected temperature rise ΔT_c is given by:

$$\Delta T_c = T_F - T_o \qquad (4.3.7)$$

where $T_F = (T_f + \Delta T_f)$, the final temperature reading corrected for

heat-exchange with the surroundings.

Thus the above procedure selects the time when the calorimeter is undergoing steady heat-exchange with the surroundings and based on this proceeds to calculate the temperature correction. In addition PROCcal_const calculates the block constant K_b, based upon electrical calibration; for which the user is prompted to input voltage and time data. PROCenthalpy calculates the enthalpy increment, $H^o_T - H^o_{298.15}$ for a drop based on the value of block constant, K_b, and the corrected temperature rise ΔT_c, calculated earlier in the programme.

4.4 Calibration of the Drop Calorimeter

4.4.1 Electrical Calibration

The block constant, K_b, is equal to the amount of energy required to raise the temperature of the block by 1 K at 298.15 K. This is conveniently done by passing a known amount of current through a heater for a fixed period of time, and noting the temperature rise, ΔT_c; thus:

$$K_b = I^2 R t / \Delta T_c \qquad (4.4.1)$$

where t is the time (s) that current I (A) is passed through a heater of resistance R (Ω). K_b is determined for a number of different

temperature rises equivalent to those which the block will normally be subjected to during drops.

Calibration was accomplished using a custom-built constant-current supply unit. This unit, along with the quartz thermometer and precision thermostat bath had previously been used in earlier solution-calorimetry studies.[112,113]

The heater element is a coil of constantan wire (40 SWG), resistance 20.67 Ω at 298.15 K. The heater coil is connected to thicker constantan leads (~5 Ω) immediately at the block surface and this connection is held in place by a blob of Araldite resin.

Constantan has a very low temperature coefficient (0.00001 ΩK^{-1}) and so the change in resistance of the heater coil as the temperature of the block rises is negligible and so the current remains constant.

The heater coil is connected to the constant-current supply unit and the current passing through the heater also passes through a standard 10.000 Ω resistance across which the voltage drop is measured, allowing the current flowing through the heater to be calculated. Voltage is measured using a Solartron 7045 digital voltmeter. The voltage is usually set to 4.000 V and the variation of this during the experiment is ± 0.001 V. The time for which current is passed is recorded on a Jacquet 309e stopwatch, with a precision of 0.01 s.

The calibration constant for the block, K_b, was determined from 15 experiments, the results of which are shown in Table 4.1 . The average value of K_b is 4235 ($\pm$ 5) J K^{-1}. The precision of this figure (0.1 %) may be considered very good when compared with the calibration results of Marchidan[114] who obtained a precision of 0.1 % and Fredrickson et al[105] who obtained a precision of 0.05 %.

4.4.2 Calibration By Dropping

The block constant, K_b, has been determined by the method of electrical calibration as described in Section 4.4.1. This alone is not enough to work on; the overall performance of the calorimeter must be assessed in terms of both the accuracy and precision of the thermodynamic data obtained. This is accomplished by dropping a standard material for which the high-temperature thermodynamic data are precisely known. National Bureau of Standards, Standard Reference Material NBS SRM 720 (synthetic sapphire) is universally used for this purpose. A variety of different materials, however, are used to encapsulate the calibrant or the sample, and the enthalpy increments for the chosen material must be established over the temperature range of interest. This is necessary, because during a drop a certain amount of heat is lost by radiation and this is dependent on the rate of drop, the emissivity of the material and the surface area of the capsule. The drop wire attached to the capsule will also have a certain heat contribution. Assuming complete reproducibility in the drop procedure and fabrication of the capsule, then for experiments

Table 4.1

Determination of Calorimeter Constant, Kb

Heater Voltage / V	Time Current Passed / S	ΔT_c / K	Kb / JK^{-1}
4.003	89.98	0.0703	4238.5
3.999	120.05	0.0939	4228.4
4.002	180.05	0.1406	4240.8
3.998	240.02	0.1871	4239.3
4.000	300.01	0.2345	4231.1
4.000	360.00	0.2817	4227.0
4.000	600.04	0.4690	4231.7
3.997	720.00	0.5624	4227.2
4.000	900.06	0.7032	4232.8
3.998	1080.08	0.8430	4233.2
3.999	1200.70	0.9340	4247.0
4.004	1500.07	1.1737	4235.3
4.001	1800.00	1.4058	4236.8
4.001	1800.11	1.4058	4236.9
3.998	2400.00	1.8732	4233.0

conducted with a sample or calibrant, the heat contribution of the capsule is merely subtracted to give the heat contribution of the sample alone. Thus it is necessary to generate a precise series of results for an empty capsule to allow a smooth graph of the data to be plotted, or for the data to be fitted to an equation as a function of T.

4.4.2.1 Calibration For Silica Glass Capsules

The material used in the present study was silica glass. This was chosen for two major reasons: sealed capsules are necessary to prevent serious decomposition of the sulphates and, given the limited facilities available to the author, it was felt that silica was easily sealed under vacuum and was resistant to corrosion at high temperatures. Platinum was considered as an alternative, but it is prohibitively expensive and difficult to seal. Silica capsules were successfully used by Conard et al.[104]

The major drawback when using silica as opposed to platinum is the high mass : strength ratio of silica. When the calorimeter was designed it was thought best to keep the temperature rise of the block to between 1.5 - 2.5 K to minimise loss by heat interchange with the surroundings; hence the use of a small capsule, 6 cm long, 1.0 cm od. To minimise the heat contribution of the capsule a wall diameter of 0.5 mm was selected.

A series of experiments was conducted using 2.313 g of Suprasil silica (0.03850 moles) which was fabricated as a container 6.2 cm long. The capsule was evacuated and filled, at room temperature, with He at a pressure of 0.2 atm. He possesses a thermal conductivity five times greater than that of air and allows heat to diffuse more quickly through the pores in a powdered sample and this allows the sample to reach thermal equilibrium with the copper block much more quickly. Appendix 3 gives the procedure for dropping and retrieving a capsule.

Due to failure of the capsule, only seven drops were completed. However, the results of these seven drops, which were done in the temperature range 1023.15 - 1162.15 K are shown in graphical form in figure 4.6. Table 4.2 shows $H^{o}_{T} - H^{o}_{298}$ for the present results and compares these with the results obtained by Conard et al, expressed as an equation of the form:

$$(H^{o}_{(T)} - H^{o}_{298.15})/J\ mole^{-1} = -27286.5 + 64.1018\ (T / K) + 4.18936 \times 10^{-3}\ (T / K)^{2} + 23.2608 \times 10^{5}\ (T / K)^{-1} \qquad (4.4.2)$$

The average deviation of the present results from those of Conard is - 1.6 % ; when one considers the different samples of glass used and the difference in drop methods (Conard uses the free-fall method), the results are very good. The discrepancy in the results is consistent with the mode of drop: using the present drop method, friction between the iron drop-weight and the drop-tube slows the

Table 4.2

Enthalpy Increment of Silica Glass by Drop Calorimetry

T / K	ΔT_c / K	ΔH / J	$H_T^o - H^o_{298.15}$ / kJ mole^{-1}	$H_T^o - H^o_{298.15}$ (Sridhar[104]) / kJ mole^{-1}	Percentage Deviation from Results of Sridhar
1023	0.4012	1699.1	44.132	44.958	-1.8
1035	0.4100	1734.5	45.052	45.804	-1.6
1042	0.4162	1762.5	45.779	46.299	-1.0
1102	0.4500	1905.9	49.504	50.491	-2.0
1120	0.4620	1956.6	50.821	51.850	-2.0
1142	0.4797	2031.0	52.753	53.428	-1.3
1162	0.4911	2079.7	54.018	54.869	-1.6

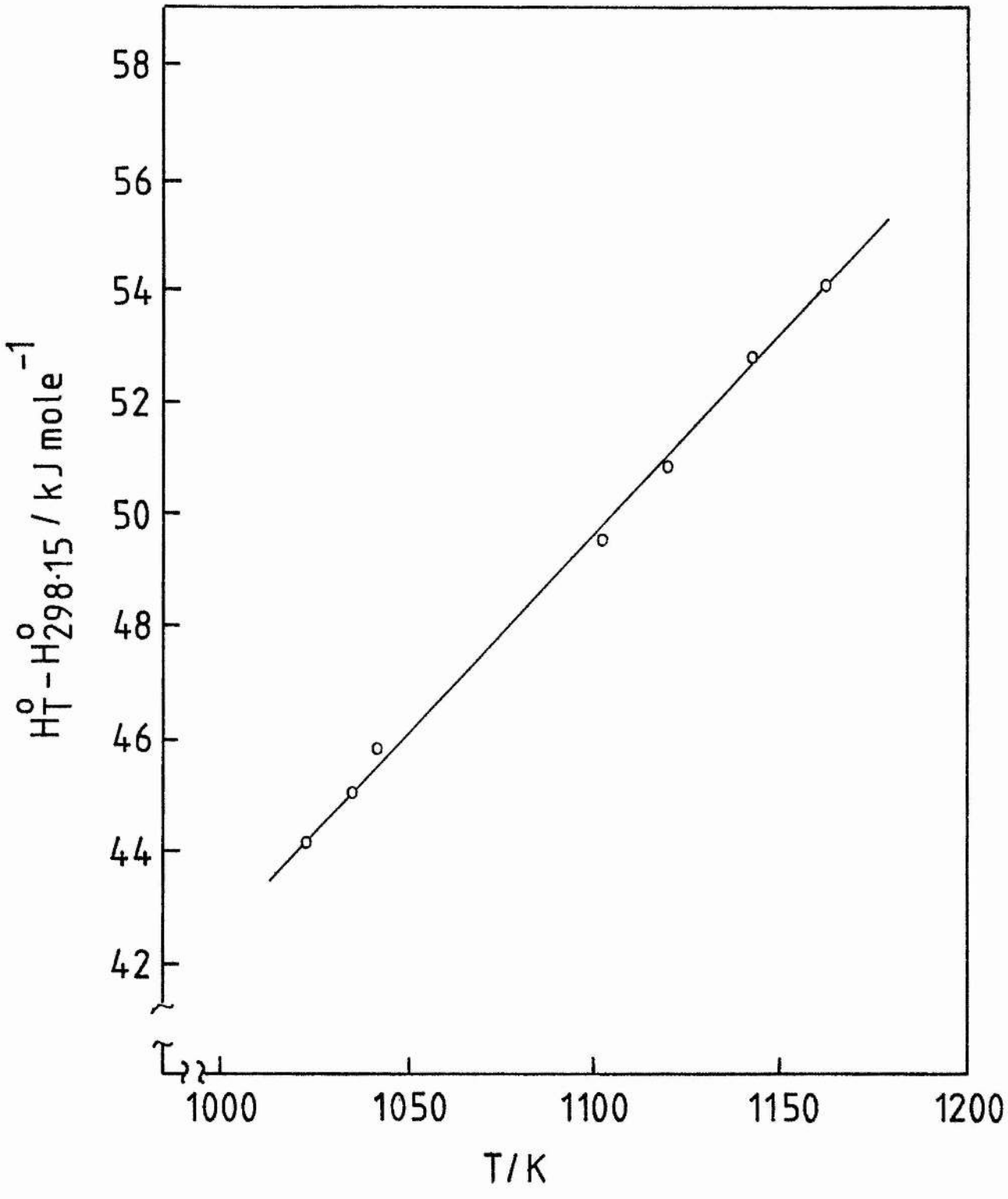

Figure 4.6 The enthalpy increment of silica glass as determined by drop calorimetry, from the data of Table 4.2.

sample down slightly, and this means that the capsule loses more heat as it falls. The empty-capsule calibration is meant to identify this type of occurrence.

Due to the lack of experimental data it was unrealistic to try to fit the results accurately to an equation of the form (4.4.2). However, from figure 4.6 it is apparent that the points lie on a straight line thus:

$$(H^{o}_{T} - H^{o}_{298.15}) \ /J \ mole^{-1} = -27519.7 + 70.115(T/K) \qquad (4.4.3)$$

Using equation(4.4.3) over the temperature range 1023 - 1162 K, the average deviation of the experimental data from the fitted data was 0.4 % and correlation coefficient was 0.999; this indicates a satisfactory fit.

As stated above, the only realistic method of assessment of calorimeter performance is by conducting a series of drops with NBS SRM 720; and a batch of this material was purchased for this purpose. However, when the capsule containing the sapphire was raised into the furnace in preparation for a drop, the capsule shattered and the sapphire was lost. The procedure was repeated, but again the capsule shattered; this occurred before the actual drop took place, in both cases. This series of experiments was therefore abandoned and it was decided to use the short time remaining to perform experiments on $CdSO_4$ in which silica capsules of wall thickness 2 mm were used. (Section 4.5).

The high-temperature enthalpy increments of SRM 720 are published by the National Bureau of Standards.[115] A study made by Fredrickson and Chasanov includes a comparison of some previous high-temperature studies, by earlier workers, on NBS SRM 720.[116] They express the enthalpy increment as a function of T:

$$(H_T^o - H_{298.15}^o)/\text{cal mole}^{-1} = -11554.31 + 27.6002\ (T / K) + 1.61393 \times 10^{-3}\ (T / K)^2 + 9.65836 \times 10^5\ (T / K)^{-1} \qquad (4.4.4)$$

The above equation has a precision of 0.2 % in the temperature range 450-1400 K.

4.5 High-Temperature Drop Calorimetry Study of Cadmium Sulphate

4.5.1 Introduction

Drop calorimetry has been successfully applied to high-temperature phase studies of a number of metal sulphates: including Ag_2SO_4,[86] $BeSO_4$[117,118] and $ZnSO_4$.[119] Phase diagrams involving these compounds have previously been studied in the present laboratories. There is interest in these compounds because they undergo high-temperature polymorphic phase transitions and, in the case of the last two compounds, these transitions are masked by decomposition of the salt (Section 3.1.1). Decomposition may be suppressed by encapsulating the material. The results of the above studies indicate that the drop method does not quench the high-temperature polymorphs; more extreme quenching methods are necessary to do this (Section 2.2.2).

It is apparent from the existing high-temperature phase studies of cadmium sulphate (Section 3.3), made using dynamic methods of thermal analysis, such as DTA, that the transition temperatures are affected by kinetics.

The drop calorimeter should yield values close to the true equilibrium values assuming that quenching does not occur. The use of a sealed capsule should prevent decomposition of the salt, as discussed in Section 3.3. From DTA studies the present author

estimates enthalpies of transition as being of the order of 4-8 kJ mol^{-1} and this should be readily detected using the drop method.

No previous high-temperature drop calorimetric study for $CdSO_4$ has been undertaken.

4.5.2 Materials and Capsule Preparation

$CdSO_4$ was obtained by heating Aldrich Gold Label $CdSO_4.H_2O$ (99.999 %) to 400 °C for 24 h. The anhydrous salt was allowed to cool over P_2O_5 before being quickly transferred to a silica capsule, after which it was heated to 400 °C for 2 h, cooled as before, and transferred to a vacuum line. A sealed capsule containing 0.2 atm of He at room temperature was prepared. The mass of the silica capsule (wall thickness 2mm) was 7.0755 g (0.11777 moles) and the mass of $CdSO_4$ it contained was 1.9838 g (9.520×10^{-3} moles). The mass ratio of the capsule to the sample is unfavourable, 12:1, but in view of the short time available to the author it was decided to use the thicker and stronger silica and attempt to obtain some preliminary high-temperature data on $CdSO_4$.

In view of some problems experienced with the thin drop-wires, it was decided to use thicker stainless steel wire, diameter 0.5 mm, for maximum strength. After five drops, however, this was showing signs of imminent failure and was replaced by 0.05 mm Pt/Rh wire, from which one result (Table 4.3,point No. 2) was obtained.

4.5.3 Results and Discussion

The results for the series of six drops are tabulated in Table 4.3 and are shown graphically in figure 4.7. It is immediately apparent from figure 4.7 that there is an uncertainty in the results which would not be expected from the results of Section 4.4.2. The experimental point at 1080 K is some 50 % lower than would have been expected. Even discarding that result, the remaining data lie on a very poor straight line. The fact that there are so few data points makes interpretation of the results difficult.

It is obvious however, that the high mass ratio of the capsule to sample severely reduces the precision of the results. Using equation (4.4.2) to calculate the heat contribution for the silica glass gives that value an uncertainty of approximately 30 J. This constitutes an error of 3 % in the heat contribution of the cadmium sulphate. When comparing the results of data points 1 and 2, whose temperatures differ by only 1 K, the percentage difference between the two values is approximately 3 %. Such errors would make the calculation of C_p impossible to any reasonable degree of accuracy. The expected enthalpies for the phase transitions would constitute approximately 5-10 % of the total heat contribution of the cadmium sulphate and an uncertainty of 3 % in the data would introduce severe limitations in the accuracy and precision of the enthalpies of transition and would also make the equilibrium transition temperature difficult to pinpoint exactly. The enthalpy increments of Table 4.3 are realistic; a study of the JANAF tables shows that many crystalline compounds have $H^o_{1000} - H^o_{298.15}$ in the range 50-150 kJ mol.$^{-1}$

Table 4.3

Enthalpy Increment of $CdSO_4$ by Drop Calorimetry

T / K	ΔT_c / K	$\Delta H_{(Silica+CdSO_4)}$ / J	$\Delta H^{\ddagger}_{(Silica)}$ / J	$\Delta H_{(CdSO_4)}$ / J	$[H^o_T - H^o_{298.15}]_{CdSO_4}$ / kJ mole^{-1}
1023	1.4694	6223.0	5294.7	928.3	97.510
1024	1.4635	6198.1	5303.0	895.1	94.019
1041	1.4849	6288.7	5444.3	844.4	88.693
1063	1.5683	6641.6	5627.8	1013.8	106.491
1080	1.4788	6262.6	5770.1	492.5	51.735
1102	1.6646	7049.5	5954.8	1094.7	114.990

$\ddagger \Delta H_{(silica)}$ calculated from equation 4.4.2.

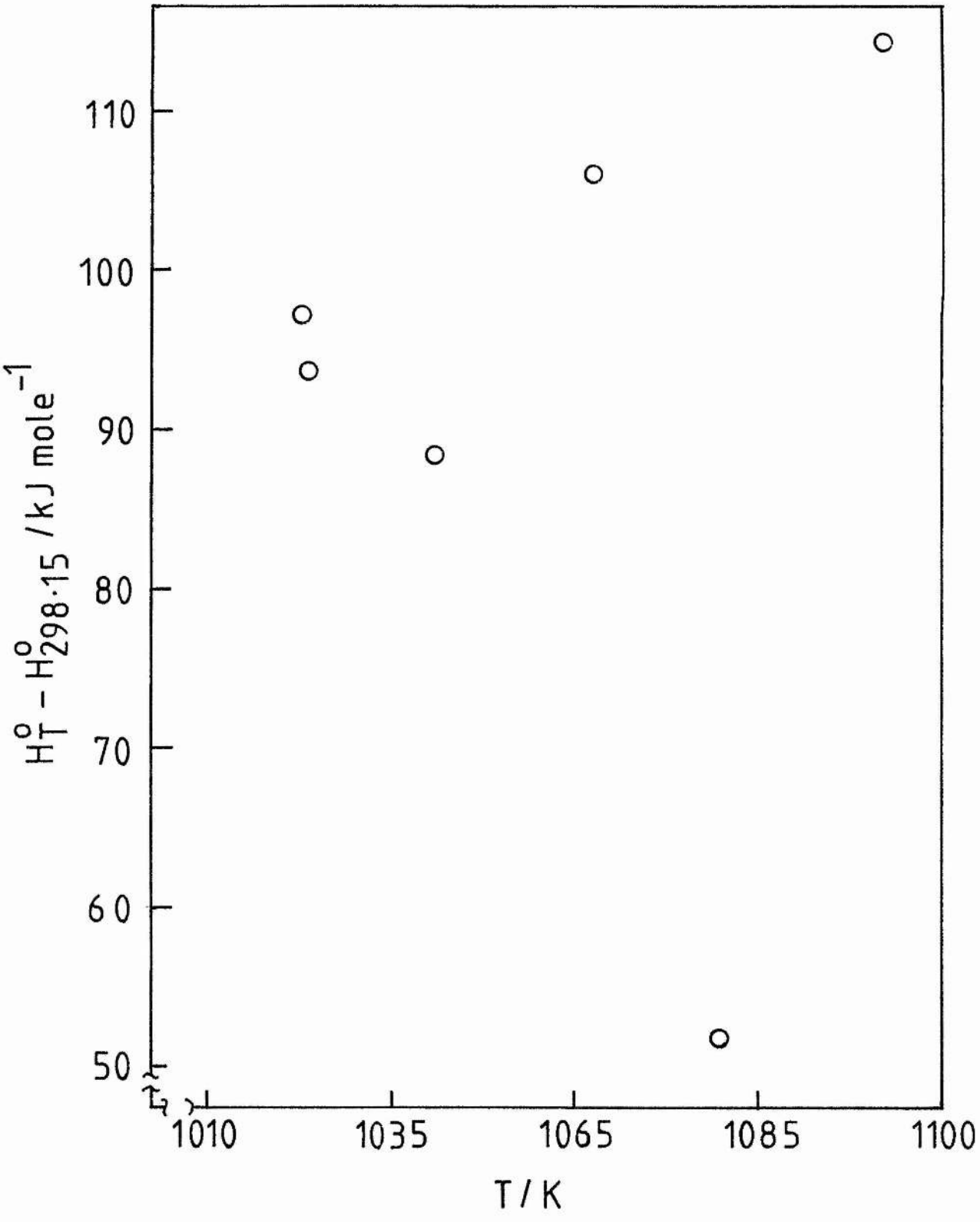

Figure 4.7 The enthalpy increment of $CdSO_4$ as determined by drop calorimetry, from the data of Table 4.3.

4.5.4 Treatment of Results

Had there been sufficient time, more results would have been obtained and the next stage would have been to express the enthalpy data as a function of T, by the method of least-squares. There are a number of suitable packages in the NAG subroutine library which may be implemented on the VAX 11/780 at St. Andrews. As a first approximation however, the data would have been fitted to an equation of the form proposed by Maier and Kelley:[100]

$$H_T^o - H_{298.15}^o = aT + bT^2 + CT^{-1} + d \qquad (4.4.5)$$

Differentiation of the above equation gives:

$$C_p = a + 2bT - CT^{-2} \qquad (4.4.6)$$

Equation (4.4.6) provides a good fit for the high-temperature heat capacity data of many crystalline compounds.[103]

Appendix 4 lists a programme which requires a specific equation, such as (4.4.5) and evaluates the coefficients by the method of least-squares. This programme runs on an Apple microcomputer but can easily be adapted to run on a BBC microcomputer.

If $C_{p_{298.15}}$ is known, the constants of equation (4.4.6) may be evaluated by the method of Shomate.[120,121] For $CdSO_4$, a literature value of $C_{p_{298.15}}$ of 100.39 J mol^{-1} K^{-1} is available.[103]

The standard entropy, S^{o}_{T}, may be evaluated by integration of (4.4.6) and substitution of S^{o}_{298} as shown in equation (4.1.7). Free energy functions may then be evaluated as discussed in Section 4.1. The literature value[103] of $S^{o}_{298.15}$ for $CdSO_4$ is 123.0 J $mol^{-1}K^{-1}$.

Errors due to differentiation and integration are introduced in the derived thermodynamic data and the subroutines for integration and differentiation which are available in the NAG library may reduce these errors.

4.6 Conclusions

The high-temperature results obtained for $CdSO_4$ are disappointing given the results obtained for silica glass (Section 4.4.2). To obtain greater precision, the mass ratio of capsule to sample must be decreased; this may be done by using silica of wall thickness 1 mm. It may be that shorter capsules (3-4 mm long) of wall thickness 0.5 mm may be sufficiently strong, and the capsule : sample mass ratio would be further reduced. One other alternative would be to enlarge the sample cavity of the copper block, to perhaps 20 mm diameter, and use capsules 20 mm wide x 50 mm length and with a wall thickness between 1 and 1.5 mm. The temperature rise of the block using such a capsule would be large (> 5 K) and this would introduce more imprecision due to greater heat loss, but the gain in enthalpy contribution of the sample itself would be so much greater that the overall precision would be improved.

Until the calorimeter is calibrated using NBS synthetic sapphire, it is difficult to assess its overall performance. The results from the silica calibration are, however, encouraging and these indicate that in most respects the drop calorimeter is functioning adequately and should be capable of achieving a precision better than 0.3 %, for a series of enthalpy increment data.

References

(1) M.L. McGlashan, Chemical Thermodynamics, (Academic Press,London, 1979).

(2) Y.K. Rao in A.M. Alper (Ed.), Phase Diagrams: Materials Science and Technology, (Academic, London 1976), Vol.1.

(3) H.C. Yeh in A.M. Alper (Ed), Phase Diagrams: Materials Science and Technology, (Academic, London,1976), Vol.1.

(4) S.T. Bowden, The Phase Rule and Phase Reactions, (MacMillan, London, 1950).

(5) J.F. Ricci, The Phase Rule and Heterogeneous Equilibrium, (Dover, New York, 1966).

(6) A. Findlay, The Phase Rule, (Dover, New York, 1951).

(7) C.W.F.T. Pistorius, J. Chem. Phys., 1965, 43, 1560.

(8) E.M. Levin, C.R. Robbins, and H.F. McMurdie (Eds.), Phase Diagrams for Ceramicists, (The American Ceramic Society, Ohio, 1964).

(9) P. Gordon, Principles of Phase Diagrams in Materials Systems, (McGraw - Hill, New York, 1968).

(10) J. Wisniak, Phase Diagrams: A Literature Source Book (Elsevier, Amsterdam, 1982).

(11) D.R. Stull and H. Prophet, JANAF Thermochemical Tables ,(US Department of Commerce, Washington, 1971).

(12) C.D. Thurmond, J. Phys. Chem., 1953, 57, 827.

(13) P.L. Lin and A.D. Pelton, High Temp. Sci., 1980, 12, 71.

(14) F.J. Dunkerly and G.J. Mills, Thermodynamics in Metallurgy, (American Society of Metallurgy, Cleveland Ohio, 1950).

(15) N.W. Taylor, J. Am. Chem. Soc., 1923, 45, 2865.

(16) G.R. Bretton and Y.K. Rao, Trans. Met. Soc. AIME, 1969, 245, 2189.

(17) L. Kaufmann and H. Bernstein, Computer Calculation of Phase Diagrams, (Academic, London, 1970).

(18) L. Kaufmann and H. Nesor in N.B. Hannay (Ed.), Treatise on Solid State Chemistry, (Plenum, London, 1976), Vol.5.

(19) C.W. Bale, P.L. Lin and A.D. Pelton, J. Am. Ceram. Soc. 1979, 62, 414.

(20) C.W. Bale and A.D. Pelton, Met. Trans., 1974, 5, 2323.

(21) R.C. Mackenzie, Talanta, 1969, 16, 1227.

(22) R.C. Mackenzie, C.J. Keattch, D. Dollimore, J.A. Forrester, A.A. Hodgson and J.P. Redfern, Talanta, 1972, 19, 1079.

(23) J.B. MacChesney and P.E. Rosenberg in A.M. Alper (Ed.), Phase Diagrams: Materials Science and Technology, (Academic, London, 1976), Vol.1.

(24) A. Ishii and K. Aikawa, Reports of the Research Laboratory of Ashai Glass Co. Ltd., 1965, 15, 1.

(25) D. Shelley, Manual of Optical Mineralogy, (Elsevier, Oxford, 1975).

(26) E. Gimzewski, Z.M. Zochowski, D.A. Campbell and P.A.H. Wyatt, Thermochim. Acta, 1981, 47, 247.

(27) G.K.T. Conn and F.J. Bradshaw (Eds.), Polarized Light in Metallography, (Butterworths, London, 1952).

(28) M. Kuhnert - Brandstaetter and L. Mueller, Microscope, 1968, 16, 257.

(29) T.J. Shepherd, Econ. Geol., 1981, 79, 1244.

(30) D. Schultze, Thermochim. Acta, 1979, 29, 233.

(31) H.A. Øye , Acta Chem. Scand., A, 1964, 18, 361.

(32) M. Gaune - Escard and J.P. Bros, Thermochim. Acta, 1979, 31, 323.

(33) R.C. Mackenzie, Thermochim. Acta,1984, 73, 249.

(34) K. Motzfeldt in J.O'M. Bockris, J.L. White and J.D. Mackenzie (Eds.), Physicochemical Measurements at High Temperatures, (Butterworths, London, 1959).

(35) P.D. Garn, Thermoanalytical Methods of Investigation, (Academic, New York, 1965).

(36) R.C. Mackenzie, Anal. Proc., (London), 1980, 17, 79.

(37) J.P. McCullough and D.W. Scott (Eds.) Experimental Thermodynamics (Butterworths, London, 1968), Vol.1.

(38) J. Braustein and H. Braustein in B. Le Neindre and B. Vodar (Eds.), Experimental Thermodynamics, (Butterworths, London, 1975), Vol.2.

(39) P.L. Start and M.W. Thring, J. Sci. Instr., 1960, 37, 17.

(40) E. Gimzewski, Thermochim. Acta, (In Press).

(41) P.D. Garn and S.S. Flaschen, Anal. Chem., 1957, 29, 271.

(42) J. Mazieres, Anal. Chem., 1964, 36, 602.

(43) R.C. Mackenzie (Ed.), Differential Thermal Analysis, vol.2 (Academic, London, 1972).

(44) H.J. Borchardt and F. Daniels, J. Am. Chem. Soc., 1957, 79, 41.

(45) H.E. Kissinger, Anal. Chem., 1957, 29, 1702.

(46) J. Tateno, J. Chem. Soc., Faraday Trans. 1, 1966, 62, 1885.

(47) D.J. David, Anal. Chem., 1964, 36, 2162.

(48) S.L. Hager, Thermochim. Acta, 1978, 26, 149.

(49) W.W. Wendlandt, Thermochim. Acta, 1978, 26, 19.

(50) P.K. Gallagher, Thermochim. Acta, 1978, 26, 175.

(51) W.W. Wendlandt, Thermochim. Acta, 1980, 37, 117.

(52) H.G. MacAdie in R.F. Schwenker and P.D. Garn (Eds.), Thermal Analysis, (Academic, London, 1967), Vol.1.

(53) W. Gutt and A.J. Majumdar in R.C. Mackenzie (Ed.), Differential Thermal Analysis, (Academic, London, 1972), Vol.2.

(54) D.S. Tsiklis, Handbook of Techniques in High Pressure Research and Engineering, (Plenum, New York, 1968).

(55) J.R. Williams and W.W. Wendlandt, Thermochim. Acta, 1973, 7, 269.

(56) C.N.R. Rao and K.J. Rao, Phase Transitions in Solids, (Mcgraw - Hill, New York, 1978).

(57) M.I. Pope and D.I. Sutton, Thermochim. Acta, 1978, 23, 188.

(58) R.C. Mackenzie (Ed.), Differential Thermal Analysis, (Academic, London, 1970), Vol.1.

(59) W.W. Wendlandt, Thermal Methods of Analysis, (Wiley Interscience New York, 1974).

(60) M.I. Pope and M.D. Judd, Differential Thermal Analysis, (Heyden, London, 1977).

(61) C.W.F.T. Pistorius in B. Le Neidre and B. Vodar (Eds.), Experimental Thermodynamics, (Butterworths, London, 1975), Vol.2.

(62) B. Wunderlich in A. Weissberger and B.W. Rossiter (Eds.), Physical Methods of Chemistry, (Wiley Interscience, New York, 1971), Vol.2.

(63) W.W. Wendlandt, Anal. Chem., 1982, 54, 97R.

(64) W.W. Wendlandt, Anal. Chem., 1984, 56, 250R.

(65) M.J. O'Neill, Anal. Chem., 1964, 36, 1238.

(66) E.S. Watson, M.J. O'Neill, J. Justin and N. Brenner, Anal. Chem., 1964, 36, 1233.

(67) R. Kohli and W. Lacom, Thermochim. Acta, 1982, 57, 155.

(68) H.H. Kellogg, Trans. Met. Soc. AIME, 1964, 230, 1622.

(69) K.H. Stern and E.L. Weise, National Bureau of Standards Report, NSRDS-NBS 7, (US GPO, Washington D.C., 1966).

(70) E.W. Dewing and F.D. Richardson, J. Chem. Soc., Faraday Trans.1 1959, 5, 611.

(71) E.M. Bollin in R.C. Mackenzie (Ed.), Differential Thermal Analysis, (Academic, London, 1970), Vol.1.

(72) E.M. Bollin and P.F. Kerr, Amer. Mineral., 1961, 46, 823.

(73) H.S. Roberts, J. Am. Chem. Soc., 1935, 57, 1034.

(74) E.W. Washburn (Ed.), International Critical Tables of Numerical Data, Physics, Chemistry and Technology, (McGraw-Hill, New York, 1926), Vol.7.

(75) C.W.F.T. Pistorius and E. Rapaport, J. Phys. Chem. Solids 1969, 30, 197.

(76) W.W. Wendlandt, Thermochim. Acta, 1974, 9, 456.

(77) W.W. Wendlandt, Thermochim. Acta, 1970, 1, 419.

(78) J.J. Rowe, G.W. Morey and I.D. Hansen, J. Inorg. Nucl. Chem., 1962, 24, 53.

(79) E. Gimzewski, Z.M. Zochowski and P.A.H. Wyatt, Thermochimica Acta, 1981, 44, 369.

(80) International Practical Temperature Scale of 1968, (English version of the official French Text), (HMSO, London, 1969).

(81) M.W. Nathans and W.W. Wendlandt, J. Inorg. Nucl. Chem., 1962, 24, 869.

(82) H. Tagawa, Thermochim. Acta, 1984, 80, 23.

(83) M.W. Prokof'ev, L.M. Kovba and A.N. Pokrovskii, Zh. Neorg. Khim., 1979, 24, 2114.

(84) B.G. Samartsev, A.N. Pokrovskii and L.M. Kovba, Vestnik-Moskovskogo Universitata Zkhimiya, 1978, 19, 727.

(85) B.N. Mehrotra, W. Eysel and Th. Hahn, Acta Crystallogr. B, 1333, 305.

(86) B.R. Conard, T.B. McAneney and R. Sridhar, J. Chem. Thermodyn., 1978, 10, 889.

(87) C.W.F.T. Pistorius, J. Chem. Phys., 1967, 46, 2167.

(88) N.S. Dombrovskaya, Izv. Sektora Fiz-Khim Analiza. Inst. Obsch. Neorgan. Khim Akad. Nauk USSR, 1938, 11, 115.

(89) A.N. Ketov, V.V. Pechkovskii, N.P. Starkov and B.N. Varskoi, Russ. J. Inorg. Chem., 1961, 6, 1028.

(90) G.V. Maksimova, Russ. J. Inorg. Chem., 1959, 4, 230.

(91) E.V. Margulis, Yu.S. Remizov and N.I. Kopylov, Russ. J. Inorg. Chem., 1963, 8, 969.

(92) E.V. Margulis, N.I. Kopylov and N.S. Grishankina, Russ. J. Inorg. Chem., 1965, 10, 542.

(93) G. Pannetier, J.M. Bregeault, and J. Guenot, Bull. Soc. Chim. Fr. 1962, 2158.

(94) M. Spiess and R. Gruehn, Z. Anorg. Allg. Chem., 1979, 455, 16.

(95) A.G. Ostroff and R.T. Sanderson, J. Inorg. Nucl. Chem., 1959, 9, 45.

(96) E.D. West and D.C. Ginnings, Rev. Sci. Instr., 1957, 28, 1070.

(97) W.A. Dench, J. Chem. Soc. Faraday Trans., 1963, 59, 1279.

(98) E.F. Westrum, G.T. Furukawa and J.P. McCullough in J.P. McCullough and D.W. Scott (Eds.), Experimental Thermodynamics, (Butterworths, London, 1968), Vol. 1.

(99) J.C. Southard, J. Am. Chem. Soc., 1941, 63, 3142.

(100) C.G. Maier and K.K. Kelley, J. Am. Chem. Soc., 1932, 54, 3243.

(101) L. Leibowitz, M.G. Chasanov and L.W. Mishler, Trans. Met. Soc. AIME, 1969, 245, 981.

(102) S. Tamura, T. Yokokawa and K. Niwa, J. Chem. Thermodyn., 1975, 7, 633.

(103) O. Kubaschewski and C.B. Alcock, Metallurgical Thermochemistry, (Pergamon, Oxford, 1979).

(104) B.R. Conard, R. Sridhar and J.S. Warner, J. Chem. Thermodyn., 1980, 12, 817.

(105) D.R. Fredrickson, R.D. Barnes, M.G. Chasanov, R.L. Nuttal, R. Kleb, and W.N. Hubbard, High Temp. Sci., 1969, 1, 373.

(106) T.B. Douglas and E.G. King in J.P. McCullough and D.W. Scott (Eds.), Experimental Thermodynamics, (Butterworths, London, 1968), Vol. 1.

(107) W.T. Thompson and S.N. Flengas, Can. J. Chem., 1971, 49, 1550.

(108) D.E. Heffer, G.A. King and D.C. Keith, Basic Principles and Practice of Microprocessors, (Edward Arnold, London, 1981).

(109) K. Davis, Using Floppy Disks With the BBC Microcomputer, (Cumana, Guildford, 1983).

(110) F.D. Rossini, Experimental Thermochemistry, (Interscience, New York, 1956), p94.

(111) N.D. Stout, R.W. Mar and W.O.J. Boo, High Temp. Sci., 1973, 5, 241.

(112) A.D. Jones and D.R. Williams, J. Chem. Soc., 1970 (A), 3138.

(113) D. Calvert, M.A. Gilchrist and P.A.H. Wyatt, J. Chem. Soc. Faraday Trans. 1, 1979, 75, 1745.

(114) D.I. Marchidan and M. Ciopec, J. Chem. Thermodyn., 1976, 8, 691.

(115) G.T. Furukawa, T.B. Douglas, R.E. McCoskey, and D.C. Ginnings, J. Res. Natl. Bur. Std., 1956, 57, 67.

(116) D.R. Fredrickson and M.G. Chasanov, J. Chem. Thermodyn., 1970, 1, 623.

(117) A.R. Taylor, Jr., T.E. Gardner and D.F. Smith, U.S. Bur. Mines, Report No. 6240, 1963.

(118) A.R. Taylor Jr., B.B. Letson and D.F. Smith, U.S. Bur. Mines, Report No. 6724, 1966.

(119) P.K. Hosmer and O.H. Krikorian, High Temp.-High Press., 1980, 12, 281.

(120) C.H. Shomate, J. Am. Chem. Soc., 1944, 66, 928.

(121) C.H. Shomate, J. Phys. Chem., 1954, 58, 368.

APPENDIX 1

The following formulae enable the parameters drop height(h), length of drop wire(l), and the length of the adjuster screw(a) ,to be calculated.

$$l = d_2 + d_4 + d_s - d_1$$

$$h = d_2 - (d_3 + 0.5\, d_1)$$

$$a = d_6 - d_5 - d_s - h$$

where:

d_1 is the length of the capsule (~ 6 cm)

d_2 is the distance to the bottom of the calorimeter well from the top flange, = 146.8 cm.

d_3 is the distance to the centre of the hot zone from the top flange, = 45.5 cm.

d_4 is the distance from the bottom of the drop weight (at rest at the bottom of the drop tube) from the top flange, = 7.0 cm.

d_5 is the distance form the top of the drop weight (at rest) to the top flange, = 9.7 cm.

d_6 is the length of the drop tube, measured to the top flange, = 117.5 cm.

d_6 is the amount of slack in the drop wire and is generally 0.5 - 1 cm.

The distances, d_2 and d_3 were measured at 1100 K using Pt - 13% Rh.

APPENDIX 2

PROGRAMME "DELTA_T"

```
 10  REM ******** DELTA_T *************
 20 CLEAR: MODE7:CLS:@%=10
 30 PROCprompt1
 40 PROCinput_file
 50 PROCprompt2
 60 PROCread_file
 70 PROCprint_fields
 80 PROCcalKA
 90 PROCdelta_t
100 PROCmenu
110 PROCprompt3
120 END
130 REM ******************************
140 DEFPROCread_file
150 INPUT#F%,SAM$,FTEMP$,BTEMP,T1$,T2$,IVAL,NPTS%
160 CLS:IF PFLAG%=1THEN VDU2:FORI%=1TO5:PRINT:NEXT
170  PRINTT1$,T2$:PRINT:PRINT;NPTS%," data points at ";IVAL;"s intervals."
180  PRINT:PRINT"Sample > ";SAM$:PRINT:PRINT"Furnace Temperature > ";FTEMP$
190 PRINT:PRINT"Bath Temperature > ";BTEMP
200 NPTS%=NPTS%-1
```

```
210 DIMT(NPTS%)
220 FORI%=0TONPTS%:INPUT#F%,T(I%):NEXT:POINT%=PTR#F%:CLOSE#0
230  PRINT:PRINT"Do you wish to alter Bath temp.?  Y/N":G$=GET$
240 IFG$="Y" THEN PRINT:INPUT"Enter new value for Bath Temp. > "BTEMP
250 IF PFLAG%=1THEN VDU3
260 ENDPROC
270 REM ******************************
280 DEFPROCinput_file
290 *CAT
300 REPEAT
310   PRINT
320   INPUT "Enter data file name: " F$
330   F%=OPENIN(F$)
340   UNTIL F%<>0
350 CLS
360 ENDPROC
370 REM ******************************
380 DEFPROCtmaxmin
390  TMAX=0:TMIN=100:TTMIN=0:TTAX=0
400 FORI%=1TONPTS%
410   IFT(I%)>TMAX THEN TMAX=T(I%):TTMAX=I%
420   IFT(I%)<TMIN THEN TMIN=T(I%):TTMIN=I%
430   NEXT
440  I%=1:REPEAT:I%=I%+1:UNTILT(I%+1)-T(I%)>0.001OR I%=NPTS%:TCHANGE=T(I%)
450 TTCHANGE=I%
460 ENDPROC
470 REM******************************
480 DEFPROCleast_squares(X,Y)
490 SX=SX+X:SY=SY+Y
500 SXX=SXX+X^2:SXY=SXY+(X*Y):SYY=SYY+Y^2
```

```
510 ENDPROC
520 REM*****************************
530 DEFPROCgrad_icept(SX,SY,SXY,SXX,N%)
540 K=((SXY*N%)-(SX*SY))/((SXX*N%)-(SX^2))
550 A=(SY-K*SX)/N%
560 ENDPROC
570 REM*****************************
580 DEFPROCinit:SX=0:SXX=0:SY=0:SYY=0:SXY=0:XMEAN=0:YMEAN=0:ENDPROC
590 REM*****************************
600 DEFPROCcalKA
610 REGMAX=0:KMAX=0:AMAX=0:INMAX%=0
620 PROCtmaxmin:TBATH=BTEMP
630 CLS:PRINTTAB(3,0);"Linear Regression Fitting Routine"
640 FORINC%=1TO 10
650   PROCinit
660   FIN%=NPTS%-(4*INC%):tfin%=10*NPTS%:N%=0
670   FORI%=NPTS% TO FIN% STEP-INC%
680     t%=(10*I%)-tfin%
690     TLN=LN(T(I%)-TBATH)
700     PROCleast_squares(t%,TLN)
710     N%=N%+1:NEXT
720   FLAG%=0:INC%=INC%*2:I%=I%-INC%
730   REPEAT
740     t%=(10*I%)-tfin%
750     PROCgrad_icept(SX,SY,SXY,SXX,N%)
760     TEST_T=TBATH+EXP(K*t%+A):DIFF=ABS(TEST_T-T(I%))
770     IFDIFF>0.00015THEN FLAG%=1:GOTO810
780     TLN=LN(T(I%)-TBATH)
790     PROCleast_squares(t%,TLN)
```

```
 800 N%=N%+1:I%=I%-INC%
 810 UNTILFLAG%=1
 820 PROCgrad_icept(SX,SY,SXY,SXX,N%)
 830 PROCreg_coeff(SX,SY,SXY,SXX,SYY,N%)
 840 IFABS(R)>REGMAX THEN REGMAX=ABS(R):KMAX=K:AMAX=A:INMAX%=INC%
 850 NEXT
 860 R=REGMAX:K=KMAX:A=AMAX:INC%=INMAX%
 870 IF PFLAG%=1THEN VDU2
 880 PRINT:PRINT;N%;" points at intervals of ";INC%:PRINT
 890 @%=PFH1%:PRINT"Gradient (k)",TAB(27);K
 900 @%=PFH2%:PRINT:PRINT"Intercept (A)";TAB(27);A
 910 @%=PFH6%:PRINT:PRINT"Correlation Coefficient";TAB(27);R
 920 IF PFLAG%=1THEN VDU3
 930 ENDPROC
 940 REM*****************************
 950 DEFPROCdelta_t
 960 SUMTHET=0
 970 ST%=TTCHANGE+1
 980 FORI%=ST% TO NPTS%
 990   THETA=-K*((T(I%)+T(I%-1))/2-TBATH)*10
1000   SUMTHET=SUMTHET+THETA
1010   NEXT
1020 TFIN=TBATH+EXP(A)
1030 DELTAT=TFIN+SUMTHET-TCHANGE
1040 IF PFLAG%=1THEN VDU2
1050 @%=PFH4%:PRINT:PRINT "Temperature correction";TAB(27);SUMTHET
1060 PRINT:PRINT"Final corrected temp.";TAB(27);TFIN
1070 PRINT:PRINT"Delta T (Corr.)";TAB(27);DELTAT
1080 IF PFLAG%=1THEN VDU3
```

```
1090 ENDPROC
1100 REM*******************************
1110 DEFPROCcal_const
1120 VDU23,1,1;0;0;0;
1130 PRINT
1140 CLS
1150 PRINTTAB(2,1);"Electrical Calibration of Calorimeter"
1160 PRINT:INPUT"Enter Voltage Reading (V) > "VOLTS:CURR=VOLTS/10
1170 PRINT:INPUT"Time current passed (min),(s) "min,sec
1180 TC=60*min+sec
1190 CALK=CURR^2*20.67*TC/DELTAT
1200 ER=(2*((.0001/CURR)^2)+((.0001/DELTAT)^2)+((.02/TC)^2)+((.01/20.67)^2))
1210  CERR=CALK*SQR(ER)
1220 IFPFLAG%=1THEN VDU2
1230 @%=PFH5%
1240 PRINT:PRINT;CURR*1000;" mA passed for ";TC;" seconds":PRINT
1250 PRINT"Calorimeter constant = ";CALK;" +/- ";CERR
1260 PRINT:PRINT"Percentage Error = ";CERR*100/CALK
1270 IFPFLAG%=1THEN VDU3
1280 @%=10
1290 ENDPROC
1300 REM*******************************
1310 DEFPROCprint_fields
1320 PFH1%=&010400:REM 1.1111E-1
1330 PFH2%=&020500:REM 0.11111
1340 PFH3%=&010200:REM 1.1E-1
1350 PFH4%=&020400:REM 0.1111
1360 PFH5%=&020200:REM 1111.11
1370 PFH6%=&020700:REM 0.1111111
```

```
1380 ENDPROC
1390 REM*********************************
1400 DEFPROCmenu
1410 PRINTTAB(0,18);CHR$(136);"HIT <C> TO CALCULATE CALORIMETER CONST."
1420 PRINTTAB(3,21);CHR$(136);"HIT <E> TO CALCULATE ENTHALPY"
1430 G$=GET$:IF G$="C" OR G$="E" THEN 1440 ELSE1430
1440 IFG$="C"THEN PROCcal_const ELSE PROCenthalpy
1450 ENDPROC
1460 REM*********************************
1470 DEFPROCenthalpy
1480 CLS
1490 @%=PFH5%
1500 PRINTTAB(3,1),"CALCULATION OF ENTHALPY INCREMENT":PRINT
1510 BCON=4235:PRINT:PRINT"Block Constant = ";BCON;" J/K ":PRINT
1520 PRINT"Do you wish to alter it? Y/N":G$=GET$:PRINT
1530 IF G$="Y"THEN INPUT"Input new value > "BCON:PRINT
1540 PRINT:PRINT:PRINTTAB(5);"H(T) - H(298.15) = ";BCON*DELTAT;" J"
1550 IF PFLAG%=1 THEN VDU3
1560 ENDPROC
1570 REM*********************************
1580 DEFPROCreg_coeff(SX,SY,SXY,SXX,SYY,N%)
1590 RXX=SXX-(SX^2/N%)
1600 RYY=SYY-(SY^2/N%)
1610 RXY=SXY-(SY*SX/N%)
1620 R=RXY/SQR(RXX*RYY)
1630 ENDPROC
1640  DEFPROCprompt1:PRINTTAB(5,10);"PLACE DATA SOURCE DISC IN DRIVE"
1650  PRINT TAB(5,14);"THEN HIT SPACE BAR TO CONTINUE":VDU23,1,0;0;0;0;
1660  REPEAT:UNTIL GET=32:VDU23,1,1;0;0;0;:CLS:ENDPROC
```

```
L
1670  DEFPROCprompt2:VDU23,1,0;0;0;0;:PFLAG%=0:SOUND 1,-15,60,10
1680  PRINTTAB(8,12);"TO USE PRINTER HIT < P > "
1690  PRINT TAB(3,14);"OR HIT ANY OTHER KEY TO CONTINUE":P$=GET$
1700  IFP$="P" THEN PFLAG%=1
1710 ENDPROC
1720  DEFPROCprompt3:VDU23,1,0;0;0;0;
1730  PRINTTAB(2,16);"TO REPEAT FOR ANOTHER FILE PRESS < F > "
1740 PRINTTAB(5,19);"TO RETURN TO MENU PRESS < M >."
1750  G$=GET$:IFG$="F"THEN 20 ELSE CHAIN "MENU"
```

APPENDIX 3

DROP CALORIMETER: PROCEDURE FOR DROPPING

The following sequence assumes that the sample has reached thermal equilibrium in the furnace.

1) 30 minutes before dropping, switch on the HP 2801 A Quartz Thermometer.

2) 10 minutes before dropping, set the HP 2801 A to read the temperature of the high-precision thermostat bath, as follows:
   (a) Select channel T2.
   (b) Set the trim switches on the rear of the HP 2801 A to 9281.

3) After noting the bath temperature, set the HP 2801 A back to reading the block temperature as follows:
   (a) Select channel T1.
   (b) Set the trim switches to 9220.

4) Record the sample temperature on the Solartron digital voltmeter.

5) "Boot" the Drop Calorimeter Master Disk and commence data acquisition as follows:
   (a) Place the Master Disk in the drive.
   (b) Press the "BREAK" key while holding down the "SHIFT" key.
   (c) Select item 1 from Menu.

Further instructions are given by the computer as a series of on-screen prompts. With the thermometer RESOLUTION set to 0.0001 K the "interval between readings" is 10 (seconds) and the "code" is 1.

6) Wait for approximately 5-10 minutes for the baseline to stabilise.

7) The drop may now be carried out as follows:

   (a) OPEN SHUTTERS as quickly as possible.

   (b) De-energise the electromagnet.

   (c) CLOSE SHUTTERS as soon as the capsule enters the calorimeter.

8) Take the furnace to the next temperature (Stanton-Redcroft LVP temperature programmer).

9) Wait for 60-90 minutes to allow the calorimeter block to reach thermal equilibrium.

10) Terminate data acquisition by pressing the "ESCAPE" key. Data is written to disk for future use.

PROCEDURE FOR SETTING UP THE NEXT DROP

11) Retrieve the sample as follows:

(a) OPEN SHUTTERS.

(b) Energise the electromagnet.

(c) Pull the magnet down drop tube to "catch" the iron slug.

(d) Raise the electromagnet to lift the capsule into view.

(e) Check the capsule for alignment and damage.

(f) Carefully let the system back up to atmospheric pressure.

(g) Raise the electromagnet to the top of the drop tube.

12) The calorimeter block should be brought back to within one or two hundredths of a degree above water bath temperature, and this is done as follows:

(a) Unplug the side-arm of the glass window and insert the funnel.

(b) Pour liquid nitrogen into the calorimeter until the temperature reaches the desired value.

(c) Replace the plug.

(d) CLOSE SHUTTERS.

13) Carefully pump down calorimeter.

14) If the block temperature is below the bath temperature, then the former can be increased by heating the block electrically using the calibration heater and the constant current supply.

15) Switch off the Quartz Thermometer.

APPENDIX 4

PROGRAMME "GRID-SEARCH"

by

I.M. FRASER

```
10 HOME
20 PRINT
30 XMAX=0:YMAX=0:CALCS=0
40 PRINT:INPUT"ENTER TOTAL NO. OF DATA PTS. ";MAX
50 DIM X(MAX),Y(MAX),C(35)
60 DIM XN(MAX),YN(MAX),F(MAX),FS(MAX)
70 FOR I=1 TO MAX
80   PRINT:INPUT"ENTER X COORD ";X(I)
90   INPUT"ENTER Y COORD ";Y(I)
100   IF X(I)>XMAX THEN XMAX=X(I)
110   IF Y(I)>YMAX THEN YMAX=Y(I)
120 NEXT I
130 REM NOW SCALE X AND Y COORDS
140 XSCALE=240/XMAX:YSCALE=70/YMAX
150 FOR I=1 TO MAX
160   XN(I)=INT(X(I)*XSCALE):YN(I)=INT(Y(I)*YSCALE)
170 NEXT I
180 PRINT:INPUT"ENTER TOTAL NO. OF UNKNOWN COEFFICIENTS ";AMAX
190 DIM A(AMAX)
200 FOR I=1 TO AMAX
210   PRINT:INPUT"ENTER ESTIMATE OF UNKNOWN(S) ";A(I)
220 NEXT I
230 PRINT:INPUT"ENTER THE ERROR LIMIT FOR CHI SQUARE ";BOUND
240 HOME:PRINT:PRINT
250 PRINT"PASS      CHI SQUARE"
260 P=0:DA=1
270 CSUM=100000!
280 IF CSUM<=BOUND THEN END
290   FOR J=1 TO AMAX
300     AHOLD=A(J)
310     GOSUB 780
320     REM J$=STR$(J)
330     REM PLOT 20,5,J$
340     REM HAVE NOW COMPUTED CHISQ
350     REM FOR INITIAL PARAMS->C(0)
360     C(0)=CSUM
370     TEST=A(J)
380     A(J)=A(J)+DA
390     GOSUB 780
400     DIRECT=CSUM
410     A(J)=TEST-DA
420     GOSUB 780
430     IF CSUM<DIRECT THEN DA=-DA
440     A(J)=TEST
450     REM SELECTS DIRECTION OF DECREASING CHI SQUARE
460     REM NOW MINIMISE THE CURRENT "A" PARAMETER
470     N=0
480     FLAG=0
490     IF FLAG=1 THEN N=0
```

```
500         REM D$=STR$(DA):PLOT 20,9,D$
510         N=N+1
520         A(J)=A(J)+DA
530         GOSUB 780
540         IF N>25 THEN DA=DA*2:A(J)=AHOLD:FLAG=1
550         IF N<=25 THEN FLAG=0
560         C(N)=CSUM
570       IF C(N)<=C(N-1) THEN GOTO 490
580       REM NOW TEST TO ENSURE >3 READINGS
590       REM OF CHI SQUARE TAKEN
600       IF N<3 THEN DA=DA/2:A(J)=AHOLD:GOTO 470
610       REM NOW CALCULATE THE OPTIMUM "A" VALUE
620       H1=C(N)-C(N-1)
630       H2=C(N)-2*C(N-1)+C(N-2)
640       HOLD=.5+(H1/H2)
650       MINA=A(J)-(DA*HOLD)
660       A(J)=MINA
670       DA=1
680     NEXT J
690     P=P+1
700     GOSUB 780
710     REM HAVE NOW COMPLETED ONE PASS
720     REM OF MINIMISATION W.R.T. EACH OF THE UNKNOWNS
730     PRINT P;"      ";CSUM
740     IF O>0 THEN GOSUB 1140
750     O=0
760     GOSUB 870
770 GOTO 280
780 REM SUBROUTINE TO CALCULATE
790 REM CHI SQUARE
800 CSUM=0
810 FOR I=1 TO MAX
820     F(I)=A(1)+A(2)*X(I)+A(3)*X(I)^2+A(4)*X(I)^3
830     CSUM=CSUM+(Y(I)-F(I))^2
840 NEXT I
850 IF J>AMAX THEN GOTO 860
860 RETURN
870 REM GRAPHICS SUBROUTINE
880 REM TO PLOT CURRENT FIT (IF POSS.)
890 FOR I=1 TO MAX
900     FS(I)=INT(F(I)*YSCALE)
910     IF FS(I)>120 THEN RETURN
920     IF FS(I)<-35 THEN RETURN
930 NEXT I
940     HGR
950     HCOLOR=3
960     HPLOT 10,10 TO 10,158
970     HPLOT 0,120 TO 260,120
980     HCOLOR=9
990 FOR I=1 TO MAX
1000      HPLOT XN(I)+10,120-YN(I)
1010 NEXT I
1020 FOR I=1 TO 50
1030      PRINT
1040 NEXT I
```

```
1050 PRINT:PRINT"PASS=";P;"    CHI SQUARE=";CSUM
1060 HCOLOR=3
1070 HPLOT XN(1)+10,120-FS(1)
1080 FOR I=1 TO MAX-1
1090   HPLOT TO XN(I+1)+10,120-FS(I+1)
1100 NEXT I
1110 IF G>0 THEN LPRINT CHR$(25);"GM"
1120 G=0
1130 RETURN
1140 REM PRINT-OUT OF CURRENT BEST FIT
1150 HOME:TEXT:PRINT:PRINT
1160 PRINT"CURRENT BEST FIT COORDS ARE:"
1170 PRINT:PRINT"XCOORD","YCOORD","FIT-Y COORD"
1180 PRINT"---------------------------------"
1190 FOR I=1 TO MAX
1200   PRINT X(I),Y(I),F(I)
1210 NEXT I
1220 PRINT:PRINT"CURRENT VALUE OF CHI SQUARE IS ";CSUM
1230 PRINT"CURRENT VALUES OF UNKNOWNS:"
1240 FOR I=1 TO AMAX
1250   PRINT"UNKNOWN";I;"=";A(I)
1260 NEXT I
1270 PRINT:PRINT"PLEASE PRESS ANY KEY TO CONTINUE"
1280 GET A$
1290 RETURN
```